TÉCNICO LISBOA

Neuromechanical Control of Ballistic Contractions

Decoding Motor Unit Activity from High Density EMG

Sofia Lopes Monteiro

Thesis to obtain the Master of Science Degree in

Biomedical Engineering

Supervisors:
Prof. Dr. Miguel Tavares da Silva
Prof. Dr. Dario Farina

Examination Committee

Chairperson: Prof. Dr. Paulo Rui Alves Fernandes
Supervisor: Prof. Dr. Miguel Tavares da Silva
Members of the Committee: Prof. Dr. Mamede Alves de Carvalho
Prof. Dr. Carlos Miguel Fernandes Quental

May 2018

In all affairs it's a healthy thing now and then
to hang a question mark on the things
you have long taken for granted.

Bertrand Russell

Acknowledgments

I would like to thank my supervisors Prof. Miguel Tavares da Silva and Prof. Dario Farina, for sharing their knowledge and trusting my ability to manage this project. Prof. Miguel Tavares da Silva lectured one of the most influential modules of my post-graduate curriculum – Biomechanics of Movement – and supported my greatest academic endeavours, both in Portugal and overseas. Prof. Dario Farina introduced me to scientific research and advised me over two masters dissertations. I would like to express my sincere gratitude for his time and valuable insights. I am most thankful for the opportunity to collaborate with Prof. Farina's lab, and for the time at Imperial College London, where I gained new perspectives into bioengineering and developed the investigation here presented.

To Dr. Alessandro Del Vecchio, my mentor throughout this project, I thank the constant availability and precious guidance. Alessandro's research inspired my work, and his advice was paramount to this dissertation. I owe him a new insight into exercise physiology, and confidence to come forward with my own ideas. I also thank Andrea Casolo for his thoughts on my methods and results, and Matteo Scorcelletti for sharing his data on ballistic contractions.

I am immensely proud to submit this dissertation to Instituto Superior Técnico. It has been a privilege to be a part of this school, along with a bright cohort of biomedical engineers who raised the standards with hard work and team spirit. A special thanks to my mates Mafalda Prazeres, Miguel Martinho, André Manso, Lino Fernandes, André Pombeiro and Carolina Leitão.

I thank Faculdade de Medicina de Lisboa for opening its doors to IST students and providing us with an exceptional background on medicine. I hope both schools will continue developing their partnership and contributing for the future of health-care with strong bridges between medicine and engineering.

This work is dedicated to my family.

To grandpa Rui, who was the first to encourage my excitement for mathematics, back in elementary school. To grandpa Zé, whose words *"Primeiro a obrigação, depois a devoção"* became my motto. They would have been happy to see me graduating.

To my aunts Maria José and Isabel, for their endless enthusiasm for my academic experience.

To my siblings, my best friends. Inês – thank you for your patience and for giving me yet a greater insight into medicine. I truly admire you. Eduardo – I am so glad to see you starting your own journey in engineering school, as I finish mine. You've earned it. I leave you my calculus notes and wish that you seize both the fun and hard times ahead.

Finally, and above all, I thank my parents, Luísa and Rui for the endless support from across the pond, the proof-reading and LaTeX hacks and, above all, for giving me independence and motivation to work for what makes me happy.

Abstract

The current work intends to contribute towards the understanding of motor control mechanisms at high rates of force development.

A first investigation validates the adoption of automatic methods for estimation of ballistic motor output onset, demonstrating the accuracy of all proposed methods with respect to the gold standard of Manual Detection (MD). Statistical processing with the AGLR algorithm outperforms MD significantly in simulated and real data ($p < 0.05$). The methods are tested on data acquired with both custom-made and commercial force transducers, and data simulated with different noise levels, obtained from a novel ballistic force model.

The second research work addresses control of motor performance through several neuromechanical factors. In order to characterize the spinal output driving sub-maximal ballistic contractions, the individual motor unit action potentials are extracted from high density EMG, using blind convolutive separation. We describe how central (e.g. recruitment and discharge rate) and peripheral (e.g. muscle fiber conduction velocity) factors collectively contribute towards mechanical output. Conduction velocity is characterized by a monotonic increase, despite a decrease in discharge rate after the initial phase of force development, and is moderately correlated with motor output ($R^2 = 0.62 \pm 0.28$). The dynamics of CV are in agreement with the transience of ionic gradient changes and may contribute to explain the late ballistic rise in mechanical output, concurrent with a decrease in neural drive, through a multiplicative relationship between peripheral and central control factors. Individual motor units exhibit short term synchronization over long step-and-hold contractions, and the motor output is highly correlated with both individual ($R^2 = 0.70 \pm 0.09$) and total ($R^2 = 0.78 \pm 0.07$) discharge patterns. The results provide evidence of the accuracy of the signal decomposition with respect to the reference invasive assessment of motor neurons and bring a new insight into how recruitment and excitation influence mechanical performance.

Keywords

ballistic contraction – motor output – onset detection – statistical signal processing – high density surface EMG – motor neuron discharge rate – muscle fiber conduction velocity

Resumo

O trabalho aqui apresentado visa contribuir para a compreensão dos mecanismos de controlo motor durante a produção rápida de tensão muscular.

Numa primeira parte são explorados métodos automáticos para a detecção do início do sinal de transdutores de força em contracções balísticas, sendo demonstrado o rigor de todos os métodos propostos e, consequentemente, a sua validade como alternativas ao método padrão manual. Os métodos são testados em sinais adquiridos com diversos tipos de instrumentação, assim como sinais simulados com diferentes amplitudes de ruído, a partir de um modelo original. O processamento estatístico do sinal com o algorítmo AGLR leva a uma exactidão superior à do processamento manual, tanto em dados reais como simulados ($p < 0.05$), apresendo-se como o método mais robusto.

Numa segunda parte, é feita uma análise dos mecânismos centrais (recrutamento e frequência de unidades motoras) e periféricos (velocidade de condução muscular), assim como da sua contribuição conjunta para a força produzida em contracções balísticas. De modo a caracterizar os sinais do sistema nervoso central durante estas contracções, os potênciais de acção de diversos neurónios motores são extraídos a partir do electromiograma de alta densidade, usando *blind source separation*. O sinal do transdutor de força é processado com o método AGLR testado na primeira parte. As unidades motoras apresentam sinais de sincronização durante a fase longa de manutenção de força, e o *output* motor está altamente correlacionado com as frequências de disparo individuais ($R^2 = 0.70 \pm 0.09$) e totais ($R^2 = 0.78 \pm 0.07$). Observamos que, apesar da redução da frequência de disparo, a velocidade de condução aumenta monotonicamente na fase final do desenvolvimento de força, e está moderadamente correlacionada com o sinal mecânico ($R^2 = 0.62 \pm 0.28$). Os resultados sugerem que a variação da velocidade de condução pode contribuir para explicar a fase final de aumento de força em contracções explosivas, através de uma relação multiplicativa entre as variáveis centrais e periféricas.

Palavras Chave

contracção explosiva – detecção de sinal – processamento estatístico – electromiografia de superfície de alta densidade – frequência de potenciais de acção – neurónios motores – velocidade de condução de fibras musculares

Contents

1 Motor Control: State of the Art and Open Questions **1**

1.1 An Overview of Motor Control . . . 2

1.1.1 Neural Control . . . 3

1.1.2 Size Principle . . . 4

1.1.3 Conduction Velocity . . . 5

1.1.4 Ballistic Contractions . . . 6

1.2 Objectives . . . 8

1.3 Experimental Considerations . . . 9

1.3.1 Onset Detection . . . 9

1.3.2 Isometric Dorsiflexion . . . 9

1.3.3 Electromyogram . . . 10

1.4 Thesis Outline . . . 12

1.5 Contributions . . . 12

2 Detection of Ballistic Action Onset **13**

2.1 Introduction . . . 14

2.1.1 State of the Art . . . 14

2.1.2 Motivation . . . 16

2.1.3 Objectives . . . 17

2.2 Methods . . . 18

2.2.1 Onset Detection Methods . . . 18

2.2.1.A Manual Detection . . . 18

2.2.1.B Noise Envelope . . . 18

2.2.1.C Statistical Processing . . . 20

2.2.1.D Simple Threshold . . . 24

2.2.2 Data Simulation . . . 24

2.2.2.A Fourier Series . . . 24

2.2.3 Experimental Data Acquisition . . . 25

2.2.3.A Preprocessing and Trial Validation . . . 25

2.2.4 Performance Analysis . . . 26

2.2.4.A Statistical Analysis . . . 26

2.3 Results . . . 26
2.3.1 Simulation . . . 26
2.3.1.A Low Noise . . . 28
2.3.1.B High Noise . . . 30
2.3.2 Experimental Results . . . 32
2.3.2.A Knee Extension . . . 32
2.3.2.B Elbow Flexion . . . 37
2.4 Discussion . . . 38
2.5 Conclusions . . . 40

3 An Insight into Central and Peripheral Control of Ballistic Contractions 41
3.1 Introduction . . . 42
3.1.1 State of the Art . . . 42
3.1.1.A Ballistic Contractions . . . 42
3.1.1.B Conduction Velocity . . . 44
3.1.2 Motivation . . . 45
3.2 Methods . . . 46
3.2.1 Motor Task . . . 46
3.2.2 Experimental Protocol . . . 46
3.2.3 Signal Processing . . . 47
3.2.4 Discharge Rate . . . 48
3.2.5 Short Term Synchronization . . . 49
3.2.6 Effective Muscle Fiber Signal Frequency . . . 49
3.2.7 Statistical Analysis . . . 50
3.3 Results . . . 50
3.3.1 Recruitment . . . 50
3.3.2 Discharge Rate . . . 51
3.3.3 Conduction Velocity . . . 51
3.3.4 Motor control and EMG . . . 54
3.4 Discussion . . . 54
3.4.1 Motor Unit Recruitment . . . 54
3.4.2 Rate Coding . . . 56
3.4.3 Conduction Velocity . . . 58
3.4.4 EMG Amplitude . . . 62
3.4.5 Motor Output . . . 62
3.5 Conclusions . . . 63

4 Final Conclusions and Further Development 65

Bibliography 69

List of Figures

2.1 Onset Distributions by Noise Level – Simulation 27
2.2 Onset Latency – Simulation 28
2.3 Onset Latency – Low Noise 28
2.4 Automatic vs. Manual Onset – Low Noise 29
2.5 Aligned Force – Simulation 29
2.6 Force measures – Low Noise 30
2.7 Onset Latency – High Noise 31
2.8 Automatic vs. Manual Onset – High Noise 31
2.9 Force measures – High Noise 32
2.10 Onset Distributions by Noise Level 33
2.11 Automatic vs. Manual Onset – Knee Extension 33
2.12 Force measures – Knee Extension 34
2.13 Automatic vs. Manual Onset – Linear Model 35
2.14 Aligned Force – Knee Extension 36
2.15 Force measures – Elbow Flexion 37
2.16 Aligned Force – Elbow Flexion 38

3.1 Double-Differential EMG – M-wave 47
3.2 EMG channel selection for CV determination 48
3.3 Motor Unit Spike Trains 51
3.4 Discharge Rate and Motor Output 52
3.5 Inter-Motor Unit DR Correlation Coefficients 53
3.6 Step-and-Hold Contraction: neural and peripheral control and motor output. 55
3.7 Ballistic Contraction: neural and peripheral control and motor output. 56

List of Tables

2.1 Onset latency with respect to manual detection. 35
2.2 Onset latency with respect to real onset. 35

3.1 Correlation between measures of neural activity and motor output. 53
3.2 Neural delays: EMD and FPP. 54
3.3 Correlation between sEMG features, bioelectrical factors and motor output. 56
3.4 Motor output and neural activity. 57

Abbreviations

AGLR Approximated Generalized Likelihood Ratio

AMU Active Motor Units

ANOVA Analysis of Variance

AP Action Potential

AR auto regressive

ASD Average Spike Density

ATP Adenosine Triphosphate

CNS Central Nervous System

CV Conduction Velocity

DR Discharge Rate

EEG Electroencephalogram

EMD Electro-mechanical Delay

EMG Electromyogram

FPP Firing to Performance Phase

MD Manual Detection

MEP Motor End Plate

ML Maximum Likelihood

MN Motor Neuron

MPF Median Power Frequency

MU Motor Unit

MVC Maximum Voluntary Contraction

NMJ Neuro-muscular Junction

NPD Negative Peak Detection

PNS Peripheral Nervous System

RFD Rate of Force Development

RMS Root Mean Square

ST Single Threshold

TA tibialis anterior

VRF Velocity Recovery Function

WF Whitening Filter

1

Motor Control: State of the Art and Open Questions

Contents

1.1 An Overview of Motor Control 2
1.2 Objectives 8
1.3 Experimental Considerations 9
1.4 Thesis Outline 12
1.5 Contributions 12

Understanding how the nervous system commands motor functions is a central issue in neurophysiology. Knowledge of the pathways that intervene in dexterous movement performance, from the brain down to the musculoskeletal system, has contributed to improve the diagnostic of neuromuscular pathologies and to formulate rehabilitation protocols. Clinical applications benefit from the non-invasive assessment of different levels of the nervous or muscle systems: upstream, the Electroencephalogram (EEG) can be used in stroke rehabilitation to induce neuroplasticity in the motor cortex, whereas downstream signals such as the Electromyogram (EMG) can be used in physiotherapy to reinforce contractions with biofeedback. In the sports industry, knowing how to adapt the physiological determinants of motor performance is useful to develop training methods.

Research on spinal signal decoding methods has direct impact on medical and human augmentation technologies, such as skilled control of prosthetic and orthotic devices. Correct interpretation of motor plans or intentions from neural and muscular signals (e.g. EEG and EMG) is the missing piece for successful implementation of man-machine interfaces that can provide manipulation or locomotion ability to people with motor limitations, such as stroke patients. The fact that adaptive signal-based mapping performs better than model-based mapping in control of direct robotic interfaces reveals the current limitations in the understanding of motor function. Moreover, recent studies on the neuromuscular system have raised doubts on already established concepts. For instance, the common distinction between Motor Unit (MU) types has been challenged by the finding that MU properties are often continuously distributed rather than clustered [1] or that the innervation number (i.e. number of muscle fibers innervated by a motor neuron) increases exponentially for progressively larger Motor Neurons (MNs), indicating that there is a continuum range of fiber properties that interpolates the features of the so called I, IIa and IIb types [2]. Also, it is now debated whether the traditional framework focusing on anatomical muscle structure should give way to a functional view based on muscle units. Such questions are relevant for the quest to unravel neural codes and peripheral determinants of movement performance. The current dissertation investigates how neural output and muscle physiology influence force development during ballistic contractions, on which only scarce reports have been published.

1.1 An Overview of Motor Control

Neural processing for motor control takes place throughout the Central Nervous System (CNS), with complex and varied neural codifications. The cortical area M1, in the frontal lobe, is a crucial center for conscious motor planning and initiation where, in general, the musculo-skeletal structures under voluntary control have a somatotopic representation, commonly know as the homunculus (i.e. relatively well defined areas of the cortex correspond to specific body parts). The size of the cortical area controlling a given limb is proportional to its motor precision (e.g. the hands have a greater cortical representation than the feet). However, these associations are not immutable, as individuals with amputations are able to reorganize their cortical connections, so that the areas from missing limbs acquire the ability to command other body parts. Moreover, outside the cortex, the cerebellum

stores pre-determined motor programs, providing fast feed-forward instructions and playing a central role in motor skill learning. Compared to the cortex, neural circuits in the cerebellum have a relatively simple organization, and some of its control mechanisms can be easily modelled. This feature has allowed studies with computational simulations to enrich the current comprehension of cerebellum activity.

Brain signals converge to the brain stem and travel down the CNS through the spinal chord, where they are directly integrated with sensory input in feedback control loops. The last point of neural signal convergence is the soma of MNs, in the spinal chord. In order for movements to be generated, the integration of inputs to MNs has to produce Action Potentials (APs) that travel down their axons, through the Peripheral Nervous System (PNS), leading to the release of neurotransmitters onto the Neuro-muscular Junctions (NMJs) (i.e. the synapses between a neuron and the corresponding muscle fibers or myocytes). Therefore, the set of action potential trains transmitted by the MNs is the final neural signal that determines muscle contraction and joint actuation.

Whilst the fibers composing a single muscle unit are typically dispersed throughout the muscle, there is a univocal (i.e. one to one) correspondence between each MN and a muscle unit – a finite collection of muscle fibers – which, together, comprise a Motor Unit (MU). In healthy individuals, a NMJ is extremely reliable, as APs in the MN axon invariably generate APs in all of the corresponding muscle fibers. The binary signal coming from the MN is converted into an equivalent signal of varying amplitude that propagates through the muscle fibers, where the contractile units – the sarcomeres – generate tension. It is currently accepted that the muscle unit translates its electro-chemical synaptic input into a mechanical output driven molecularly by the establishment of cross-bridges in the protein filaments of the sarcomeres. Each muscle unit can thus be seen as an amplifying element that filters a binary signal from a MN and behaves mechanically with a magnitude proportional to its frequency content. The muscle unit is the active functional component driving the musculo-skeletal system, composed of both viscoelastic and rigid elements (e.g. muscles, tendons, ligaments and bones) whose main function is to generate tension in a more or less controlled fashion.

The capacity to exert muscle tension is dependent on factors such as muscle length, speed of contraction, fatigue level and even interference between the activity of adjacent fibers. Macroscopically, contraction of the whole muscle tissue, in either a concentric, isometric or eccentric manner, produces torque around the joints. However, the torque at the joints is further dependent on the mechanical properties of the connective tissues of the system (e.g. tendons) and their anatomical position, as the moment arm varies throughout the range of movement [3]. Motor output thus reflects the overall muscle activity filtered by viscoelastic structures, including the muscle itself, and limited by anatomy.

1.1.1 Neural Control

The CNS regulates muscle contractions by varying the number of active units and the intensity (e.g. frequency) of the activation signal [4]. These mechanisms are commonly referred to as recruitment and rate coding, respectively, and are both steadily increased in gradually rising contractions. In such contractions, the upper limit of MU recruitment is about 80% of Maximum Voluntary Contrac-

tion (MVC), from which any additional tension generation is due to increased discharge rate. The neural drive from spinal neurons leads to muscle activation as the neurotransmitters (i.e. acetylcholine) released in the NMJ depolarize the sarcolemma, creating local currents that propagate through the muscle tissue. These currents can be detected with electrodes placed on the skin, over the contracted muscles, and the extracted interference signal is the so-called EMG. While EMG contains information on muscle activation and is widely used to infer the underlying neural mechanisms, the value of commonly extracted features (e.g. Root Mean Square (RMS), or spectral features) as measures of neural drive is currently under debate [4][5](see Section 1.3.3). Yet, state-of-the-art sensors and processing methods can now decode individual motor neuron spike trains (i.e. timing of action potentials) from high density EMG, and have introduced a new paradigm for accurate and non-invasive assessment of rate coding and recruitment strategies.

1.1.2 Size Principle

The size principle was initially formulated as the positive correspondence between the size of motor neurons and their rank of recruitment, and is a central concept for the understanding of movement control strategies [6]. In gradually increasing contractions, at a constant rate of force development, motor units are recruited at well defined force levels [7]. Motor neurons with smaller somas, and corresponding to smaller muscle units (i.e. smaller innervation numbers), start firing at lower force levels, whereas larger units are recruited towards higher force levels [1][6][7]. Thus, smaller motor units are said to have a lower recruitment threshold. The size principle has been complemented with the findings that additional functional, mechanical and anatomical features of muscle units, such as maximal twitch force or fiber diameter and composition, are also correlated with recruitment threshold [8]. Given that increased fiber diameter reduces cytoplasmic resistance and increases conduction velocity [9], it is unsurprising that muscle fiber Conduction Velocity (CV) is also correlated with the features of motor units and, consequently, with recruitment threshold [8][10][11].

Since action potentials generated at the motor neuron hillock are always propagated to the corresponding muscle fibers, the property of recruitment threshold has to be determined at the central level. The size principle reflects the correspondence between the central command structure (i.e. innate organization of motor strategies) and the properties of the peripheral conducting and actuating units (e.g. axon of the motor neuron and corresponding muscle units). Most of the early investigation on neural control strategies was based on small, and potentially non-random, populations of neurons (e.g. stimulation and recording with micro-needles [8]). Recently, the size principle was verified in large populations of motor units assessed with non-invasive methods, using hdEMG decomposition [1]. However, it is still not fully understood how this correspondence contributes toward motor function [12]. Moreover, while the size principle has been demonstrated in ramp contractions, it is not yet clear whether it applies to ballistic contractions.

1.1.3 Conduction Velocity

Once a spinal signal reaches the end of the PNS, the transmission of motor commands continues from the innervation zone through the length of muscle fibers [13], so that muscle units essentially behave as amplifiers of the nervous system commands [14]. Once an action potential reaches a motor plate, the maximal contribution of the fiber towards force production is delayed by the time to peak twitch contraction [15]. This time is intimately related to the composition of the fiber and its conduction velocity. Therefore, motor performance relies not only on proper integration of conscious commands with programmed circuits and sensory information in the CNS, but also on the quality of the amplification by the peripheral effectors.

Action potentials are propagated over the length of muscle fibers, along the sarcolemma and T - tubules, leading to the release of Calcium ions (Ca^+) from the sarcoplasmic reticullum into the cytosol or sarcoplasm, leading to the cycle of cross-bridge formation in the sarcomeres. As a result, there is a mechanical contraction of the muscle fiber, whose stimulated force profile is known as a muscle fiber twitch; a combination of voluntary fiber twitches drives the musculo-skeletal system. Skillful tension generation is thus dependent on the structure and biochemical state of muscle units (i.e. neural signal amplifiers) which determine their propagating and contractile capacity [16][17][18][19].

Muscle fiber Conduction Velocity (CV) is the speed of propagation of the electrochemical signal (i.e. action potentials) along the sarcolemma, from the end-plate towards the muscle fiber ends. CV is an important factor in motor precision and power output [16] and has clinical relevance in several diseases and conditions, including diabetes [20], fibromyalgia [21] and several types of myopathies [22][23][24]. In some conditions, the diagnostic yield of CV has been reported to overcome that of EMG [22]. Increased CV is associated with improved balance and performance of isometric and dynamic exercises. It is also relevant for peripheral control in power exercises, such as the leg press [16] or cycling sprints [19], and it is related with Adenosine Triphosphate (ATP) turnover and fiber type content [19].

Andreassen and Arendt-Nielsel [8] demonstrated the correlation between conduction velocity and strength of individual motor units in elicited contractions. Later on, the relationship between motor unit conduction velocity and recruitment threshold was confirmed to follow the size principle in voluntary contractions [1][10]. Likewise, CV is correlated with fiber type and cross sectional area, and can be used to estimate muscle fiber composition [1][11][16][25]. The relationship between myocyte structure and CV can be attributed to two main factors: cell diameter, which tends to be larger in type II fibers [9], leading to greater sarcoplasmic conductance and thus faster electro-chemical signal transmission along the fibers [16]; and the proportion and type of Na^+/K^+-ATPase pumps, which are more abundant and efficient in type II and whose activity increases membrane excitability[1] [18][28]. At the muscle unit scale, the size principle is also consistent with the higher impact of larger fibers on CV, since conduction is promoted by simultaneous activity of different fibers and larger motor units have larger innervation numbers [2].

[1] By increasing the K^+ gradient across the sarcolemma, its resting potential is lowered (i.e. hyperpolarization). Consequently, the AP area becomes smaller and the repolarization time is decreased [26][27].

Besides the intrinsic features of muscle units and fibers, CV is dependent on cellular conditions: it increases significantly with temperature [13][19] and decreases with H^+ accumulation (i.e. pH reduction) [17]. Temperature may impact CV by reducing the time constant of opening and closing of voltage-gated Na^+ channels [19] or by decreasing the extracellular concentration of K^+, leading to a lower resting potential and repolarization time [13], and consequently increasing CV. Both ATP turnover and CV are positively influenced by temperature, which may explain why CV and power output increase simultaneously in dynamic contractions [19]. On the other hand, pH reduction enhances the membrane permeability to K^+, whose concentration in the extracellular space is then increased, with the reverse effect on CV [29]. Simulation with computational neural models supports the role of K^+ channels in conduction velocity variation [30], while relating it to the discharge rate. CV decreases with blood restriction, due to metabolite build-up rather than lack of energetic substrate [31], and lactic acid is a possible agent for CV decrease during fatigue, in accordance with the lower CV with pH reduction [17]. However, not only H^+, but also Na^+ and K^+ gradients change with the onset of fatigue [32]

CV can be non-invasively estimated from the multi-channel EMG recordings. In pioneering neurological studies, muscle fiber conduction velocity of selectively stimulated units was determined from the time lag of potentials detected with two electrodes placed over the fiber [8]. The cross correlation method is widely used to estimate the average CV in voluntary contractions involving multiple muscle units [1][33][34]. Other methods proposed in the literature include the spectral dip method [35], time-frequency/scale representations [36], application-specific integrated circuits (ASIC) [37] or optical flow models [38].

1.1.4 Ballistic Contractions

The capacity to produce strong movements in a short time is crucial for safety, object manipulation and sports performance. For instance, moving powerfully in a restricted time (e.g. 50-250 ms) is required in sports such as martial arts and sprint running [39]. Explosive contractions (the terms explosive and ballistic shall be used interchangeably) consist in generating voluntary muscle tension with the highest Rate of Force Development (RFD) possible. The level of execution of voluntary ballistic isometric contractions is related to balance in the elderly [40] and with athletic skills (e.g. jumping) [41], and is attributed to increased neural drive [42]. In athletes, force development seems to be emphasized in the first 50 ms of contraction through increased firing rate, rather than different peripheral characteristics, when compared with control subjects [41].

Although scarce, the existing literature on neuro-physiological control of ballistic contractions describes a very distinct nature from paced contractions with a sustained RFD (i.e. the slope of the force-time curve) [15][39]. Whereas the size principle is verified in ramp contractions, in ballistic contractions (i.e. with unrestricted RFD) there is no sound evidence of such ordered recruitment [15]. Despite the idea that recruitment order could change in strong contractions [43], the supporting results might be misguiding, since spike detection/decoding methods may not yield a precise assignment of the first action potentials to the respective units (because the units activated in a ballistic contraction are re-

cruited within a few milliseconds, their APs may be highly superimposed). Nevertheless, Desmedt et al. [15] determined a more robust parameter to classify ballistic thresholds – considering the final levels of force for which a given motor neuron would be recruited in the initial discharge – and observed that it was well correlated with the corresponding recruitment threshold for ramp contractions.

In gradual contractions of the tibialis anterior (TA), motor units are progressively activated at thresholds up 8 kg [15]. Even when performed with high RFD, tracked contractions are marked by gradual increases in both recruitment and firing frequency. Neural coding of ballistic contractions is markedly different since recruitment occurs within a brief period of extremely high instantaneous discharge rate. Nevertheless, despite most MNs being excited even before motor output is detected, the motor neurons are still ranked in the sense that their participation in a ballistic contraction is strongly associated with peak force [15]. Indeed, activation of a given motor unit in a ballistic contraction depends on the estimated level of maximal force (e.g. a motor neuron will not fire in a ballistic contraction bellow a certain low force threshold, and will always fire above higher threshold[2]). Moreover, whilst in ramp contractions the discharge frequency of each MU increases progressively after activation onset, in ballistic contractions all units start firing at a high firing rate, ranging from 50 to 130 Hz, and followed by a decrease in frequency [44]. The maximal Discharge Rate (DR) is associated with maximal RFD, and can be improved with strength training, with possible adaptation mechanisms occurring both at the supra-spinal and motor neuron levels [44][45][46].

When comparing contractions with different maximal force levels, recruitment of additional motor units increases the target force, but only up to a certain point. In ballistic contractions, recruitment of the maximal number of active units seems to occur at lower peak forces than in ramp contractions with the same target force (e.g. 5 vs. 8 kg), from which further increments of peak force are obtained only by increasing frequency [15]. Experimental evidence of fundamental differences between neural strategies for explosive and gradual tasks confirms that the former are performed in a mostly pre-programmed manner, with most of the commands being generated before muscle sensory feedback can be processed. Feed-forward control of ballistic tasks involves fast recruitment of units that would be slowly recruited over a ramp contraction with a proportionally higher maximum force. Several factors may intervene in these contractions by modulating excitability in the spinal circuts. For instance, there is evidence of pre-synaptic inhibition of Ia-afferent neuron signals from the soleus (i.e. antagonist muscle) prior to ballistic dorsiflexion onset [47]. Upstream, brainstem activity affects MU excitability and thus the drive to muscles through the monoaminergic input; furthermore, the noradrenegic and serotonergic systems also interfere with motor performance [46].

While the neural signal underlying electrical muscle activity has been researched for decades, its investigation classically required either 1) invasive recodings that could potentially undersample or damage neural tissues; 2) simulations with models such as the one proposed by Fuglevand and Winter [48]; 3) inference from limited measures of EMG signal. Apart from the aforementioned studies, investigation on control of ballistic contractions has generally been limited to non-invasive studies that employ simple measures of sEMG amplitude in a low resolution time-scale, whose accuracy is

[2] Desmedt et al. [15] defined ballistic threshold as the force half way through these two limits and showed that it was proportional to recruitment threshold in gradual contractions

debatable (see Sections 1.3.3 and 3.1). Recent advances in signal processing have led to successful decomposition of high density multi-channel EMG recording, resulting in the accurate extraction of the individual firing times of populations of motor neurons [14][49]. With this technique, it is possible to thoroughly investigate how neural activity mediates muscle contractions non-invasively, and to sample larger and possibly more representative populations of motor units. In Chapter 3, state-of-the-art high density EMG decoding is used to investigate the neural strategies in ballistic contractions, and how they relate to both motor output and electrochemical changes within the muscle. However, full high density EMG decomposition requires custom hardware, a restricted experimental setting and computationally heavy processing. Since regular surface EMG is widely available and can be employed in both real-time and a greater range of conditions, it shall also be investigated to which extent the simple global variables obtained from this signal reflect the decoded neuro-muscular drive.

1.2 Objectives

The following dissertation presents methodological and physiological studies, addressing ongoing questions on neuromechanics and exercise physiology, and focusing particularly on ballistic contractions.

The first investigation compares algorithms for accurate detection of force onset in ballistic contractions. Its results support the adoption of automatic methods, by validating a practical and reliable alternative to the elementary processing methods endorsed by modern literature for force onset detection. Besides using experimental data acquired with two types of force transducers to test the algorithms, the author introduces a simulation method based on random harmonic generation to compare the accuracy of different methods at varied noise conditions.

The newly validated automatic detection is then employed in the second study, for an investigation of the neuromuscular mechanisms of force generation during short and powerful contractions, which are seldomly described in the literature. For the first time, state-of-the-art motor unit activity decoding – using high density EMG and blind convolutive separation – is used to study the neurophysiology of ballistic contractions and to describe how central (e.g. recruitment and discharge rate) and peripheral (e.g. conduction velocity) factors collectively contribute towards motor output. Finally, we investigate whether the amplitude of the interference EMG signal reflects the underlying neuromuscular changes. We show that, despite the recently reported limitations of conventional EMG, this practical signal acquisition modallity may be used to characterize neural and muscular performance during ballistic contractions.

Before presenting the research work, we introduce some experimental considerations that are relevant for the investigation and its applications.

1.3 Experimental Considerations

1.3.1 Onset Detection

The first 50 ms of rapid contractions are determinant for overall ballistic performance [46][50]. For instance, differences between motor output of athletes and untrained subjects seem to lay on the neural drive during this phase [41]. Given the high rates of increase of most variables of interest at the beginning of contraction (e.g. force/torque, motor unit recruitment, discharge rate), small differences in onset placement may lead to significant differences in the resulting measurements. Therefore, it is essential to detect the beginning of tension development as accurately as possible. However, the currently accepted gold standard for force detection is a manual method which, despite its simplicity, is tedious and time-consuming [46]. Whilst the automatic methods employed in the literature have been shown to lead to inaccurate results [51], such poor performance likely owes to the excessive simplicity of the algorithms. We start our work by investigating the possibility of using an automated method for detection, rather than the manual counterpart, without compromising accuracy. A thorough investigation of the performance of more complex automatic detection methods is the topic of Chapter 2.

1.3.2 Isometric Dorsiflexion

One of the greatest challenges in biomechanics is solving the redundancy of the muscle system actuating anatomical joints. For that reason, when estimating muscle tension from external force or trajectory measurements, it is convenient to do so in movements with one degree of freedom and with a small number of intervening muscles for a given action. Single joint movements allow body positions to be easily replicated and properly compared [46]. Additionally, when using EMG arrays, it is important to place the electrode grid in the direction of the muscle fibers for accurate CV calculation and MU activity decoding. Therefore, the TA, a monoarticular muscle with parallel fibers, which is mostly responsible for dorsiflexion, is one of the preferred muscles for such studies. Other muscles with parallel fibers, such as the first dorsal interosseus or the brachioradialis, are also commonly observed in the literature.

Motor output can be measured from the force exerted on external sensors and/or the changes in joint position. For instance, the magnitude of elicited twitch contractions of stimulated TA fibers can be inferred from external measurement of the torque around the ankle [8]. Indeed, the force applied to a fixed sensor during a voluntary contraction is a common measure of motor output, rendering a simple framework for experimental protocols where subjects aim at a goal aided by visual or auditory cues. However, such non-invasive measures of force production are unavoidably influenced by factors other than mechanical muscle fiber tension.

The capacity to produce force varies with muscle length and contraction velocity; also, the moment arm of the muscles generating torque around a joint typically changes throughout the range of movement, and so do the relative contributions of different muscles. When studying neuromuscular control, the influence of passive musculo-skeletal properties contributing for motor output, such as

the viscoelactic elements of muscle and tendon and the stiffness of the actuated body part, should be controlled or, ideally, minimized. To minimize their confounding effect, the measure of motor output evaluated in our neuro-physiological investigation (see Chapter 3) is the force produced in isometric dorsiflexion. Isometric contractions ensure a constant moment arm (i.e. torque is linearly proportional to force applied on sensor), stiffness, fiber muscle length and null velocity of fiber shortening. Due to these experimental advantages, measures of motor performance (such as RFD [39][46]) are typically measured in isometric conditions. Moreover, the accuracy of hdEMG decoding and CV estimation is improved by minimizing the relative displacement between the approximated filters (in the muscle fiber membranes) and the sensors (Section 1.3.3).

1.3.3 Electromyogram

Over the last decades, understanding of the bioelectrical properties of contractile tissue allowed the recording and processing of EMG, to become a useful technique in clinical practice (e.g. for diagnostic or physiotherapy). The relationships between muscle electrical activity and motor output or adaptation (e.g. joint torque, fatigue, hypertrophy) have been extensively described.

EMG changes in a relatively predictable way with different neural strategies, typically increasing monotonically with recruitment and discharge rate [48]. In dynamic loaded multijoint movements, ballistic contractions generate higher rectified EMG amplitude than slow controlled contractions with the same load. In isoinertial contractions, EMG amplitude has been found to vary with load, movement speed and acceleration [52][53], whereas the effects on Median Power Frequency (MPF) are not clear. There is also a strong relationship between joint angle and EMG activity [39][54], in line with the aforementioned complexity of the changes in muscle activation, and thus control mechanisms, throughout the range of movement in dynamic contractions.

Sakamoto and Sinclair [52] found no changes in MPF in different conditions, whereas Jakobsen et al. [53] found significant reduction of MPF in ballistic contractions, and Linnamo et al. [55] found significant increase in ballistic contractions. MPF reduction can be caused by lower conduction velocity, which is commonly observed during fatigue or, conversely, by synchronization of fiber excitation, in which case MPF can be accompanied by an increase in RMS [56]. In gradual contractions, as force increases, newly recruited units have higher innervation numbers and thus may increase overall synchrony [53]. On the other hand, synchronization of different motor units might increase EMG amplitude without a corresponding increase in force, but with a concurrent reduction of force steadiness [56]. This increase in amplitude, however, is not proportional to recruitment, given the exponential distribution of innervation numbers across the motor unit pool [4]. Furthermore, neural drive can be globally estimated as the spike density (i.e. the number of action potentials per time unit); it has been shown that the relationship between spike density and number of active motor units, or the number of active muscle fibers, becomes progressively less linear in fatiguing contractions [57].

Whilst computational models can replicate experimental recordings to some extent [57] and are widely used to study EMG properties and estimate physiological phenomena [48][57][58], the algebraic sum of action potentials observed in simulated signals [58] does not necessarily translate into

real signals. Therefore, the relationship between global (e.g. time and frequency domain) features of surface EMG and the underlying neural drive is not as straightforward as it is often assumed in the literature [4][5][59]. Estimates of muscle activity – and hence neural drive – from EMG, can be confounded by several factors. More concretely, amplitude cancellation can induce up to 63% loss of signal [60]; amplitude and, especially, spectral features have been shown to be poorly correlated with neural strategies [5].

Although EMG is extensively used in research and therapeutic applications to extrapolate the neural activity during specific motor tasks, the aforementioned non-linearities have recently raised speculation on the informative value of global features of the EMG [4][5][61]. Although high density EMG decomposition yields a more accurate estimate of neural drive, this technique requires a strict experimental set-up and additional instrumentation and computational costs. Therefore, the more elementary EMG amplitude analysis is available for a much greater range of experimental conditions, and can be easily employed in dynamic contractions. It is thus important to compare the performance of both types of analyses in order to reassert the feasibility of sEMG global variables to extract the underlying neural changes and accurately predict adaptations (e.g. muscle hypertrophy) or diagnose pathologies [5][62]. In Chapter 3, the relationship between surface EMG and the neural determinants of ballistic contraction is examined through the course of contractions.

hdEMG Decomposition

The interference Electromyogram (EMG), detected with surface electrodes, results from the combination of action potentials travelling across the length of muscle fibers. The weighting of multiple fiber currents depends on the relative location of the fibers with respect to the electrodes, the properties of the volume conductor (e.g. adipose and cutaneous tissues) and properties of the fibers themselves. As an action potential travels down the muscle fibers, the time-dependent local depolarization at each longitudinal point of the sarcolemma can be seen as the impulse response to the motor neuron signal [49]. For every recording point (i.e. electrode), the muscle fibers can thus be approximated by finite impulse response filters, and the multichannel EMG signals are related to the spinal output through a convolutive relationship (in other words, the EMG signals reflect combinations of filtered MN AP trains). Given the finite duration of the impulse responses, it is possible to decompose the recordings into linear instantaneous mixtures. Algorithms developed for speech processing are extensively employed in bio-electrical signal decomposition. For instance, Independent Component Analysis (ICA) is commonly used to separate neural sources from EEG [63]. However, the activities of the different motor neurons contributing towards surface EMG recordings are correlated and clearly not independent, and deeming ICA inappropriate in this case. Recently, another decomposition approach was applied in solving the EMG convolutive mixture by selecting the most scattered sources, taking advantage of the sporadicity of MN discharges at the analyzed time scale. Negro et al. [64] introduced Convolutive Blind Source Separation (BSS), using a sparseness optimization criterion for convergence of component separation to accurately extract the binary signal of individual motor units from hdEMG. In the current work, we employ the BSS algorithm to extract complete AP trains from different motor units.

1.4 Thesis Outline

Having introduced ballistic contractions as a relevant framework for performance and injury risk assessment, the following chapters present my independent research in two parts, following the natural course of the investigation. Each of the subsequent chapters is self-contained and undertakes a different scientific problem. Yet, the conclusions drawn in Chapter 2 are crucial to validate the methods adopted in Chapter 3.

Chapter 2 addresses technical issues related to the measurement of motor output in fast contractions, focusing on the current debate on onset detection; it includes a methodological study of detection strategies, and challenges the prevailing gold standard.

Chapter 3 covers the central investigation of this project, exploring the temporal progression of motor control variables, the relationships between neural and muscular states, potential neurophysiological mechanisms, and the resulting motor output during ballistic contractions. The experimental set-up and protocol are also presented in Chapter 3.

In each of the following segments, the respective investigation is motivated and contextualized within the relevant literature; the computational and statistical methods employed are detailed, and referenced when appropriate; the results and their implications are discussed, along with possible limitations and suggested improvements.

Chapter 4 summarizes the dissertation, highlighting the most critical results and limitations, and clarifying its applications and contributions.

1.5 Contributions

Two papers are being finalized from the research here presented and will be submitted for publication shortly. These extended abstracts are provided along with this dissertation.

The methodological investigation of Chapter 2 includes a novel simulation model and a thorough evaluation of several automatic methods for force onset detection in different experimental and simulated conditions; the results demonstrate that the proposed automatic methods perform at least as well as the current gold standard.

The neurophysiological study of Chapter 3 employs state-of-the-art hdEMG processing in the study of explosive contractions, and addresses several literature gaps on both ballistic neural control and conduction velocity. It provides a characterization of the evolution of motor unit recruitment, discharge rate and conduction velocity over the course of fast and powerful contractions, and an original analysis of their relationships and impact on motor output. Furthermore, the results provide evidence of the accuracy of the signal decomposition with respect to the reference invasive assessment of motor neurons.

2

Detection of Ballistic Action Onset

Contents

2.1 Introduction 14
2.2 Methods 18
2.3 Results 26
2.4 Discussion 38
2.5 Conclusions 40

2.1 Introduction

Several measures of motor performance, such as absolute force, rate of force development and electro-mechanical delay, can be obtained directly or indirectly from force transducers. Unbiased measurement of these variables depends on the precise detection of the instant of force onset, especially in the case of ballistic contractions. The present literature claims that the gold standard for detection of sudden force signals is a manual method requiring time consuming visual analysis. This methodological study introduces a new automatic and robust framework for detection of ballistic contraction onsets. We start by implementing an algorithm to replicate the manual gold standard technique, and then take advantage of fast computational tools for statistical analysis and signal filtering to further improve the original method. Finally, we test the performance of statistical processing on force transducer signals, employing a whitening filter and likelihood ratio tests, which have been proved to outperform manual detection in kinematic signals.

2.1.1 State of the Art

Force production during the first 50 ms of a ballistic contraction reflects the ability to perform balanced motor tasks and powerful athletic movements. RFD has been found to vary with athletic capacity [41] and to increase after strength training [45], but its accurate measure is dependent on proper force onset detection. Likewise, evaluation of intrinsic delays in the neuromuscular system, such as reaction time and neuro-motor delay [41] – which can be affected in pathological states, such as Parkinson's disease [65][66] – is highly sensitive to correct onset determination. Electro-mechanical Delay (EMD) estimates the time-difference between the arrival of the electric signal to the actuator (i.e. muscle) and the onset of motor output, and is a function of the electrochemical events occurring within the fibers and the viscoelastic properties of the muscle and tendon. Therefore, improper choice of detection method may lead to systematic errors on neuro-mechanical parameters [51].

The current gold standard for force onset estimation in ballistic contractions is the manual detection method (MD) proposed by Tillin et al. [41], which employs a set of well-defined procedures to determine the onset based on the signal's deviation from noise amplitude levels. When correctly performed, this method yields consistent onset estimations, and has thus been adopted in numerous protocols throughout the literature [46]. Recently, Tillin et al. [67] refuted claims that a threshold-based method would outperform MD, for these assertions were based on improper signal processing and detection methods [68].

Tillin's manual approach takes advantage of the human cognitive capacity to recognize different scales and infer relevant patterns [67]. Although this would in principle be a rather subjective approach, the MD robust protocol minimizes arbitrary choices. The spread of MD results from different investigators has been analyzed to demonstrate the method's consistency leading to onset errors with an order of magnitude of only 1 ms across several subjects and detection sessions [67].

Comparison of several methods for onset detection in kinematic signals revealed a bias introduced by the use of single threshold (ST) methods and their poor performance when compared to MD [69].

Later on, this bias was extensively analyzed in force signals [51]; not surprisingly, while performing better than absolute force thresholds (e.g. 4 N), relative-thresholds (e.g. computed with respect to a subject feature such as MVC) were still found to perform worse than MD. Thresholds based on the standard deviation of the signal offer a more adaptive solution, but the literature uses conservative thresholds (e.g. 3 standard deviations [42][54]) which inevitably compromises the accuracy of results.

Given that the signals meet the quality requirements for MD, the protocol uses the raw signal exclusively, and therefore there is no need to design proper digital filters. The input signal is thus free from any distortions introduced by pre-processing that could lead to a lag in the onset, and the onset is estimated as the last local minimum before deflecting above baseline-noise levels. Indeed, for the purpose of onset detection in a high-resolution time scale, processing signals corrupted by high levels of noise or particular frequencies (e.g. 50 Hz) is not a trivial task, as it may shift the onset of the rising phase and remove the frequency components (e.g. local peaks) on which the manual detection relies [46][67]. Indiscriminate use of filtering techniques has led to delusive reports in the literature. Indeed, the aforementioned allegation that a single-threshold outperformed manual detection was based on a protocol that included arbitrary pre-processing, in which the force signal was filtered with an excessively wide non-causal moving-average prior to detection [68]. Besides not accounting for the lag in the filtered signal due to non-causality, the resulting signal was not suitable for the standard manual detection, and thus acquired a systematic bias favouring the absolute-threshold method [67].

Manual detection, however, is time-consuming and compromises analysis of large data-sets[69]. Also, studies claiming its superiority often compare it against simple thresholds that are excessively high and necessarily compromise accuracy, even in fast contractions, such as 5% MVC or three standard deviations (e.g. much greater than 2 standard deviations of the noise) [51]. Tillin et al. [67] do not thoroughly acknowledge the existing literature on more powerful automatic detection methods with respect to manual detection [69]. Furthermore, the accuracy of manual detection relies on stringent criteria for signal quality, whereas signals with sufficiently high SNR cannot currently be obtained with commercially available instrumentation [67]. Indeed, published reports on accuracy of the manual method are based on signals obtained with custom-made strain gauges with low noise levels [70]. For signals with higher noise levels, the authors vaguely mention an alternative detection method that has performed well on unpublished data [67]. Hereafter, force transducers available in neuro-muscular research and diagnostic facilities may not yield the signal quality required for the manual method accuracy attributed to Manual Detection (MD). Concurrently, higher noise amplitude also requires higher thresholds for detection, which further worsens performance of single-threshold methods.

Wyatt [71] detects onset of rapid kinematic movements (e.g. eye saccades) from the third order derivative of the position with respect to time, commonly designated jerk. Jerk provided better estimates than either position or first and second derivatives. However, such methods still require the use of a single threshold, which can bias the results [72]. Soda et al. [73] tested a range of automatic methods on force signals, applying derived quantities such as the RFD (i.e. the first derivative of the force profile). Since high variability of these signals compromises the establishment of proper thresholds, the applicability the automatic methods was not generalized. Although the study proposed a

classifier to determine the best method to adopt in each detection, this is not a robust solution, due to the potential introduction of inconsistencies by employing different methods for different signals. Ultimately, the study did not show improved accuracy/consistency of the automatic methods with respect to the gold standard MD.

Finally, a method proposed by Staude [69], employing a whitening filter and the Approximated Generalized Likelihood Ratio (AGLR) for onset estimation, has been shown to yield rigorous detection in kinematic signals and to outperform manual detection[1]. To our knowledge, there are no published data on detection of force onset using this method. This method employs statistical modelling of the signal, combining an adaptive whitening filter with template matching to distinguish between noise and a signal of interest as drivers of a biomechanical model. The whitening filter eliminates the effects of the biomechanical system on the final output, so that the resulting signal is composed of stochastic noise, plus an eventual generating signal (i.e. muscle tension). When the latter is present, convolution of the whitened signal with an appropriate inverted template can reflect its location. Whilst the model templates for noise and signal are predetermined by the user, the whitening filter coefficients are obtained from the real signals, in an adaptation phase that occurs early during the noise period. Decision relies on computation of the log-likelihood ratio, to infer the odds of a given portion of the signal being generated by the force model, rather than the noise model. This is a more refined approach to detection than the gold standard, where "adaptation" to the signal consists in simply detecting the limits of noise and prior knowledge on the behaviour of underlying signal sources is not taken into account. Despite this method having shown promising results with respect to MD, it has not been adopted in ballistic force research, possibly due to its technical complexity.

2.1.2 Motivation

The literature proposes a manual detection method MD as the gold standard for accurate onset detection. Yet, there seem to be insufficient published reports on this methodology in two fronts: first, to our knowledge the gold standard method has not been computerized despite its simplicity; and second, the gold standard has not been compared to sturdy automatic methods, even though other published methods have produced precise detection in signals akin to ballistic force. Indeed, up to date, most of the proposed alternatives did not go beyond threshold methods, and it is not surprising that they could not achieve the precision of manual detection. The present investigation addresses these gaps by introducing an automatic implementation of the gold standard method, and comparing its performance against the original and widely adopted manual version; it also proposes further adaptations to the original method, to improve performance without compromising computational complexity. Finally, Staude's AGLR method, which has been shown to outperform manual detection of kinematic signal onsets, is also included in the investigation [69].

[1] It is worth noting that Tillin et al. [67] acknowledge Staude's investigation [69], yet they do so to improperly suggest that it supports the use of their manual method.

Automatic Implementation of the Gold Standard Detection Method

Manual detection involves observing the signal in two well-defined force vs. time scales. In the first scale, which includes the initial rising phase of the signal, the observer identifies the noise envelope (e.g. maximal amplitude of baseline noise) and selects the threshold as the last local minimum before deflection away from the baseline (i.e. before signal crosses the upper baseline limit for the last time). The location of the onset is then confirmed in the second time scale. Whilst involving very low-level cognition, this process is time consuming and constitutes a handicap in studies on neuromuscular control of explosive contractions. In order to take full advantage of advanced technologies, such as hdEMG decomposition (see Chapter 3), and to analyze high amounts of data, the methods for force onset detection should be not only accurate, but also automatic.

The current study was prompted by the conjecture that the demand for manual implementation of the reference detection method might be excessive, since the required steps involve nearly no subjectivity and can be easily implemented in an efficient algorithm. Firstly, the signal portion used in detection is well defined in both the time and force dimensions by the specified scale of 5 N by 250 ms, and therefore automatic selection of the analysis window should be consistent with the manual one. The only potentially subjective step is the selection of the last moment of the noise period. However, given the ballistic nature of the force, the rising phase occurs in a very short time period at the scale of manual detection, and the signal portion within the observation window should not exceed a few dozens of milliseconds. We can thus employ a conservative criterion for automatic selection of the noise-portion; considering its stochastic nature and the large size of the window, a difference of the order of milliseconds should have no significant impact on the resulting noise envelope, which simply consists in the global force *extrema* (i.e. *maximum* and *minimum*) within the noise period. The moment of deflection from baseline is then objectively defined as the point at which the signal ultimately crosses the noise envelope. Finally, the estimated onset is simply the last local minimum before the moment of deflection. Given the considerations above, there seems to be no hindrance to the automatic implementation of the gold standard method, which motivates the present study.

2.1.3 Objectives

The null hypothesis, which this study intends to support, is that automatic methods can perform as well as, or better than, the gold standard. The alternative hypothesis represents the gold standard claim, i.e. that MD is more accurate than automatic detection. In order *not* to reject the null hypothesis, there shall be no significant difference between accuracy of MD and automatic methods, measured from the onset timings and dependant measures (Force and RFD).

To ensure the robustness of the proposed methods, they are applied to different types of signals: 1) simulated signals with different noise levels; 2) signals obtained with custom force transducers, with minimal noise levels; 3) signals obtained with commercial dynamometers, with higher noise amplitude.

2.2 Methods

2.2.1 Onset Detection Methods

The following detection methods were implemented in a custom MatLab program to analyze ballistic force signals. The processing pipeline included a user-friendly interface to assist in Tillin's manual detection method [70], and an adapted AGLR algorithm.

2.2.1.A Manual Detection

The manual method consists in observing a section of the force transducer recording with a consistent and appropriate scale (e.g. 5 N by 250 ms) such that the initial rising phase is included [41] [51] [67].

From that window the observer selects the maximum and minimum amplitudes of noise, which forms the baseline envelope, and identifies the onset as the last local minimum (i.e. negative peak) occurring within the envelope (i.e. before the signal definitely deflects away from the baseline noise envelope). Then, at a smaller scale, the user confirms the proper location of the selected peak.

2.2.1.B Noise Envelope

In the manual method, the user selects the noise-containing region from which the envelope is determined intuitively, which requires observation of the initial rising phase of the signal. Automatic bounds to the noise portion can be established by detecting the rising phase with a threshold (e.g. a high threshold corresponding to the magnitude of the larger force scale in the manual method) at an alarm time t_a, and then selecting a 200 ms long segment that terminates with a conservative lag (e.g. 50 ms) *before* the alarm time for each event. In a single trial:

$$t_a = \min\{t : F(t) \geq 2\sigma_N\} \tag{2.1}$$

Where F is the measured signal, t is the discrete time, σ_N is the standard deviation of the noise segment N, which is given by:

$$\begin{gathered} N = F(t_a - a_N + 1), F(t_a - a_N + 2), ..., F(t_a - a_N + b_N) \\ a_N = \lfloor 0.25 f_{samp} \rfloor, \;\; b_N = \lfloor 0.20 f_{samp} \rfloor \end{gathered} \tag{2.2}$$

where N_- and N_+ are the global force extrema in the noise interval. The previous selection rules result in a detection scheme with the scale specified by the gold standard (Section 2.2.1.A) [70]. The noise envelope E is determined as:

$$E = \{N_-, N_+\} = \{\min(N), \max(N)\} \tag{2.3}$$

The onset t_{on} corresponds to the last local minimum before crossing the upper envelope limit for the last time at t_D:

$$\begin{aligned} t_{on} &= \max\{t : F(t) < F(t+1) \wedge F(t) < F(t-1) \wedge F(t) < N_+\} = \\ &= \max\{t : F(t) < F(t+1) \wedge F(t) < F(t-1), t < t_D\} \end{aligned} \tag{2.4}$$

where the time of deflection t_D is approximated in discrete time as:

$$t_D = max\{t : F(t) > N_+ \wedge F(t-1) < N_+\} \tag{2.5}$$

From that, implementation of the previous detection rules to find t_{on} is trivial.

In summary, the algorithm for last Negative Peak Detection (NPD) is equivalent to the following strategy: a forward search to detect the moment t_a when the absolute value crosses an "alarm" threshold; selection of analysis window up to the alarm time (i.e. ensuring a "consistent" scale [67]) and, within the latter, the noise section. Determination of a new – and, in principle, stricter – threshold N_+ from noise features. The last time the signal crosses N_+ occurs by t_D. Finally, from t_D, a backward search for the nearest negative peaks finds the onset t_{on}. NPD replicates the gold standard (see Section 2.2.1.A). Its only potential drawback is the lack of robustness against instabilities in the first 100 ms of the analysis window, since signals with instabilities in the later phase are discarded in the gold standard criteria. In Section 2.3, we shall confirm whether this leads to statistical difference. Two alternative versions of this method are introduced, to improve performance: NPD-SD computes the noise envelope from standard deviation, and NPD-MA smoothes the signal lightly prior to detection.

From the preliminary analysis for this study, it appeared that the force envelope was exceedingly conservative, leading to overestimation of the perceived onset with both MD and NPD. A simple solution to this issue is to determine the noise envelope from statistical moments of the noise signal rather than its global maxima:

$$E_\sigma = \{N_{-,\sigma}, N_{+,\sigma}\} = \{\bar{N} - \sigma_N, \bar{N} + \sigma_N\} \tag{2.6}$$

and substitute N_- and N_+ by $N_{-,\sigma}$ and $N_{+,\sigma}$, respectively, in Equation 2.4 for the method NPD-SD.

Finally, NPD-MA is inspired on the literature suggesting to tackle signals corrupted by high amplitude noise with a digital filter and detect the onset at the point then the first derivative of the filtered force ultimately crosses zero [67]. Although the design of a proper zero-phase filter is beyond the scope of this study, given the fast-rising nature of the signal, it is reasonable to assume that, with some sort of light filtering, the last negative peaks prior to deflection could be closer to the actual onset (as long as the filter does not completely eliminate the peaks between the onset and deflection). Hence, NPD-MA smoothes the signal with an un-weighted causal moving average (after determining the noise envelope):

$$F_i^{MA} = \frac{1}{L} \sum_{n=i-L+1}^{i} F(n) \tag{2.7}$$

where L is the size of the running window. The onset is determined by substituting F by F^{MA} in Equation 2.4. It follows from the causality of the filter that NPD-MA does not incur the fallacy of Thompson et al. [68][67]. NPD-MA does not underestimate the onset by generating a negative phase, since only samples taken at $t \leq n$ are used to determine $F^{MA}(n)$. The running average covers a window of less than 4 ms (i.e. $L = 8$ samples, with $f_{samp} = 2048$ Hz), reducing the impact of the high amplitude peaks that may reduce accuracy of manual detection. By using a short window, NPD-MA avoids both over-filtering and inducing a pronounced lag toward later time values. In order to avoid

confounding the effects of changing the noise envelope and smoothing the signal, whenever applying NPD-MA the original MD noise envelope (i.e. N_+) is used.

2.2.1.C Statistical Processing

Staude's algorithm achieves accurate detection by relying on a biomechanical statistical model; it employs both whitening and matched filters, and estimates the onset based of statistical hypothesis testing. Although originally developed for kinematic signals, the current work intends to show that it also yields precise results in ballistic force signals, since these may be modelled as a random process. The following explanation is based on a particular implementation that was developed by the author from a script provided by Staude. A more abstract description of the general method may be found in Staude's paper [69].

The biomechanical system included in the signal model is described as an autoregressive filter H_{BM}, whose input and output are corrupted by noise (e.g. non-modelled biological phenomena, instrumentation noise, etc.). The input to the system is a stochastic process x_k, reflecting the sum of the activity of neuro-muscular elements (e.g. muscle unit contractions) at each point in discrete time k. The expected value of x_k, $m(k)$, may vary in time and is modelled depending on the underlying state, which can either be resting or active. Ultimately, we are interested in finding the moment when the active state replaces the rest state as the input of the biomechanical system. In other words, the force onset occurs when the generating process goes from the rest model to the active model. The idea behind the use of a Whitening Filter (WF) is that accurate detection of the transition time should be based on x_k, which can be obtained by processing the measured output y_k (e.g. discrete force transducer signal).

The Gaussian generating process x_k is described as:

$$x_k = m(k) + \omega_k, \;\; \omega_k \sim \mathcal{N}(0,\, Q) \tag{2.8}$$

where Q is the constant variance of the zero-mean white noise signal ω_k. For simplicity, the rest state is assumed to have constant zero mean, so that $m_R(k) = 0$. The active state can be modelled as any reasonable discrete sequence, preferably with positive difference (i.e. $m(k+1) - m(k) > 0$) as the total actuating units should be sequentially activated at the onset. Indeed, while there is no strong evidence that the size principle holds in ballistic contractions, motor unit recruitment is still expected to have some level of progression at the beginning of contraction (see Chapter 3). For instance, the active dynamic mean $m_A(k)$ can be modelled as a ramp signal, such as the following finite template with unit slope:

$$m_A(k) = \begin{cases} \frac{k}{L_T}, & 0 \leq k < L_T \\ 0, & o.w. \end{cases} \tag{2.9}$$

where L_T is the maximum size of the template and $m_A(0)$ occurs at the onset, and $m_A(k) = 0, \;\; 0 \leq k < L_T$. The onset is the transition time t_{on} such that:

$$x_k = \begin{cases} \omega_k, & k < t_{on} \\ m_A(k - t_{on}) + \omega_k, & k \geq t_{on} \end{cases}, \;\; \omega_k \sim \mathcal{N}(0,\, Q) \tag{2.10}$$

Having defined appropriate templates, and knowing that a matched filter allows optimal detection in the presence of white noise, it follows x_k contains all the relevant information for detection. However, in order to employ a template matching approach, the filtering effect of the joint system H_{BM} must be removed from the raw signal y_k.

Each anatomical joint is a unique system influenced by active and passive elements with viscoelastic properties, intertwined both in series and in parallel (see Chapter 1). Since our prior knowledge, $m(k)$, pertains to the input signal x_k (i.e. the shape of the mean generating process or template), it accounts only for the overall recruitment as a function of time, which is related to the total muscle contractile response. However, there are several other factors determining the ultimate torque generated at the joint and, consequently, the measured force (see Chapter 1). Those factors include muscle and tendon viscoelasticity, the relative engagement of agonist and antagonist muscles, the restrictions on range of movement placed by ligaments, the joint itself and the action of stabilizing muscles. All these factors are dynamic in time: they depend of the joint configuration and are inherently time-dependent due to viscosity. As a consequence of this complex architecture, the force signal measured experimentally, y_k, can be interpreted as a filtered version of the generating signal, x_k.

Rather than individually characterizing the above mentioned factors (e.g. modelling the stiffness of the system), the system H_{BM} is represented by an auto regressive (AR) filter H_{BM} that can be automatically adapted on a trial-by-trial basis. The filter is defined as:

$$H_{BM} = \frac{b_0}{A(z)} = \frac{b_0}{1 + a_1^{-1} + a_2^{-2} + ... + a_p^{-p}} \tag{2.11}$$

where b_0 is the gain of the system, a_n are the AR coefficients, p is the order of the filter and z is the complex frequency. In the discrete time domain, the system output is related to the generating signal x_k by [69]:

$$\tilde{y}_k = b_0 x_k - \sum_{i=1}^{p} a_i \tilde{y}_{k-1} \tag{2.12}$$

and the measured signal is given by:

$$y_k = \tilde{y}_k + v_k, \;\; v_k \sim \mathcal{N}(0,\, R) \tag{2.13}$$

where R is the constant variance of the zero-mean white noise signal v_k from the measurement device.

As the name suggests, the output of a WF is a white noise sequence with variance σ^2 and dynamic mean $\mu(k)$:

$$w_k * h_W \sim \mathcal{N}(\mu(k), \sigma^2) \tag{2.14}$$

with w_k being and arbitrary signal in discrete time and h_W is the impulse response of H_W. We want to determine a WF H_W that ideally reverses the previous operation so that:

$$y_k * h_W = b_0 x_k \tag{2.15}$$

When applied to y_k, H_W yields a scaled version of the generating signal, which can be used as the input to the matched filter and decision rule. In the limiting case where $R = 0$ (i.e. the noise

from experimental devices is negligible), the WF is the inverse of the AR part of $H_B M$ (i.e. $H_W = b_0 H_B M^{-1}$) and is thus given by [69]:

$$H_W(z) = 1 + a_1^{-1} + a_2^{-2} + ... + a_p^{-p} \tag{2.16}$$

where p and $a_1, ..., a_p$ are the order and AR coefficients of $H_B M$, respectively (see Equation 2.11). Note that H_W corresponds to the frequency response of a weighted running average, with a p sample long window and weights a_n.

An AR model is fitted to every new trial, from an adaptation interval consisting of a small period of rest where the generating signal is known to be $x_k = m_R(k) + \omega_k$. The covariance method is used to minimize the error in the coefficients in the least squares sense. Given the assumption of zero mean m_R in the rest signal, the adaptation interval consists in (scaled) noise filtered by an AR filter. From this interval, the autocorrelation matrix and autocorrelation vector are determined as:

$$R_{xx}(i,j) = \frac{\sum_{n=p+1}^{N} x_{n-i} x_{n-j}}{N-p} \tag{2.17}$$

$$r_{xx}(i) = \frac{\sum_{n=p+1}^{N} x_{n-i} x_n}{N-p} \tag{2.18}$$

where p is the order of the AR model and N is the length of the adaptation period. The coefficients are estimated by approximating the following expression:

$$a = [a_1, ..., a_p]^T = -R_{xx}^{-1} \times r_{xx}^T \tag{2.19}$$

for which the least squares solution can be obtained, for instance, with a MatLab solver.

Once the AR coefficients are determined, the filter H_W is applied to the remaining signal to recover x_k. Subsequently, onset detection *per se* is implemented on x_k. Detection is based on evaluation of the binary statistical hypothesis of the generating random process having dynamic mean m_A (alternative hypothesis H_A) against it having mean m_R (null hypothesis H_0). The algorithm AGLR divides detection in two phases to reduce the computational burden of the method. Recall that, in the presence of a resting phase (i.e. constant mean process) the variability of the WF output is merely the result of white noise. However, in the active phase, the whitened signal will have an additional rising component that cannot be explained by a constant mean Gaussian process alone. As mentioned before, if the profile of the signal of interest can be supposed *a priori*, then a matched filter is an optimal method to maximize the SNR in the presence of white noise. In practice, the first phase of detection with the log-likelihood ratio approach described by Staude can be depicted as applying a threshold to the output of a matched filter.

Although the shape of the active process m_A can be estimated, there is no prior knowledge on the exact magnitude and length of the initial rising force (the first 50 ms of ballistic contractions are extremely variable [46]), which is required for maximal precision. This limitation is initially overcome by using a template of fixed-length to *roughly* locate the onset. For that, the whitened signal is convolved

with an inverse template with predefined size L_{MF}, allowing a fast search for a matching segment in the signal[2]:

$$h_k = m_A^{MF}(L_{MF} - k) \tag{2.20}$$

$$y_k = \sum_{n=-\infty}^{\infty} h_{k-n}x_n = \sum_{n=-\infty}^{\infty} h_n x_{k-n} = \sum_{n=0}^{L_{MF}-1} h_n x_{k-n} \tag{2.21}$$

where h_k is the impulse response of MF and m_A^{MF} is obtained from Equation 2.10 with L_T replaced by $L_{MF} \approx 15\,\mathrm{ms}$. This result can be related to the log-likelihood ratio of the statistical hypotheses between two generating processes. The assumption of white noise reduces the log-likelihood estimation to a linear combination of the normalized correlations of the x_k with the templates m_A and m_0, scaled by their variance σ^2 (active and resting processes are assumed to have equal variance) [69]. Adding the assumption of null mean noise m_0, the measure of likelihood is condensed into the scaled output from the matched filter in Equation 2.21.

When a predefined threshold for the matched filter h is crossed, at time t_a, the algorithm assumes having found the signal of interest and moves to the second detection part, where the processing required for accurate detection is only performed locally. This phase considers a sub-sequence of x_k, x_k^W, corresponding to a signal window starting at $L_T \approx 100ms$ before t_a and ending less than $10ms$ after t_a. Note that L_T is also the maximum size of the template and that $L_T >> L_{MF}$. Therefore, convolving x_k^W and maximum template m_A yields the correlation of the signal with successively smaller sub-templates through the window (e.g. since both sequences have similar length, their overlap varies as the template slides over the window)[3]. Apart from a different normalization step[4], the likelihood function within the window is computed as before, and the onset t_{on} is defined as the point k at which the log-likelihood ratio is the greatest. t_{on} maximizes likelihood of the generating random process having active dynamic mean m_A starting at t_{on} against it being at rest.

The method's parameters were adapted when appropriate. In particular, different window sizes for adaptation were tested in a preliminary study: while in some cases the algorithm would yield successful detection with an adaptation size of 500 noise samples (i.e. about 250 ms, the size of the observation window in the gold standard method), in general, a larger noise portion was required. The default adaptation phase was set to half a second, which consistently ensured correct detection. In cases where the noise segment is less than the default value, our algorithm still attempts detection with the available data and is prompted to automatically select a smaller window, based on the location of the rising phase. L_{MF} and the h were set to 25. The deadzones and AR model order were kept at the default values [69].

[2]Note that this search can be implemented online.

[3]If the user defines multiple templates besides the default, which is always used for the matched filter, the algorithm performs the described convolution for every template. Several different templates were tested, with no noticeable difference relative to the ramp template, and thus chose to use only the ramp in order to reduce the number of potential confounding factors.

[4]Since the generating signal is now correlated to templates of different sizes, normalization of the MF output does not correspond to homogeneous scaling.

2.2.1.D Simple Threshold

The last detection method is an adaptive threshold based on each subject's MVC:

$$t_{on} = \min\{t : F(t) > 0.01 \times \text{MVC}\} \tag{2.22}$$

This method is hereafter referred to as the Simple Threshold. Recall that, according to the literature, ST is expected to perform poorly with respect to the manual method. It is nonetheless included in this study to assess the consistency of our findings with previously published results.

2.2.2 Data Simulation

Simulations and detections were implemented in MatLab 2016b.

2.2.2.A Fourier Series

The general ballistic force model is obtained from a Fourier series in the form:

$$f(t) = \sum_{n=0}^{N} a_n \cos(nwt) + \sum_{n=1}^{N} b_n \sin(nwt), \tag{2.23}$$

In particular, an eight term series is adopted:

$$f(t) = a_0 + a_1\cos(wt) + b_1\sin(wt) + a_2\cos(2wt) + b_2\sin(2wt) + ... + a_8\cos(8wt) + b_8\sin(8wt) \tag{2.24}$$

The series yields force values as a function of discrete time corresponding to a sampling frequency of $2048\,\text{Hz}$ (e.g. a typical sampling frequency for signals of this nature) so that, for any subsequent variable transformations (e.g. discrete into continuous time), the simulated data is processed as the experimental data.

The use of a relatively high number of coefficients allows replication of a physiological shape, whilst providing more degrees of freedom in the random coefficient generation. The ranges of coefficients a_n and b_n and fundamental frequency w were determined by fitting the model to experimental data obtained from isometric ballistic contractions of the tibialis anterior, the main muscle responsible for dorsiflexion (see Section 2.2.3). From the regression, the 95% confidence intervals for the coefficients in the fitted model were obtained. The simulation employs the confidence intervals for the coefficients (rather than for estimated forces, which would take into account the noise) because noise is added to the signal in a separate phase.

Analysis of the coefficient ranges reveals that the baseline a_0 and the fundamental frequency (i.e. first harmonic) terms a_1 and b_1 have the greatest magnitude, such that $a_0 \approx -a_1, -b_1 \gg \gg |a_2|, ..., |a_8|, |b_2|, ..., |b_8|$. Therefore, the sum of the most important sinusoidal components rises to its maximum in a period of T_{nat}, which can be estimated from the expected value of the fundamental frequency $\bar{w}$ as,

$$T_{nat} = \frac{2\pi}{\bar{w} f_{samp}} = 0.93\,\text{s}, \quad \bar{w} = 0.0033 \tag{2.25}$$

As expected, T_{nat} is less than one second, but still larger than the typical rising time in real ballistic contractions. The rising time of the full time-series is reduced when the remaining terms are added,

leading to a plateau phase as seen in experimental signals. The average upper limit of the series bandwidth is

$$f_H = \frac{8}{T_{nat}} = 8.6\,\mathrm{Hz} \tag{2.26}$$

In each simulated trial, the coefficients are randomly chosen from the corresponding ranges and the resulting curve is computed. The real force onset is determined as the theoretical minimum of the curve within the first period. To remove the ordinate off-set, the force value at the real onset is subtracted from the signal; the sub-sequence preceding the real onset is then substituted by an array of zeros.

Finally, white noise is added at two different levels, to simulate signals acquired with both custom and commercial sensors. Different sets of trials are generated for the two noise conditions. The lower noise level corresponds to the same standard deviation as the noise in the knee extension data (obtained with custom transducers), leading to a visually identical pattern of transition between noise and ballistic signal. The higher noise level simulates the use of a commercially available force transducer, having the same standard deviation as the dorsiflexion data. 50 trials were simulated for each of the noise levels (each discarded simulation trial was repeated until a valid one was obtained, yielding 50 valid trials).

2.2.3 Experimental Data Acquisition

Twelve subjects performed ballistic contractions to 80% MVC. The experimental set-up for dorsiflexion force is detailed in Section 3.2.2. The dorsiflexion trials were used to obtain the parameters of the simulation. The knee extension results were obtained with an equivalent set-up, with the knee flexed to about 60°; a strain gauge loading cell was attached to the shin surface, frontally to the distal end of the tibia of the dominant side. Elbow flexion force was measured with a commercial isokinetic dynamometer, with a considerably higher level of baseline noise. A considerable part of the elbow flexion data was widely corrupted by pretension and countermovements and thus could not be assessed with statistical significance.

2.2.3.A Preprocessing and Trial Validation

Stretching muscle right before explosive contraction generates elastic tension and may interfere with antagonist activation. Preforming any kind of tension prior to the explosive contraction may also change the dynamics of contraction and thus confound the results. It is thus advised to ensure that ballistic contractions start from rest [44][46][74]. Trials with counter-movements or pretension were therefore discarded, according to the trial selection criteria for manual detection[5]: discarding trials in which overall variations in noise exceed 0.5 N in amplitude within the last 100 ms before the perceived

[5] In a side study, I evaluated the robustness of an automatic trial selection method based on a parameter obtained from the AGLR algorithm – the scaling factor of the template – and employing a double threshold criterion (e.g. using the parameter h, with a marginal increase in computational costs). The performance of a such method was highly dependent on the data set and on the AGLR parameters. Although it is not employed in the present study, the AGLR-based selection detects instabilities, pretension and counter-movements with relatively good accuracy; thus, with further adjustments, this trial validation method may have potential to enable a fully automatic and real time framework for ballistic force onset. It is also noted that manual analysis of raw signals corrupted by the 50 Hz line signal leads to a noticeable systematic bias, which in general does not occur with AGLR.

onset. Ideally, the signal should be minimally processed, to avoid removal of the low amplitude and high frequency peaks on which the manual method relies [67]. The only processing method that was applied prior to detection is the 8 sample running average on the automatic method NPD-MA; the input to the remaining methods was the raw signal corrected for the gravitational force and converted to Newton.

2.2.4 Performance Analysis

The automatic methods NPD, NPD-SD, NPD-MA, AGLR and ST were compared against the gold standard MD. After selecting the onsets with the methods above in both simulated and experimental data, the force f was measured at every 50 ms after each onset (e.g. detected with each method) up to 150 ms and RFD was determined as $\Delta f/\Delta t$ in the corresponding 50 ms intervals. In simulated trials with known real onset, automatic methods and MD were also compared against the real onset. The measures compared in the statistical analysis were time of onset, force at 50 ms after onset, and mean RFD in the first 50 ms after onset.

2.2.4.A Statistical Analysis

The effects of detection methods on onset placement and force measures at 50 ms were tested for significance with two-way Analysis of Variance (ANOVA) and corrected with the Tukey's honest significant difference criterion *post hoc* test. In the simulation study, the reference was the real onset; the factors considered in the ANOVA were methods and noise levels. In the experimental study, the reference was the MD onset (i.e. the gold standard) and the factors tested for statistical significance were methods and subjects. Significance was accepted for $p < 0.05$. For the largest experimental data-set, the isometric knee extension, a linear model was fitted to AGLR onsets against MD onsets.

2.3 Results

2.3.1 Simulation

The onset difference relative to MD is shown for the NPD, NPD-SD, NPD-MA and AGLR methods in Figure 2.1, for each of the noise levels applied in the simulated isometric dorsiflexions. A positive difference means that automatic algorithms placed the onset later than user, and vice-versa. The markers are proportional to the number of events with a given onset difference value. The large proportion of zero-difference NPD detections (in orange) show that NPD coincided exactly with MD onset in the majority of detections. NPD-SD, NPD-MA and AGLR anticipated MD detection in all but two outlying cases.

Between the two noise levels it is observed that: the relationship between MD and NPD is unaltered with the change of noise level; NPD-SD and NPD-MA have the same range of distances with respect to the manual method, but with different distributions; different noise levels lead to a markedly different range of AGLR detections *with respect to MD* onset.

Figure 2.2 shows the distribution of the pooled simulation data, this time showing the difference with respect to the real onset (see Sections 2.3.1.A and 2.3.1.B for independent analyses of the different noise cases). The histograms for manual detection and automatic detection onset latencies are in agreement with the distributions in Figure 2.1: they reveal a dual distribution for MD and all NPD methods, while AGLR has a single distribution with markedly smaller variance.

Latency of MD and all NPD methods seems to be dependent on noise level, with the difference in onset being shifted toward later values in the presence of higher noise. MD and NPD are distributed identically and NPD-SD and NPD-MA follow the trend of MD, although with a less delay. AGLR is more robust against higher noise levels, with a consistent (e.g. single distribution with small variance) relationship with real onset. Most importantly, in no circumstance does any of the methods anticipate (e.g. underestimate) the real onset (i.e. all the onset difference values are positive). Therefore, methods that anticipate the onset with respect to MD (e.g. NPD-SD, NPD-MA and AGLR) always result in greater accuracy.

ANOVA confirmed that the factor noise level led to significant differences in onset placement and all measures of force (force, force normalized to MVC, RFD and normalized RFD). The factor detection methods led to differences ($p << 0.01$) in onset placement and force (normalized and absolute) but not in RFD. Multiple comparisons were made for onset and force: all methods led to significant difference from the real values; AGLR was significantly different (i.e. more accurate) than all other methods; there was no difference between NPD-MA and NPD-SD or between MD and NPD; ST was significantly higher than all other methods.

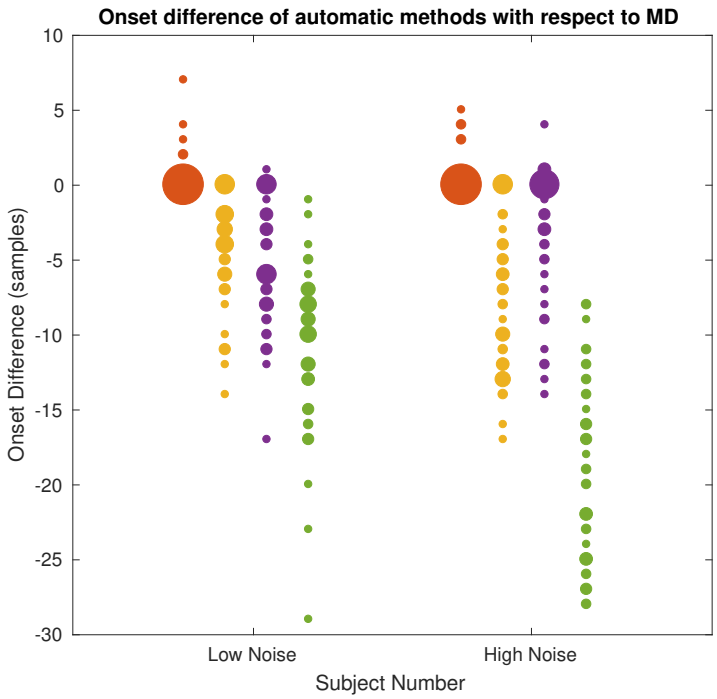

Figure 2.1: Distribution of differences between automatically and manually detected onsets, in number of samples, by subject, in simulated trials with two different noise levels. Negative values correspond to anticipation relative to MD. Legend: orange – NPD; yellow – NPD-SD; purple – NPD-MA; green – AGLR. Markers proportional to number of events.

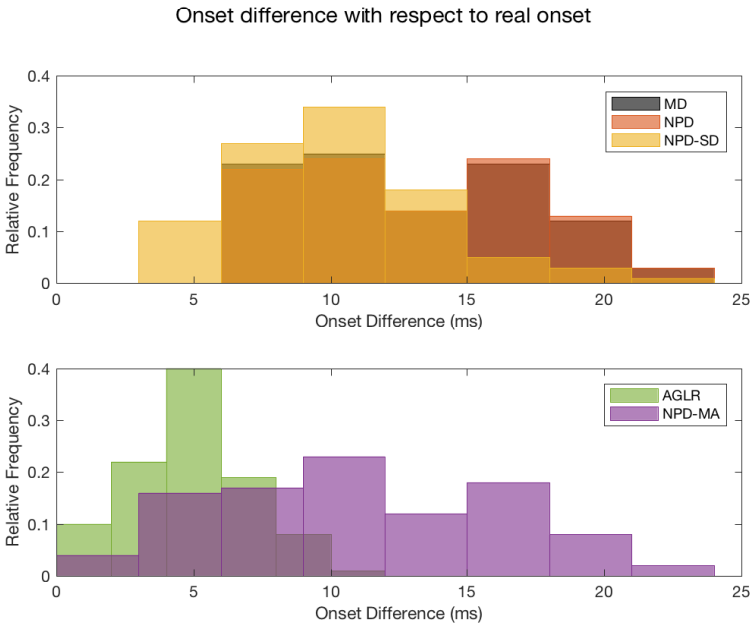

Figure 2.2: Distribution of differences between detected and real onsets, in milliseconds.

2.3.1.A Low Noise

Figures 2.3 and 2.4 show the differences in onset detection of automatic methods with respect to real onset and manual detection, respectively. Figure 2.3 reveals that MD and NPD are nearly identically distributed, while NPD-SD, NPD-MA and AGLR are more skewed towards the real onset. AGLR has the lowest mean, variance and range, denoting more consistency and accuracy.

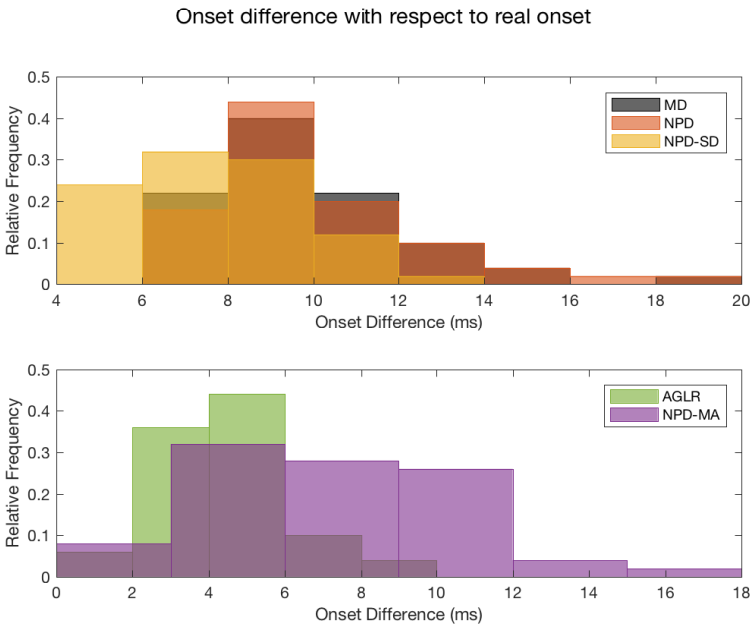

Figure 2.3: Distribution of differences between detected and real onsets in simulations with low noise level, in milliseconds.

Figure 2.4 shows that about 90% of the NPD detections coincide with MD, supporting the validity

of the automatic version of the gold standard. The standard deviation of the difference between MD and NPD was 0.6 ms (or 1.25 samples) in the lower noise data set. NPD-SD and NPD-MA onsets are within -8 ms before and 2 ms after the gold standard detections. AGLR detects the onset up to 16 ms before MD (without underestimating the onset as revealed by Figure 2.3).

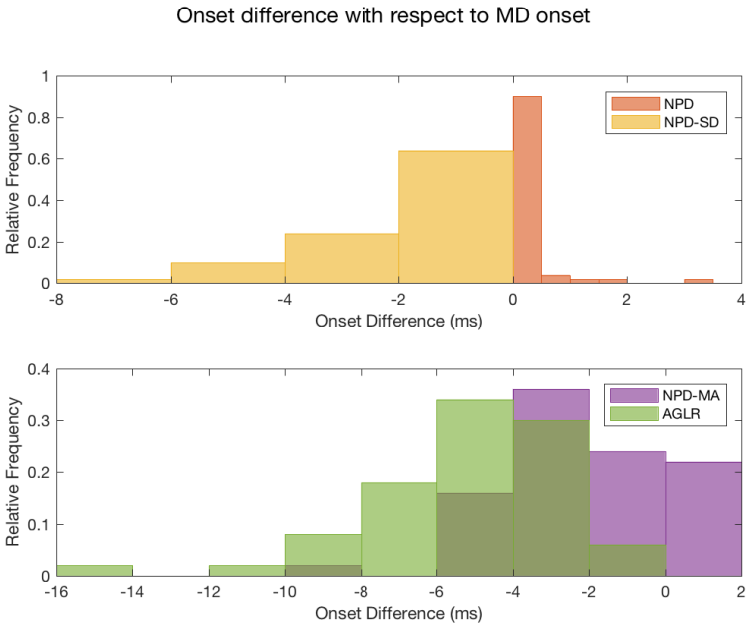

Figure 2.4: Distribution of differences between automatic and manual onsets in low noise simulations, in milliseconds.

Figure 2.5 shows all the simulated trials aligned in the discrete time axis according to the onset estimated with AGLR. The dark markers identify the manually detected onset. Observation with the naked eye confirms that the manual method detects the onset with visible delay, while the AGLR method is very accurate with respect to intuitive human detection. It also confirms that MD is more consistent and accurate in low noise conditions (Figure 2.5a) than in high noise conditions (Figure 2.5b).

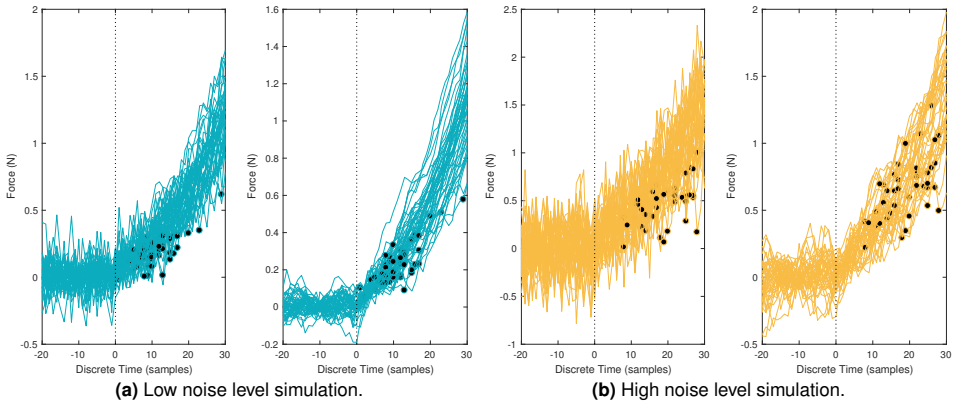

(a) Low noise level simulation. **(b)** High noise level simulation.

Figure 2.5: Initial phase of force production, aligned in the discrete time axis according to the AGLR estimated onset (at zero), in a) low noise and b) high noise simulations. The left hand side of each sub-figure shows the raw forces; on the right hand side the force has been smoothed with a 4 backward sample moving average, to enhance the signal of interest. The dark markers identify manually detected onsets.

Figures 2.6a-2.6d show the measured force features in absolute units and normalized to MVC, averaged over all trials. AGLR yielded the closest measures to the real values consistently, while ST introduced a strong bias as expected.

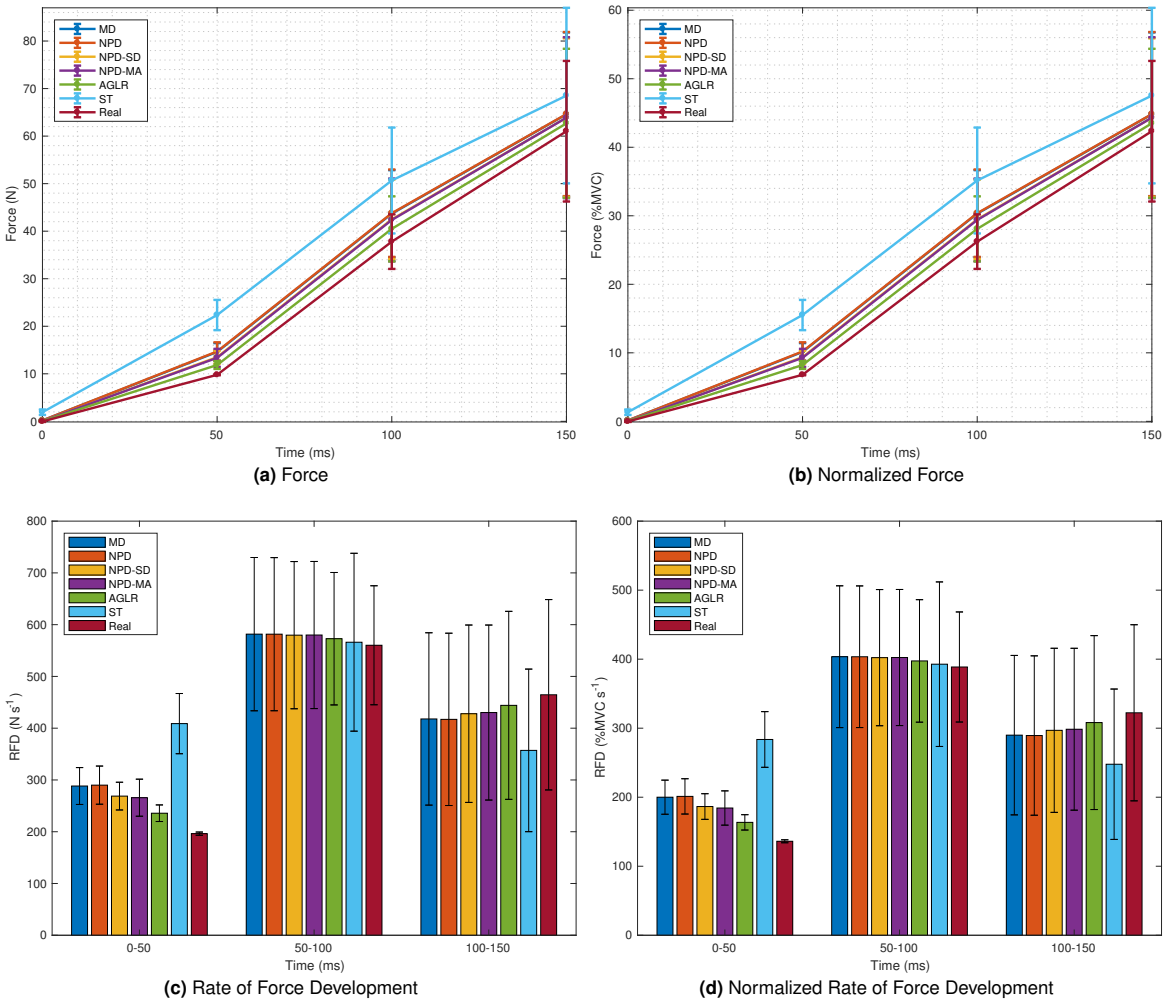

(a) Force **(b)** Normalized Force

(c) Rate of Force Development **(d)** Normalized Rate of Force Development

Figure 2.6: Force and Rate of Force Development after real and estimated explosive force onsets in simulated isometric dorsiflexions with low noise levels. Onsets estimated with manual (MD) and automatic methods (NPD, NPD-SD, NPD-MA, AGLR and ST). Average over all trials.

2.3.1.B High Noise

In the case of high noise, detection latency has a somewhat wider variance, but keeps the same trends as with low noise (Figure 2.7). With respect to the onset of MD, NPD-SD and AGLR are always more accurate, and NPD-MA is consistently identical or more accurate (Figure 2.8).

As in the low noise condition, about 90% of the NPD detections match the MD detections. The cases where they differ are due to visual artifacts in the signal plots for visual detection. In the second, closer scale used to confirm the onset placement in MD, it is often not visibly perceptible whether a peak is under or above the threshold. In such cases, where a peak is ambiguously touching the threshold line, a human observer may adequately assume that the unclear peak is above the line and select the previous peak as the onset. On the other hand, the automatic version will consider the latter peak as the onset. This incoherence is exacerbated by the finite precision of the plotting tools at

the scale required by the MD method. Those cases lead to the small difference between the manual and automated GS methods.

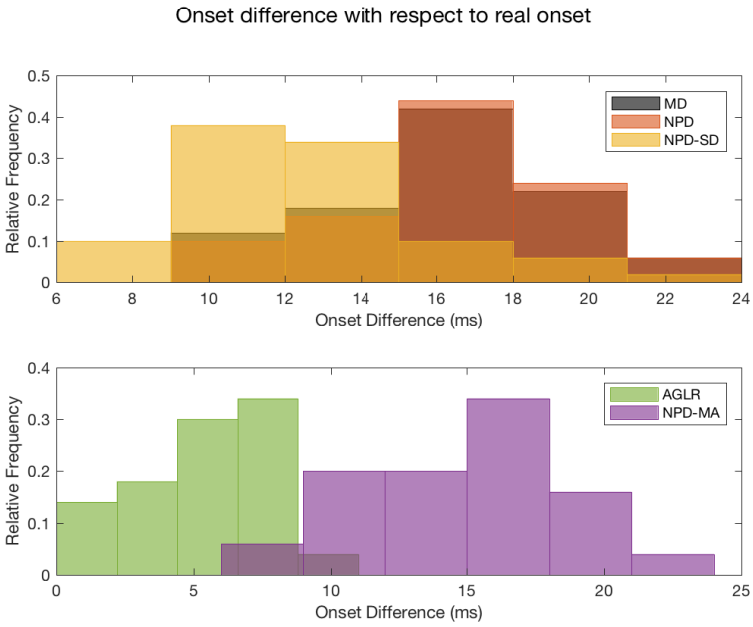

Figure 2.7: Distribution of differences between detected and real onsets in simulations with high noise level, in milliseconds.

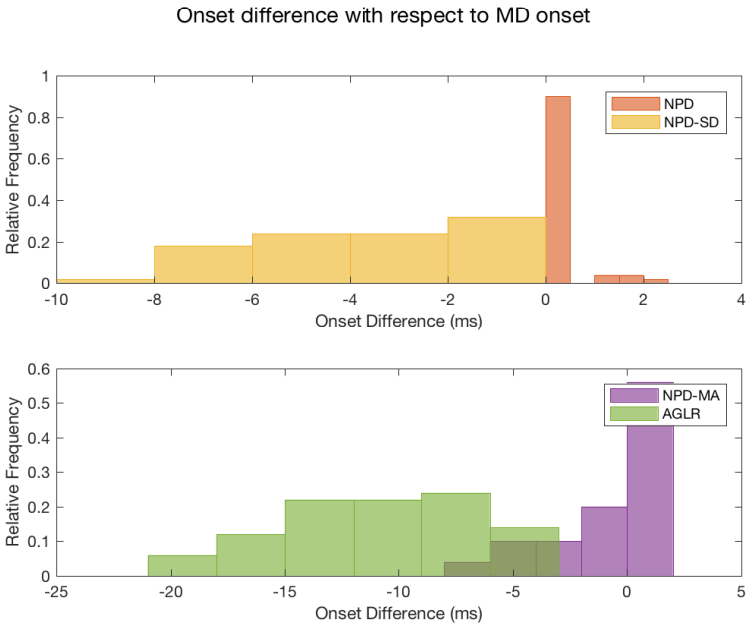

Figure 2.8: Distribution of differences between automatic and manual onsets in high noise simulations, in milliseconds.

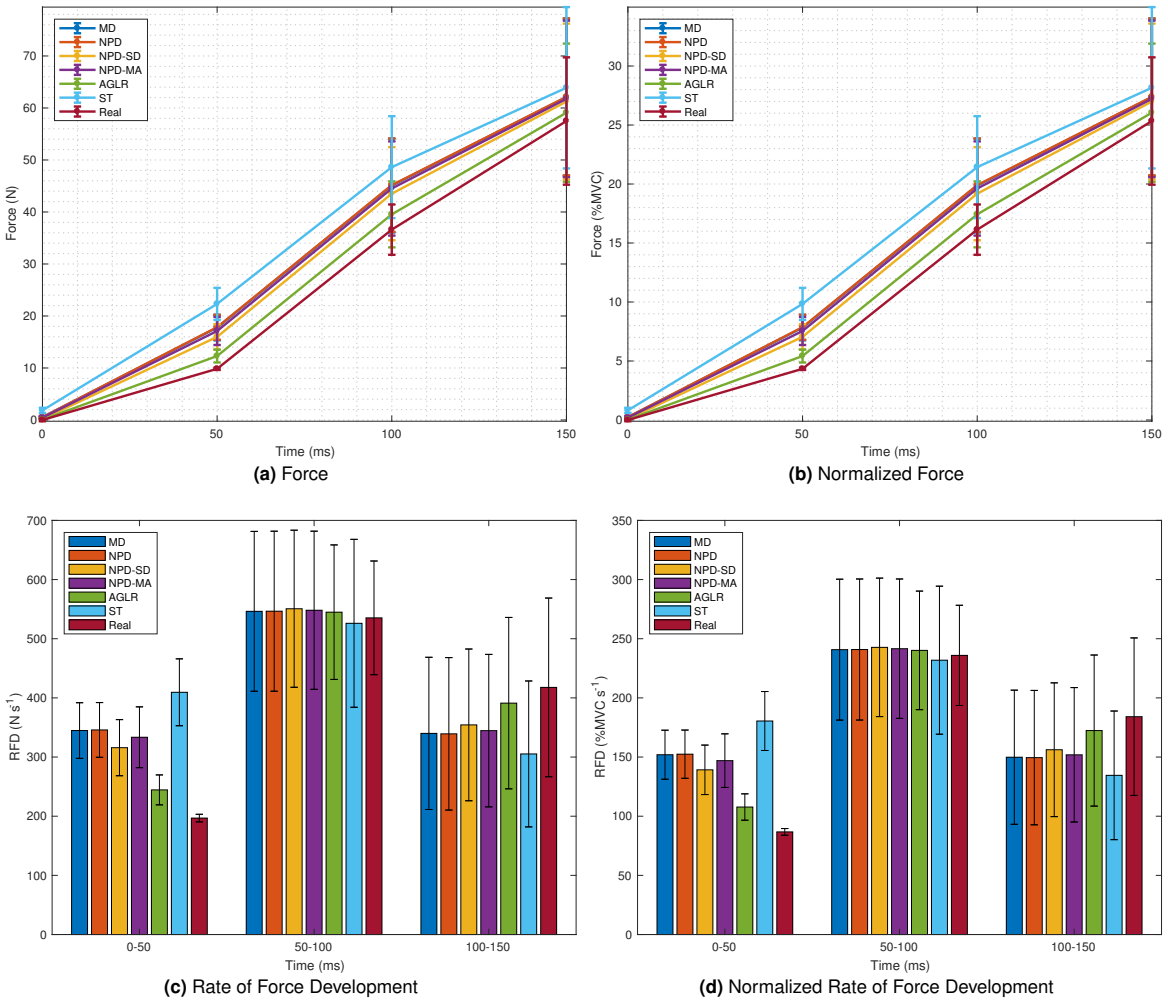

(a) Force **(b)** Normalized Force

(c) Rate of Force Development **(d)** Normalized Rate of Force Development

Figure 2.9: Force and Rate of Force Development after real and measured explosive force onsets in simulated isometric dorsiflexions with high noise levels, determined with manual and automatic methods. Average over all trials.

2.3.2 Experimental Results

Voluntary force and RFD are presented in absolute and normalized (i.e. %MVC) values.

2.3.2.A Knee Extension

The onset difference relative to MD is shown for the NPD, NPD-SD, NPD-MA and AGLR methods in Figure 2.10, for each of the subjects performing isometric knee extension. As observed in simulated data, the majority of NPD detections (in orange) coincides exactly with the MD onset, and NPD-SD, NPD-MA and AGLR tended to anticipate MD detection. Since the distributions were similar for all subjects, the results were pooled and represented in histograms in Figure 2.11, which show the distribution of onset differences in milliseconds.

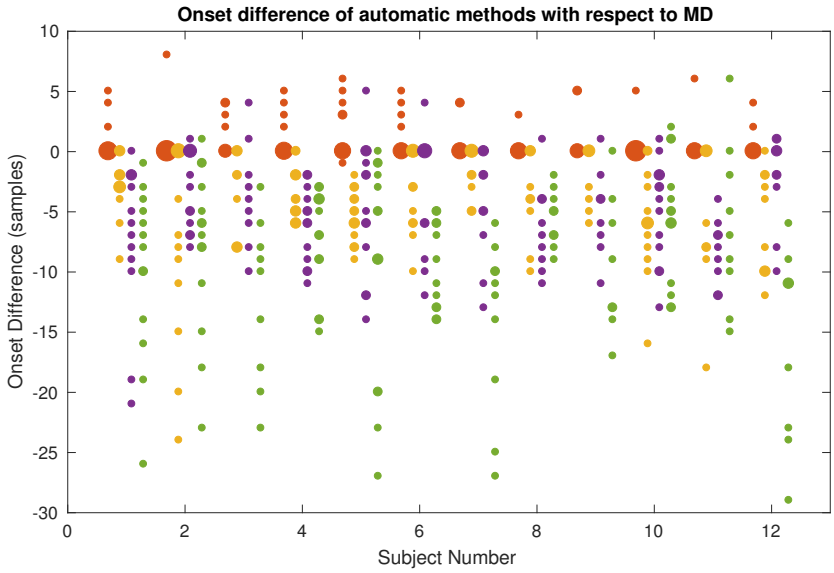

Figure 2.10: Distribution of differences between onsets estimated with automatic methods and MD, in number of samples, by subject. Negative values correspond to anticipation relative to MD. Legend: orange – NPD; yellow – NPD-SD; purple – NPD-MA; green – AGLR. Markers proportional to number of events.

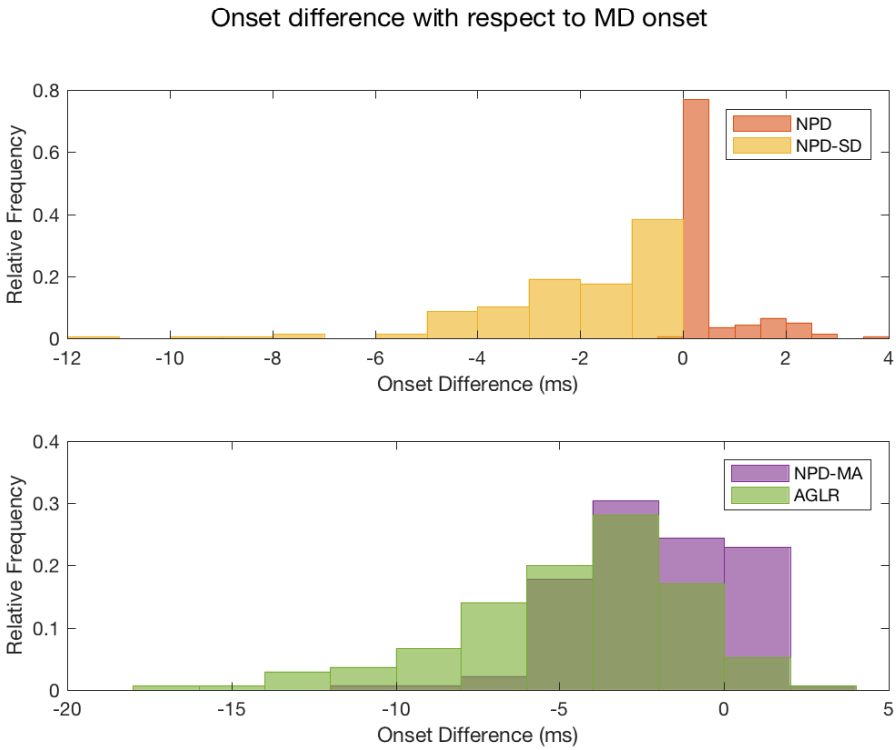

Figure 2.11: Distribution of differences between automatic and manual onsets in isometric knee extension, in milliseconds. Negative values correspond to anticipation relative to MD.

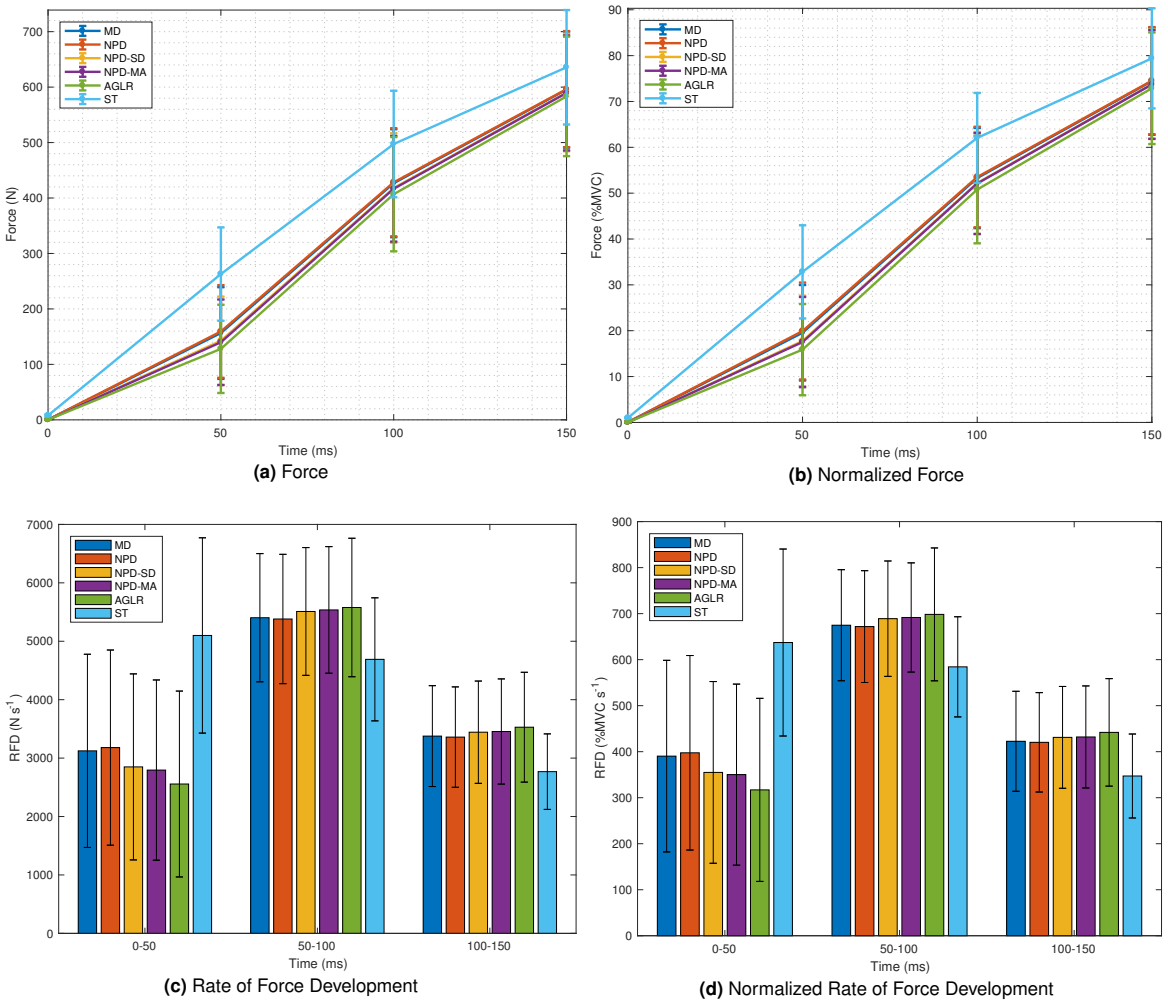

(a) Force **(b)** Normalized Force

(c) Rate of Force Development **(d)** Normalized Rate of Force Development

Figure 2.12: Force and Rate of Force Development after estimated explosive force onsets in isometric knee extension, determined with manual and automatic methods. Average over all subjects.

Despite the reported variability in force profiles in the first 50 ms of contraction, the forces measured from MD and AGLR onsets are well correlated. Indeed, the pooled data fit a linear regression model (Figure 2.13), indicating consistency between the measure obtained from different onset detection methods, and the measures obtained from one method can be related to the other.

In Figure 2.14 the MD onset is marked in signals aligned through the AGLR axis. In the vast majority of trials, the signal is already clearly rising by the time MD selects the onset, while AGLR tends to place the onset close to where intuitive human pattern recognition would.

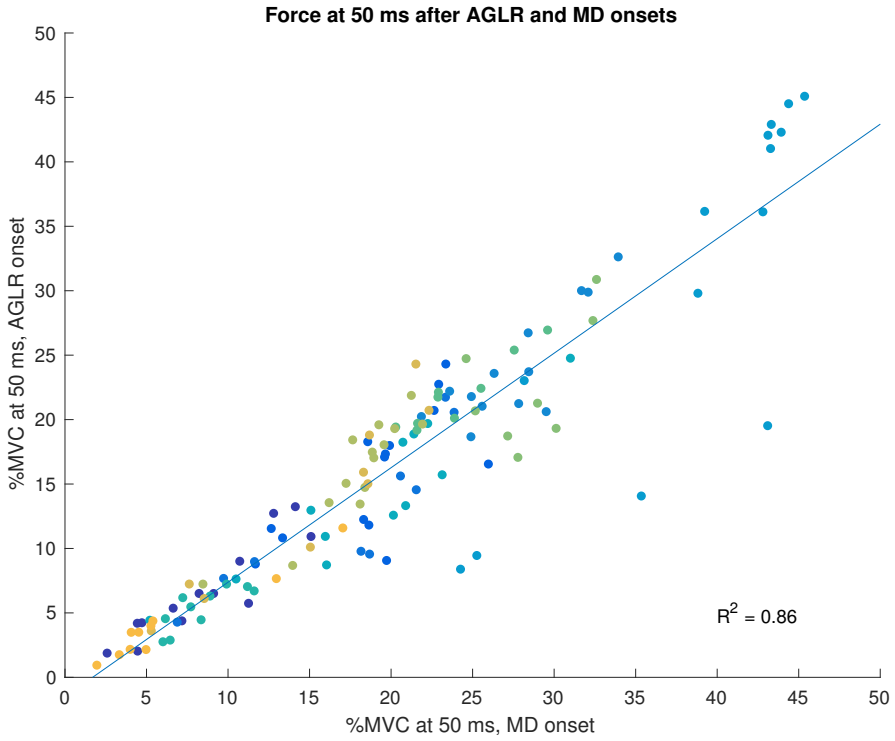

Figure 2.13: Scatter plot of the forces at 50 ms after AGLR onset vs. MD onset for all knee extension trials (different subjects are assigned different colours). The blue line represents the linear model estimated from the data, with $R^2 = 0.86$.

Table 2.1: Onset latency with respect to manual detection.

	Simulated		Experimental	
Method	Low Noise (ms)	High Noise (ms)	Knee Ext. (ms)	Elbow Flex. (ms)
NPD	0.18 ± 0.60	0.19 ± 0.57	0.43 ± 0.87	3.30 ± 4.94
NPD-SD	-2.04 ± 1.70*	-3.54 ± 2.46*	-2.15 ± 2.11*	-1.10 ± 2.28
NPD-MA	-2.47 ± 1.96*	-1.27 ± 2.07*	-2.39 ± 2.22*	-2.59 ± 7.89
AGLR	-5.28 ± 2.46*	-10.76 ± 4.09*	-4.63 ± 3.48*	-4.73 ± 7.10
ST	14.21 ± 3.92*	8.28 ± 3.06*	17.50 ± 4.74*	12.97 ± 6.74*

Timing of automatic detection with respect to the gold standard manual method MD (mean $\pm$sd). *$p < 0.05$ for testing the difference between the mean time of automatic detection to MD.

Table 2.2: Onset latency with respect to real onset.

	Simulated	
Method	Low noise (ms)	High Noise (ms)
MD	9.83 ± 2.35	16.27 ± 3.11
NPD	10.01 ± 2.46	16.46 ± 2.96
NPD-SD	7.79 ± 1.92	12.72 ± 3.17
NPD-MA	7.36 ± 3.08	15.00 ± 3.69
AGLR	4.55 ± 1.57	5.51 ± 2.36
ST	24.04 ± 3.63	24.55 ± 3.18

Timing of detection with respect to the real force onset (mean$\pm$sd).
All were significantly different from real onset.

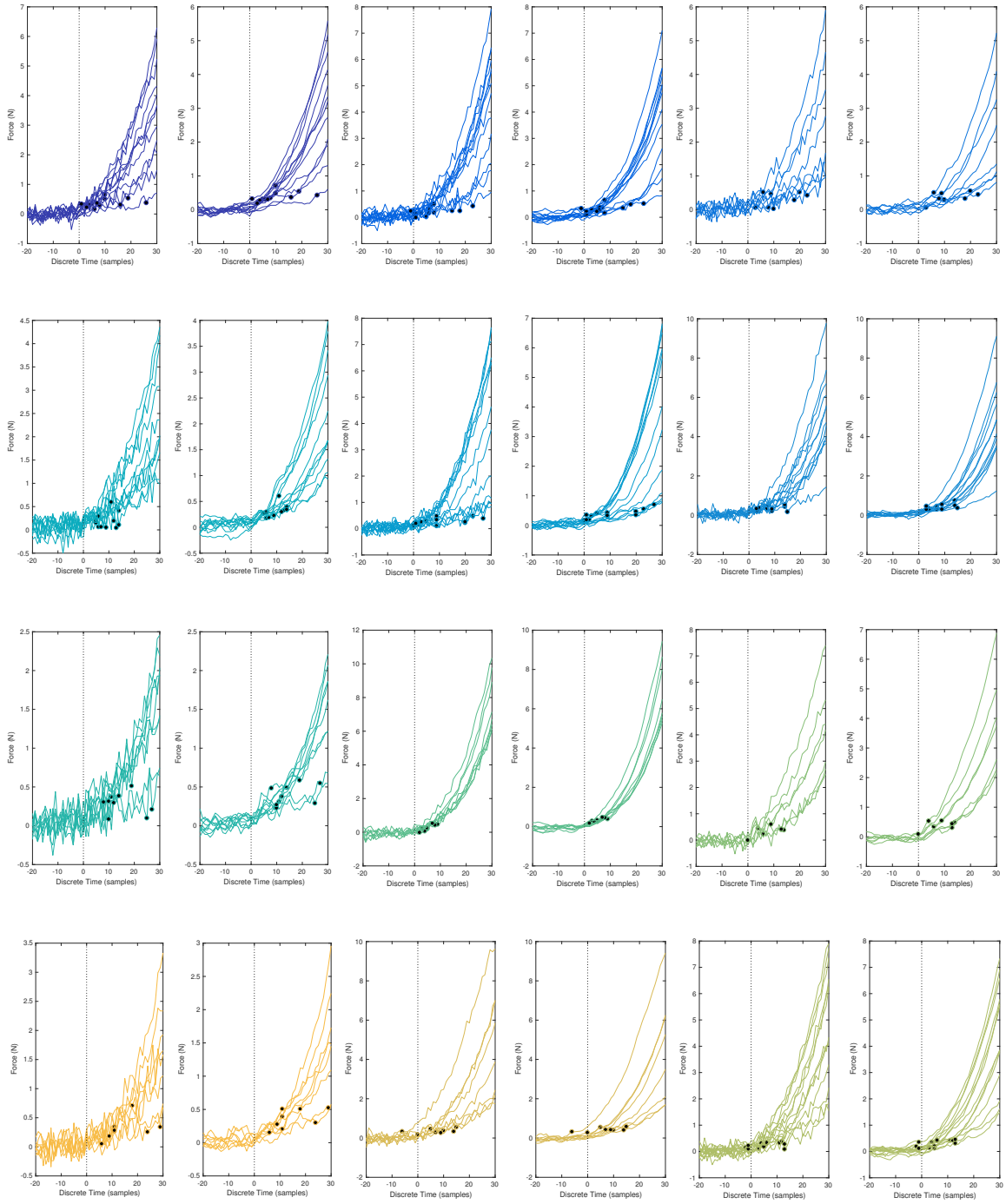

Figure 2.14: Initial phase of force production, aligned in the discrete time axis according to the AGLR estimated onset (at zero), for all twelve subjects who performed ballistic isometric knee extension. The left hand side of each sub-figure shows the raw forces; on the right hand side the force has been smoothed with a 4 backward sample moving average, to enhance the signal of interest. The dark markers represent manually detected onsets.

Knee flexion results were significantly affected by the factor subjects in force and rate of force development ($p < 0.01$) but not in onset placement ($p = 0.04$). Detection methods affected all measures of performance ($p < 0.01$). Multiple comparisons revealed that ST was different and less accurate than all other methods. For the remaining methods: there were no differences in rate of force development (both absolute and normalized); AGLR and NPD-MA (but not NPD and NPD-SD) had different forces

at 50 ms than MD, and lower expected value; NPD was no different from MD in onset placement, but all other methods had significantly smaller latency.

2.3.2.B Elbow Flexion

Most trials in the isometric elbow flexion data set were preceded by counter-movements and were consequently discarded. Due to the small amount of samples, the distributions of onset detection differences among methods do not yield relevant visual interpretation. Also, different types of noise occurred in different trials, which further contributed to the variance in results. However, despite the poor quality of the signals, both manual and automatic detection methods allowed proper force measurements in the trials that passed the validation criteria. In the subset of trials shown in Figure 2.16, the majority of detections seem to be more accurate with AGLR, which becomes more evident when the force profiles are lightly smoothed. The differences between measures of force obtained with the different methods follow the same trend observed in ballistic knee extension (Figure 2.15).

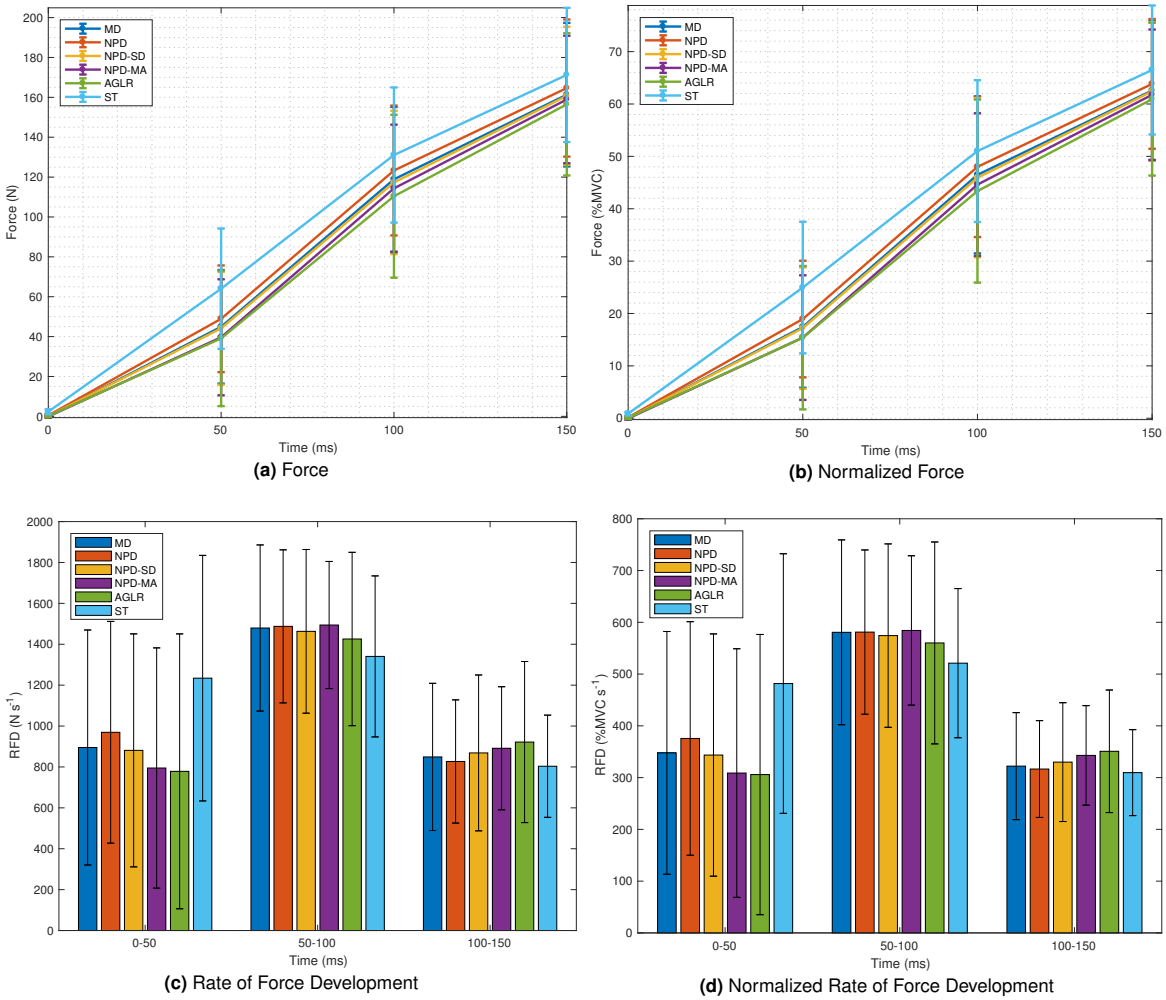

(a) Force **(b)** Normalized Force

(c) Rate of Force Development **(d)** Normalized Rate of Force Development

Figure 2.15: Force and Rate of Force Development after estimated explosive force onsets in isometric elbow flexion, determined with manual and automatic methods. Average over all subjects.

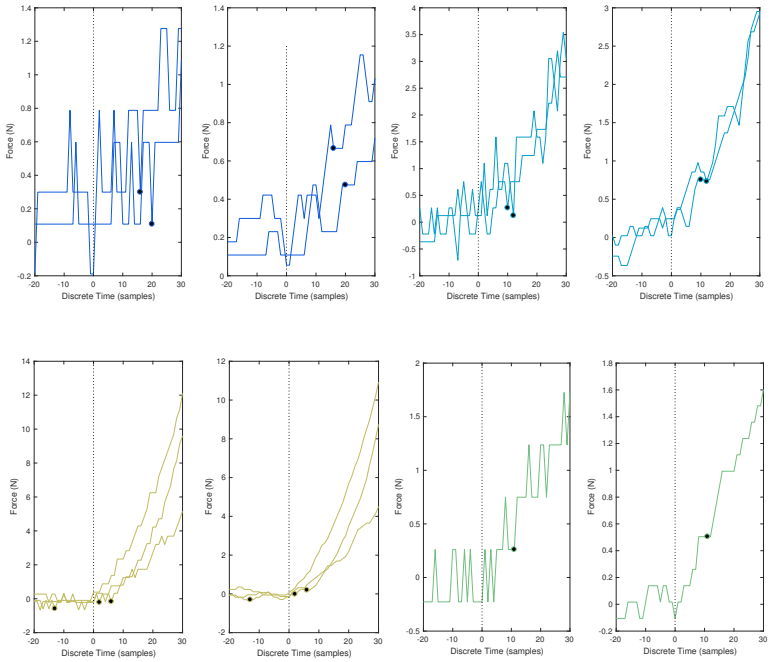

Figure 2.16: Initial phase of force production, aligned in the discrete time axis according to the AGLR estimated onset (at zero), for four subjects who performed ballistic isometric elbow flexion. The left hand side of each sub-figure shows the raw forces; on the right hand side the force has been smoothed with a 4 backward sample moving average, to enhance the signal of interest. The dark markers represent manually detected onsets.

The factor subjects was significant in force and rate of force development ($p < 0.01$) but not in onset placement ($p = 0.2$). Detection methods affected onset and force ($p < 0.01$) but not rate of force development. Multiple comparisons revealed that all methods except ST resulted in no difference from MD in regard to absolute and normalized force, supporting the null hypothesis.

2.4 Discussion

As expected, the use of a simple threshold high enough to avoid false positive detections leads to an overestimation of the onset and, subsequently, to significant differences in the measures of force with respect to both manual and more complex automatic methods. We confirmed that even a low relative threshold (i.e. 1% MVC) leads to significant differences in measures of motor output (e.g. force and RFD), emphasizing the limitations of this automatic method already reported in the literature [46][51]. However, this study brings a new prespective into the methodological guidelines for onset detection, by showing that manual detection is not the most accurate method. Having verified the inadequacy of the simple threshold and its poor performance against the remaining methods, from this point onward, when mentioning automatic methods, the author shall refer only to the NPD and AGLR.

The simulation results demonstrate that automatic methods can outperform manual detection. Since automatic detection never occurs before the real onset, the simulations certify that automatic methods do not underestimate the onset (i.e. they do not lead to false positives). Therefore, automatic methods detecting earlier onsets than MD may be assumed to be more accurate. It must be noted

that, since simulation noise was generated by a single Gaussian process, AGLR is optimal for its onset detection, and thus it may not be inferred that its high accuracy level in simulations can be replicated in experimental results. Similarly, as noise modelling is based on standard deviation, it was pre-determined that NPD-SD would perform significantly better than NPD.

As expected, detection performance of MD, measured from the difference between real and detected onset, varies with noise level. Noticeably, when data of different noise levels are pooled, the narrow distribution on AGLR onsets contrasts with the bimodal distribution of the remaining methods. This indicates that, contrary to the common assumption that accuracy of onset detection methods – especially MD – is highly dependent on noise levels [46], AGLR is robust to reduction in signal quality in the presence of white noise. From Figures 2.1 and 2.5 it is evident that the difference between AGLR and MD is smaller and less variable with lower noise levels. At the same time, Figure 2.3 corroborates that AGLR detection is more consistent for different disturbance levels, in the presence of additive Gaussian noise. Indeed, Tillin et al. [67] claim that the gold standard is adequate specifically in the case of high frequency low amplitude noise. We show that MD performance is affected when noise levels are higher than the ones of custom strain gauges, and its accuracy may be compromised in common set-ups using commercial sensors. All automatic methods were as accurate or more than MD, supporting the null hypothesis and rejecting the alternative hypothesis of the gold standard.

Visual inspection of Figure 2.5 strongly supports that AGLR does not underestimate the subjectively perceived onset, suggesting that the accuracy results from the simulation study hold for experimental trials as well. Results from the regression model are another indicator of the validity of the AGLR method. The good correlation between the outcomes of both methods indicates that their effects (i.e. biases) on the measured force relative to the real force shall be proportional. If AGLR were to underestimate the onset (i.e. detect before actual onset), the relationship of such false positives with the gold standard, assuming that the gold standard is accurate and consistent, would likely be less coherent.

Oftentimes, the last peak before deflection appeared to coincide with the threshold-line, due to the poor resolution of the plotting system at the scale of observation in the manual detection protocol. In such visually dubious cases, the subjective interpretation of the manual method led to greater accuracy, rendering the gold standard potentially more accurate than its automatic version by half a millisecond. This slight discrepancy did not lead to significant differences between MD and NPD, which supports the null hypothesis.

As expected, not only MD could be automatized, as the automatic version allowed implementation of modifications on the original method to further increase accuracy: Having shown that the automatic method NPD performs *as well* as the so called gold standard in experimental data, the remaining automatic methods are even more accurate. However, the automatic method may be improved if the noise-bounding limits are relaxed, by determining them from statistical properties rather than global extrema. Once the NPD was computerized, its improvement consisted in a trivial adjustment based on simple statistics, which nonetheless led to significant performance gains.

The state-of-the-art paradigm yields accurate detection when noise has high frequency and low

amplitude. Automatic methods employing statistical choices, soft filtering or templates can outperform manual detection, particularly in signals with high amplitude noise. In general, NPD-SD and AGLR were identical or more accurate than MD, and in most cases NPD-MA onsets were more accurate than MD. AGLR is likely to estimate the onset closer to the real start of contraction, and to be more robust against higher noise levels. However, its computational burden is much higher than the one of NPD-SD and NPD-MA, and thus the latter may be acceptable in the case of limited computational costs or real-time processing capacity. Besides its complexity, AGLR has a larger adaptation phase than the manual inspection window. On the other hand, the thorough adaptation allows it to make accurate estimates in signals with small instabilities in the 100 ms prior to the onset, even in cases where the trials have to be discarded with the gold standard method.

2.5 Conclusions

The manual method commonly employed for onset detection in ballistic contractions is unnecessarily time consuming and painstaking. This method can be replicated by an automated routine with no prejudice to performance in validated trials (i.e. leading to no significant differences in onset placement and subsequent force measures). Moreover, automatic detection can be significantly improved by making simple changes to the current gold standard, without compromising computational efficiency. Finally, AGLR, a more sophisticated method employing statistical processing and making use of previous knowledge about events of interest yields the best performance in simulated and experimental data, along with robustness against high levels of noise. However, the performance of AGLR in simulated trials may be enhanced due to the chosen noise model. In order to fully demonstrate that the accuracy of automatic methods holds in a greater range of conditions than MD, further studies might evaluate simulations with added statistical complexity (e.g. non-white noise) and higher volumes of experimental data obtained with commercially available dynamometers. Our findings validate the use of a range of automatic methods, rather than the current gold standard of manual detection. The possibility of unmanned detection opens a new way to investigation of large volumes of data and can substantially contribute towards filling the gap in the literature on ballistic contractions.

3

An Insight into Central and Peripheral Control of Ballistic Contractions

Contents

3.1 Introduction 42
3.2 Methods 46
3.3 Results 50
3.4 Discussion 54
3.5 Conclusions 63

3.1 Introduction

3.1.1 State of the Art

3.1.1.A Ballistic Contractions

Ballistic contractions consist in voluntary generation of muscle tension to achieve a target force as fast as possible, with undefined Rate of Force Development (RFD). The ability to execute rapid and forceful movements can be related to aging and neuro-muscular disorders and is crucial for sports performance. In daily living, explosive contractions may be important to ensure safety when movement stability is disturbed [41][70], and explosive voluntary force has been associated with balance ability in aged populations [40].

The mechanisms of neural control of ballistic contractions were investigated and compared against ramp contractions by Desmedt et al. [15], who described the fundamental features of neural activity in the TA during ballistic isometric dorsiflexion. One of their main findings was the almost simultaneous recruitment of several motor units at the onset of contraction, starting at a high firing frequency [15]. This strategy is markedly different from the gradual recruitment and discharge rate increase occurring in fast but tracked contractions [7]. Although it has been argued that such behaviour challenges the size principle, the motor neuron sub-populations recruited in ballistic contractions are consistent with the peak-force of the contraction [15]. Also, given the practical limitations in the accurate assignment of the first discharge to the corresponding motor units resulting from the nearly simultaneous discharges, the measured recruitment threshold has limited reliability in ballistic movements. Desmedt et al. [15] introduced the ballistic threshold concept, which reflects the probability of recruiting a given motor unit in a contraction with a certain maximal force [15](e.g. units are recruited at the onset depending on a specific target force, corresponding to their ballistic threshold, rather than being recruited at a specific force – the recruitment threshold). Ballistic thresholds are linearly related to the recruitment thresholds properties of the same neurons in paced contractions, where the size principle holds [15]. Therefore, the group of motor units recruited in ballistic contractions with different maximal force follows a well programmed assignment of neuron sub-populations, whereas the rank of recruitment onset seems to be of lesser relevance in this context. In both gradual and explosive contractions, higher peak forces can be achieved by increasing the number of discharges over the initial sudden burst, and this becomes the primary mechanism for achieving greater maximal force above a certain level (however, this level is lower in ballistic than in ramp contractions with the same target force). Additionally, maximal RFD capacity has also been related to maximal discharge rate in rapid contractions [44].

Another consequence of the study by Desmedt et al. [15] is the reduction in motor unit ballistic threshold with respect to its recruitment threshold. If generalized, this property implies that a given ballistic contraction requires the activation of more motor units than a ramp contraction with the same maximal force. This is in accordance with the fact that, for different ramp contractions, the recruitment threshold of a given MU varies proportionally with the rate of force development [46], and supports a generalized spinal organization of motor units dependent on the goal force.

Given that the neuro-muscular junction is a completely reliable synapse, the generalized MU organization must be programmed at the CNS. Since larger motor units tend to have faster twitch forces, it would be reasonable to expect the recruitment mechanisms to be reversed in the case of sudden forces. Although episodes of reversal of the size principle have been documented, they do not provide significant evidence, as the very short time between consecutive onsets and the consequent overlap of many action potentials may lead to inaccuracy in determining the exact moment of recruitment of each motor unit [15]. Also, in contractions elicited from invasive stimulation, small motor units are activated in greater proportion [8], which supports the preservation of recruitment of *weaker* units regardless of the mode of contraction. The CNS seems not to adjust the control for fast and forceful tasks by preferentially recruiting larger and faster units, but rather by recruiting them at the beginning of contraction, along with the smaller MUs. This mechanism might increase the efficiency of force production through the simultaneous activation of parallel units [15].

Ballistic capacity may be affected by the maximal voluntary contraction, fiber type composition, stiffness of the muscle-tendon unit twitch profile and the strength of neural signals [39][70]. Ballistic performance is typically assessed in isometric contractions, by measuring force and rate of force development (either absolute or normalized to MVC) in standardized intervals [46][67][70]. When evaluating central control from sEMG amplitude, or innate muscle contractile properties from evoked contractions, the most significant factor underlying differences in ballistic motor output between athletes and un-trained individuals is the intensity of the neural drive to muscles [41]. However, Folland et al. [70] found that the correlation between agonist muscle EMG activity and force changes throughout the contraction, within a range from 0.45 to 0.71, and EMG correlation with RFD ranges from 0.16 to 0.71. While EMG amplitude yields an overall estimate of neural activity, it provides limited insight into specific neural control strategies (e.g. recruitment and rate coding). For instance, Del Vecchio et al. [5] have recently reported the limited predictive value of EMG amplitude and spectral features with regard to neural factors, in particular recruitment, but is not known whether similar results should be expected in ballistic contractions.

The existing report on motor unit activity in ballistic contractions [15] is based on relatively limited populations of neurons, and does not investigate peripheral mechanisms (e.g. conduction velocity). Apart from the characterization of ballistic contractions in terms of a time-independent ballistic-threshold, no other relationships between control variables (e.g. recruitment, discharge rate and conduction velocity) and the motor output have been investigated up to date. Folland et al. [70] reported changes in relative contribution of neural and morphological factors throughout ballistic contractions, but seldom physiological interpretations can be drawn from their results. Moreover, a strong linear relationship between neural drive estimated from EMG amplitude and motor output has only been confirmed in the first 40 ms of ballistic contractions [41].

Until recently, accurate assessment of motor neuron activity required invasive procedures [7] [15], which limited and possibly biased the sampled neurons [1]. On the other hand, recent investigations on the relative contribution of neural and contractile properties towards performance of ballistic contractions were based on elementary assessment of neural activation, whose accuracy is smaller than

state-of-the-art EMG decoding. To the author's knowledge, there are no studies of neural activity in ballistic contractions using individual MU discharge rate information from significantly large MN populations. Furthermore, ballistic contractions have not been characterized with regards to changes in muscular electrical properties throughout the contraction, namely conduction velocity, which has been included in the size principle parameters [8].

3.1.1.B Conduction Velocity

The spinal chord integrates inputs from higher centers (e.g. motor cortex, brainstem, cerebellum) and peripheral sensory information (e.g. skin receptors, golgi tendon organ, etc. [75]), in circuits that converge into the somas of motor neurons. The spinal output is propagated through the peripheral axons and across the NMJs (i.e. the synapses between MNs and muscle fibers). In non-pathological cases, a NMJ is an extremely reliable synapse, where the transduction of MN action potentials into chemical signals (mediated by the neurotransmitter acetylcholine) inexorably originates action potentials in the motor plates of the corresponding muscle units. These action potentials are in turn propagated along the muscle fiber membranes to generate contraction across their length.

Analysis of stimulated tibialis anterior fibers shows that muscle fiber CV is closely related with functional and structural features included in the size principle: CV is higher in muscle fibers with larger diameter, greater twitch force, and shorter rise time [8]. CV has been reported to decrease with fatigue, either throughout maximal contractions [19] or contractions sustained for long periods [25][29][76][77]. As described in Chapter 1, the literature explores the relationships between muscle fiber properties and conduction velocity, describes fatigue-related changes in CV (correlating them with EMG), and evaluates motor performance with respect to general CV properties. Most published studies focus on CV changes in the course of very long contractions (e.g. 40 to 300 s [78][79]) and have poor time resolution (e.g. 0.5 or 1 second [79][80]). Conversely, the progression of CV at the beginning of contraction has received minor attention. The existing reports confirm that CV follows the size principle in voluntary contractions [1][81]. Particularly, Masuda and De Luca [10] found a correlation between CV and recruitment threshold in gradual contractions. In their study, the rise in CV followed the rise in force, and was mostly attributed to the activation of larger fibers, according to the size principle; in this study, even though the individual motor unit discharges were extracted, the relationship between measures of rate coding and CV was not investigated. More recently, Del Vecchio et al. [1] corroborated the strong correlation between CV and recruitment threshold in larger populations of neurons, whose activity was decoded with convolutive blind source separation method in ramp contractions. They also reported the uni-modality (i.e. absence of distinct classes) of motor units with regards to CV and fiber diameter.

In agreement with the contribution of MU synchrony and DR towards CV development [25][82], there is experimental evidence of an increase in CV with increased rate of muscle stimulation (i.e. induced discharges) [83]. Yet, it still is not clear how this translates into voluntary contractions with natural neural firing, since most studies considering the effects of DR on CV employ a fixed discharge rate for each single contraction [29][84]. Nevertheless, the Velocity Recovery Function (VRF), relating

the inter-spike intervals to the excitability and conductivity of muscle fibers, reveals both subnormal and and supranormal regions [30][85]. Using computational simulations of muscle excitation at different rates, Fortune and Lowery [30] have obtained an estimate of the variation in muscle fiber CV with respect to the instantaneous firing rate, which is consistent with experimental data. Noticeably, K^+ channels and T-tubular system were central parameters in this VRF derivation, supporting their strong impact on conduction velocity development. Finally, it is not known how CV progresses in the case of ballistic contractions, where recruitment and DR have a markedly different behaviour.

Whilst the literature on CV variation with fatigue is relatively vast, to the author's knowledge there is only one account of the relationships between neural control and changes in CV at the onset of gradual voluntary muscle tension, which considers recruitment and disregards DR [10]. Furthermore, no literature was found on the impact of physiological discharge rates on CV, or on the variation of CV during ballistic contractions.

3.1.2 Motivation

Our investigation addresses the gap in the literature on neural and peripheral control of ballistic contractions, using hdEMG decomposition to extract the individual MU spike trains from significantly large MN populations. Over the last decade, the development of new EMG decomposition methods [49], particularly the blind convolutive source separation of high density multi-channel recordings [14], introduced the possibility of non-invasive assessment of the complete discharge profiles of large populations of neurons [5]. In the current study the activity of 188 motor neurons is assessed during ballistic contractions of the tibialis anterior and its association with motor output (e.g. force and rate of force development) or muscle conductivity.

The following research intends to contribute to clarify the basic neural strategies and electrophysiological features in fast production of a target force, complementing the scant literature on neuromotor control of ballistic contractions. Its main goal is to analyze motor neuron excitation patterns during ballistic contractions and to quantify how they relate to both motor output and global surface EMG variables, aiming to provide new insights into performance mechanisms for power-oriented tasks. This investigation involves interpreting signals transmitted from the CNS and their relationship with muscle physiology, and estimating how motor output depends on conduction velocity, recruitment and discharge rate.

Despite being widely employed in research and clinical practice (e.g. to infer the quality of therapeutic or resistance exercises [50]), global surface EMG interpretation is not trivial and has recently been questioned (see Section 1.3.3) [5]. Nevertheless, surface EMG remains an extremely versatile technology, with a much wider application range than high density EMG decomposition and allowing real-time processing. Besides describing the evolution of control parameters during ballistic contractions, this investigation analyzes the predictive value of the surface EMG signal for the assessment of neuro-muscular variables, contributing for the open discussion on whether EMG is over-exploited for inference of neuro-mechanical variables, such as motor unit recruitment and the type of recruited muscle fibers, or prediction of neuro-muscular adaptations, such as hypertrophy.

3.2 Methods

3.2.1 Motor Task

With isometric dorsiflexor contractions, it is possible to approximate muscle tension and measurement of motor output with force transducers, whereas its parallel fibers of the TA allow proper decoding of the hdEMG and CV in static conditions. When using rigid force transducers (e.g. custom built strain gauges [70]) and restraining the subject's movement with a proper set-up, the changes in joint angle and compliance of soft-tissue can be minimized [46]. Consequently, the moment arm and muscle length are approximately constant (i.e. torque is linearly proportional to force) and, since TA is responsible for the gross of ankle dorsiflexion, the relationship between force output and TA tension can be assumed to be linear. In isometric contractions, with respect to dynamic contractions, the passive influence of tissue visco-elasticity is reduced, and the relative contribution of different muscles is maintained throughout non-fatiguing contractions. In these conditions, although the measured force may not be exclusively generated by the observed muscle (e.g. tibialis anterior) it may be assumed that those two variables are highly correlated. The force transducer signal is used as a standardizing factor and feedback signal for performance of contractions by the subjects, and due to the aforementioned approximate linearity, it can be related to the concurrent measurements of muscle activity. Likewise, many studies on the neural mechanisms of motor control employ isometric contractions of the dorsiflexor muscles, and its properties are extensively related in the literature (e.g. [1][5][8][15][25][86]).

3.2.2 Experimental Protocol

Fifteen healthy subjects performed isometric dorsiflexions at sub-maximal and maximal contraction levels. While sitting on a chair, the subjects extended their dominant leg and dorsiflexed the ankle to 30° from neutral position. The ankle position was strongly fixed with Velcro tapes placed around the foot and the ankle. A strain gauge load cell was attached in series with the tape on the ankle, perpendicularly to the lateral malleolus.

With the aid of a dry electrode array, the proximal and distal innervation zones of the TA were determined; in each zone, the direction of the fibers was identified by detecting the position with greatest consistency in AP shape propagation when moving the array over the skin surface. A 64-electrode high density EMG grid, with 5 columns and 13 rows of 1 mm wide gold-coated electrodes, with a 8 mm interelectrode distance d_G. was placed on the skin, after shaving, abraising and cleaning it with 70% ethanol, so that 4 electrode rows were over the innervation, and the columns were parallel to fiber direction. The electrodes were individually covered with a conductive ointment before placement of the grid, which was attached to the skin with adhesives. The monopolar multi-channel EMG signals were acquired with an amplifier (bandwidth 3 dB, 10-500 Hz).

Force and EMG signals were sampled simultaneously at 2048 Hz and 12 bits per sample. The experimental sessions started with three MVC trials, separated by at least 30 s, where subjects received auditory incentive to contract as forcefully as possible for at least 3 s. The greatest force achieved in

the course of the three trials was selected as the MVC. Subsequently, the subjects performed at least four ballistic contractions to 70% of their MVC. The subjects had to reach the goal force as fast as possible, guided by a feedback monitor showing the desired force level and the transducer signal in real time. Each ballistic contraction was followed by a plateau, in which the subject tried to hold the tension at the goal level (this type of contraction has been referred to as *step-and-hold* [44]). Motor output (i.e. force transducer signal) was normalized to peak trial force.

The proximal electrode grid signals were used for MU source separation, whereas the distal ones were used to determine CV.

3.2.3 Signal Processing

The following signal analysis was performed with custom MatLab programs, using the Signal Processing and Statistic and Machine Learning toolboxes.

Force signals were corrected for the gravitational force and converted to Newton. The recording was segmented into separate trials and force onset detection was performed with the AGLR method (see Section 2.2.1.C).

The multi-channel surface EMG was decomposed with blind source separation [64], yielding the individual motor unit spike trains:

$$ST_m(t) = \begin{cases} 1, & if\ t \in T_m^{AP} \\ 0, & otherwise \end{cases} \tag{3.1}$$

where T_m^{AP} are the times of AP arrival to the m^{th} unit's motor end plate.

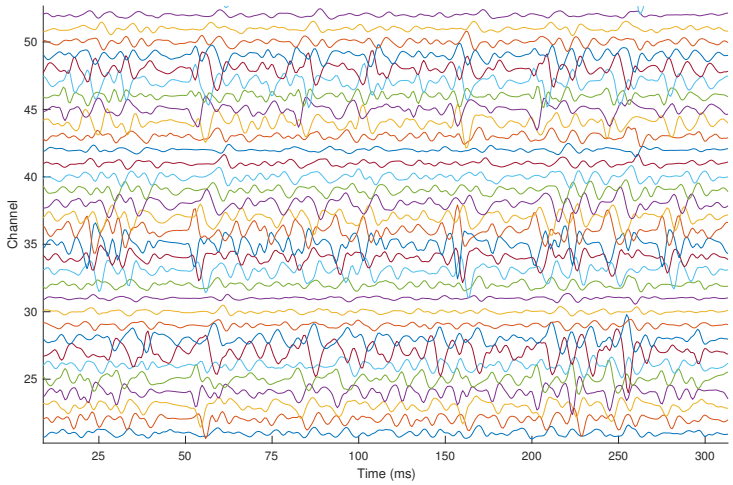

Figure 3.1: Time-scale of observation of double-differential EMG signals for selection of consecutive channels for CV estimation.

EMG Amplitude and Conduction Velocity

High density EMG signals were spatially filtered by computing the double-differential:

$$EMG_{r,c}^{dd} = -EMG_{r-1,c} + 2 \times EMG_{r,c} - EMG_{r+1,c} \tag{3.2}$$

RMS, CV, Average Spike Density (ASD), RFD and the percentage of firing units were determined in 75 sample long (ca. 36 ms) intervals plus a 5 sample overlap ($L = 75$, $o = 5$). When comparing the above variables by superimposing plots and calculating correlations, the remaining variables (e.g. DR) were averaged over the same intervals. Furthermore, RFD, RMS, mean DR and CV were also determined as a function of force (in intervals corresponding to 10% increases in trial peak force).

In each discrete time interval i, RMS was averaged across all the double differential signals.

$$RMS_i^{dd} = \frac{1}{K}\sum_{k=1}^{K}\sqrt{\frac{1}{L}\sum_{n=Li-o+1}^{L(i+1)+o}|EMG_k^{dd}(n)|^2} \tag{3.3}$$

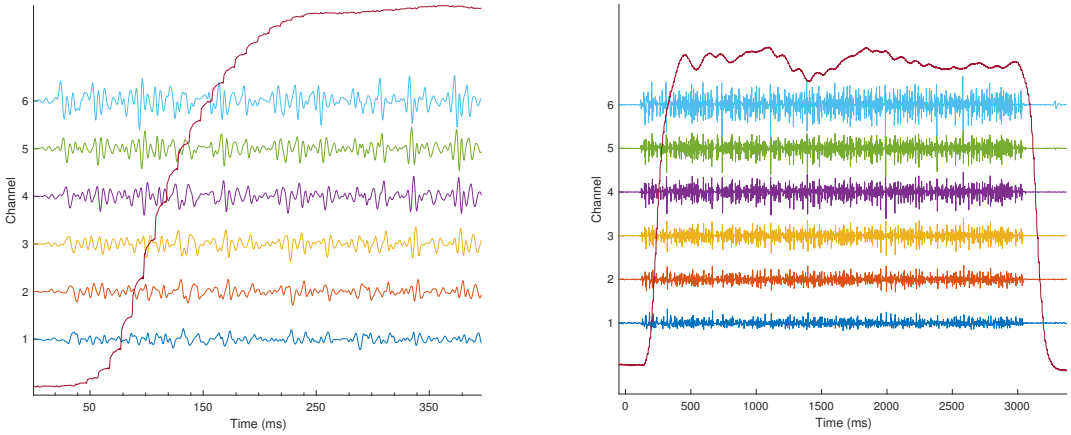

Figure 3.2: Double differential EMG signals selected for CV determination with the cross-correlation method.

For each subject, the double differential signals were visually inspected. The observer selected four to six consecutive channels, with clear AP propagation in the same direction from the innervation zone and the least changes of shape and scale (Figure 3.1). For each subject, the same channels were used in conduction velocity computation of each (discrete) time interval in all trials (Figure 3.2). After a first estimation of the signal delay θ between multiple detection points in consecutive channels, using cross-correlation, θ was approximated with Maximum Likelihood (ML), using Newton's criteria [87], and CV was determined from:

$$CV = \frac{d_G \times f_{samp}}{\theta} \tag{3.4}$$

3.2.4 Discharge Rate

Average Spike Density

When estimating variables over 75 sample windows, ASD is determined in each discrete time interval w by counting the number of decoded AP's among all neurons and dividing it by both the interval length and the number of decoded motor neurons M:

$$ASD = \frac{f_s \times \sum_{m=1}^{M}\sum_{t=w_i}^{w_f} ST_m(t)}{M(w_f - w_i)} \tag{3.5}$$

where w_i and w_f are the first and last indexes of the time window, f_s is the sampling frequency and $ST_m(t)$ is given by equation 3.1. While Average Spike Density is a commonly employed measure of neural activity, it requires a relatively large time resolution, given the sparseness of action potentials with respect to the sampling time-scale.

Instantaneous Motor Neuron Firing Rate

As the measurement intervals become smaller, ASD becomes less accurate. We employ an alternative method for firing frequency estimation, which approximates the real instantaneous discharge rate of each motor unit DR_m. Let us consider that the time difference between any two consecutive spikes of the m^{th} motor neuron, i.e. at times $T_m^{AP}(n)$ and $T_m^{AP}(n+1)$ (see Section 3.2.3) is the instantaneous firing period. Then, since firing frequency is the inverse of firing period:

$$DR_m = \frac{f_s}{T_m^{AP}(n+1) - T_m^{AP}(n)}, \quad T_m^{AP}(n) \leq t < T_m^{AP}(n+1) \tag{3.6}$$

The total discharge rate (DR) is the average over all motor unit instantaneous discharge rates. This measure allows overall DR to be estimated with the same time-resolution as the sampling frequency, which in turn allows determination of Short Term Synchronization and Firing to Performance Phase (FPP, see Section 3.2.5). When comparing DR to variables measured in larger time-scales (e.g. EMG amplitude and conduction velocity), the total DR is averaged through time in the same intervals.

Recruitment

Recruitment order is determined from the rank of the time of each unit's first spike. At each time interval, recruitment is quantified as the proportion of Active Motor Units (AMU): the percentage of units whose neurons are activated (e.g. transmit an AP) within the time window.

3.2.5 Short Term Synchronization

The level of synchronization is assessed from the statistics of the coefficients of correlation between the instantaneous discharge rate profiles DR_m of all motor units [88].

Firing to Performance Phase

In each trial, two measures of neuro-mechanical lag are determined: both at the onset and within the contraction. EMD is the difference between the onsets of force and EMG activity. Firing to Performance Phase (FPP) is the time-shift that maximizes the cross correlation between the instantaneous total DR and the force transducer signal.

3.2.6 Effective Muscle Fiber Signal Frequency

Physiologically, CV is the velocity of propagation of a signal from a stationary source. Since CV is not constant, from the perspective of a peripheral sarcomere (e.g. signal receiver) the binary signal emission process is equivalent to a moving source, whose speed can be estimated as $\Delta CV = CV_f - CV_i$. This results in a shift of the frequency at the sarcomere with respect to the discharge

frequency at the source (i.e. the Motor End Plate (MEP)), alike the Doppler Effect. The equivalent rate of AP arrival to a given point of the muscle fibers with respect to the initial rate can be approximated as:

$$DR^{MF} = \left(1 + \frac{\Delta CV}{CV_i}\right) DR^{MEP} \tag{3.7}$$

We can roughly estimate the difference in peripheral AP frequency between two moments, by considering a 40 ms time-scale and averaging DR at each of those intervals as in Figure 3.6. Albeit leading to a significant reduction in DR, this approach is consistent with the findings that the effective neural drive to muscle (i.e. the signal that generates muscle tension) corresponds to a common low frequency component of a MN population [88].

3.2.7 Statistical Analysis

To evaluate the linear relationships between different factors across time, the correlation coefficient between variables α and β – $\rho(\alpha, \beta)$ – was obtained with Pearson Statistics:

$$\rho(\alpha, \beta) = \frac{\mathrm{cov}(\alpha, \beta)}{\sigma_\alpha \sigma_\beta} \tag{3.8}$$

where cov is the covariance and σ is the standard deviation. The correlations among discharge rates or between discharge rate and force were determined from the profiles at the sampling rate (Table 3.1). The correlations between motor output, neuro-muscular activity variables and EMG amplitude were determined over the full length of contraction, with the profiles determined in 75 sample intervals, and averaged over all subjects. The data were pooled and plotted as a function of time (Figures 3.6 and 3.7). The natural logarithms of the data in Figure 3.7 (up to 650 ms after tension onset) were fitted to a multiple linear regression model, with CV, DR and recruitment as predictor variables and force as the dependent variable. All variables were re-scaled, by subtracting the value at the onset (and then normalized) before determining their natural logarithm. The multiple linear regression was generated with the Statistics and MatLab Machine Learning Toolbox. Results are presented as mean $\pm$ standard deviation. Statistical significance was accepted for $p < 0.05$.

3.3 Results

3.3.1 Recruitment

In general, recruitment and rate coding obtained with high density sEMG decomposition were in agreement with the invasive studies on TA in ballistic contractions [15]. The same discharge burst described in previous research was observed [15], with full recruitment generally being completed before 21% of the peak force is reached. The proportion of motor units firing before force onset was less than the one suggested in the literature [15], which is coherent with the use of a more accurate force detection method in the present study. After an initial firing burst where most motor units were recruited, they remained active but firing rate decreased noticeably overall.

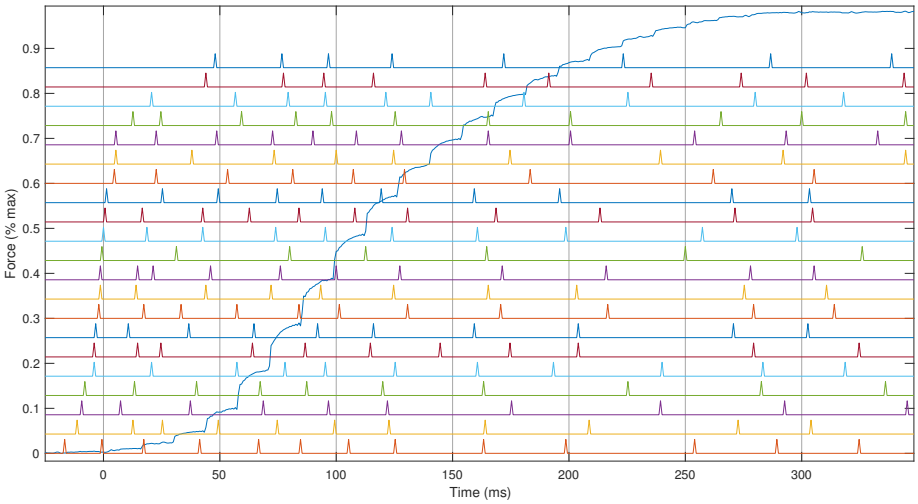

Figure 3.3: Decoded motor unit spike trains and motor output during ballistic contractions.

3.3.2 Discharge Rate

Besides being recruited within a short period and before the gross of force development, the instantaneous firing rates of different motor units are highly correlated throughout the whole contraction (e.g. 90% of the inter-unit correlations were between 0.6 and 0.95 in subject 12), thus individual motor units exhibit short term synchronization over long step-and-hold contractions. Individual neural profiles are strongly correlated with each other. In some subjects the distribution of correlations appears to be weakly bimodal (e.g. Figure 3.5). In such cases, the correlations are slightly reduced and bimodality disappears when the discharges of different trials are grouped according to the rank of the generating unit, instead of gathering neural activity by the motor units themselves (i.e. when the data are rearranged according to recruitment rank rather than units).

When aligned to eliminate FPP, the electro-mechanical time-offset within the contraction period determined from cross correlation, both the averaged instantaneous discharge rate and the discharge rate from individual units were highly correlated with total force. The motor output is highly correlated with both individual ($R^2 = 0.70 \pm 0.09$) and total ($R^2 = 0.78 \pm 0.07$) discharge patterns. This feature of the derived variables denotes the reliability of the methods employed, validating hdEMG decomposition as an instrument for neural control assessment during ballistic contractions. When comparing individual MUs with motor output, the mode of the distribution of correlation coefficients was above 0.85. Additionally, there was no correlation between ASD and motor output (Table 3.3). When averaging force and total DR profiles, either across trials or over time windows, small fluctuations during the plateau phase are eliminated and there is no significant correlation between motor output and DR (Table 3.3).

3.3.3 Conduction Velocity

Conduction velocity was collectively analyzed for the twelve subjects with the best quality CV measurements in ca. 40 ms intervals. The average MFCV increased from 3.5 to 4.5 m/s over ballistic

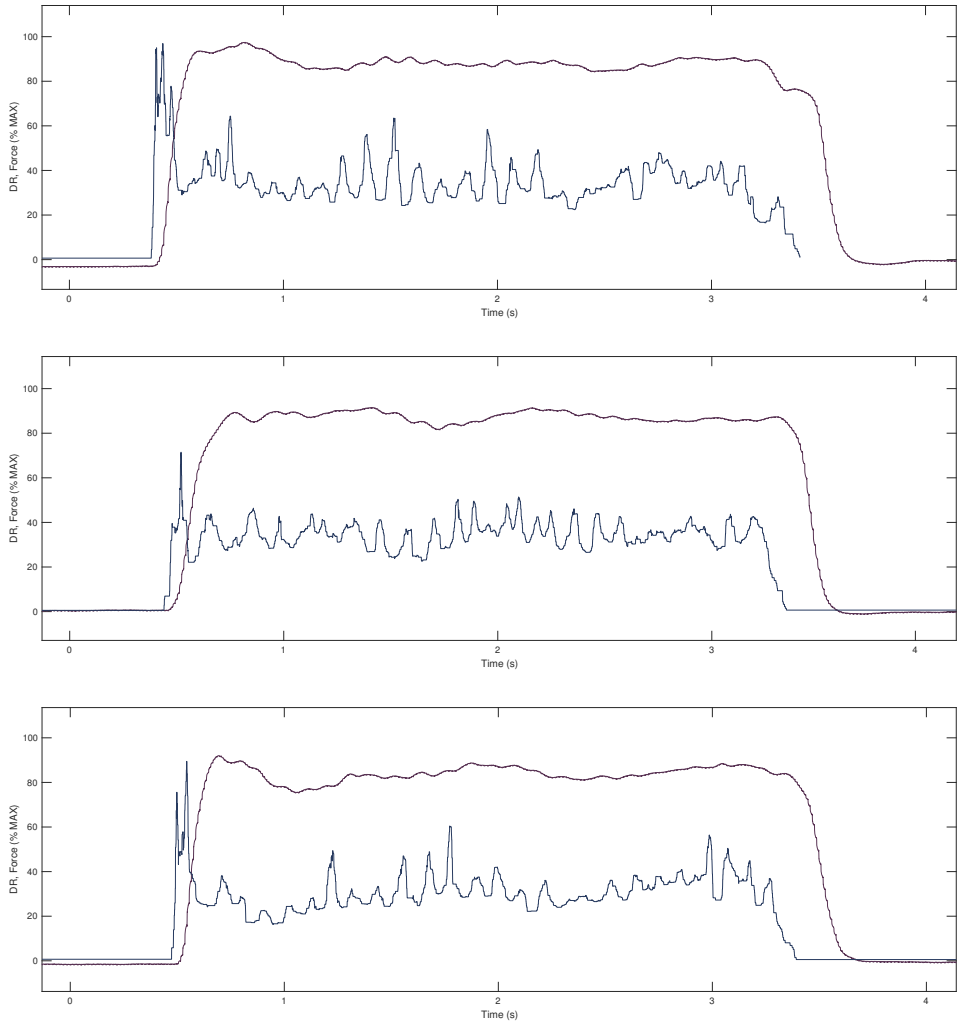

Figure 3.4: Normalized profiles of force and instantaneous discharge rate (mean over motor units) in step-and-hold trials.

contractions, which is within the range of velocities in elicited TA twitch contractions reported by Andreassen et al. [8] . The change in conduction velocity in a 400 ms long contraction is consistent with the measurements in submaximal contractions of the vastus lateralis [33] and with slow ramp contractions of the TA up to 80% MVC [10]; the average CV is consistent with the rise in conduction velocity from 3 to 4 m/s as full recruitment occurs [10], and a standard deviation under 0.5 m/s is in agreement with the accuracy of the ML method [87]. Assuming a mean TA fiber length of 70 mm [89], an action potential should take up to 20 ms (i.e. much less than the time resolution for CV) to travel from the motor end-plate to each end of the fiber at the beginning of contraction (i.e. when CV is minimal), up to 17.5 ms around the peak of DR, and up to 15 ms once force is sustained (i.e. when CV is maximal).

Conduction velocity is characterized by a monotonic increase, despite a decrease in discharge rate after the initial phase of force development, and is moderately correlated with motor output ($R^2 = 0.62 \pm 0.28$, Table 3.3). Figure 3.6 depicts the average and standard deviation of force, RFD, CV, DR and recruitment. While the initial rise in CV is consistent with the rise in single unit DR and torque, once DR starts decreasing, both CV and torque continue rising, reaching a plateau at roughly the

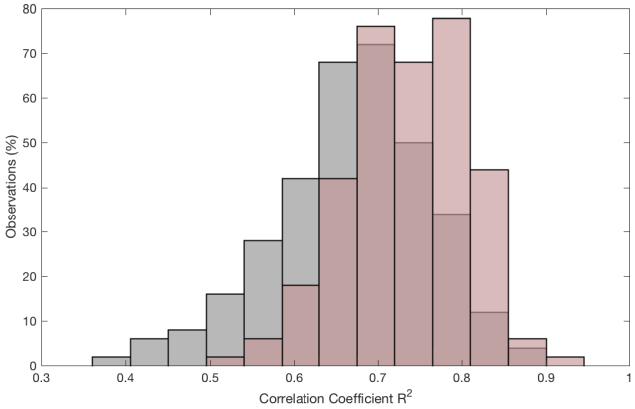

Figure 3.5: Distribution of coefficients of correlation between discharge rate profiles of different motor units – purple; between ranked DR profiles – grey.

Table 3.1: Correlation between measures of neural activity and motor output.

	Correlation	
Subject	Mean DR	MU DR
1	0.75 ± 0.05	0.70 ± 0.09
2	0.77 ± 0.05	0.71 ± 0.09
3	0.80 ± 0.05	0.80 ± 0.05
4	0.82 ± 0.06	0.72 ± 0.11
5	0.88 ± 0.01	0.81 ± 0.10
6	0.89 ± 0.02	0.80 ± 0.11
7	0.88 ± 0.02	0.82 ± 0.06
8	0.74 ± 0.00	0.63 ± 0.11
9	0.82 ± 0.04	0.72 ± 0.11
10	0.75 ± 0.21	0.66 ± 0.21
11	0.64 ± 0.24	0.54 ± 0.21
12	0.73 ± 0.41	0.70 ± 0.35
13	0.76 ± 0.21	0.74 ± 0.19
14	0.66 ± 0.10	0.52 ± 0.22
15	0.78 ± 0.09	0.62 ± 0.18
Mean	0.78 ± 0.07	$0{,}70 \pm 0{,}09$

Pearson correlation coefficient between DR (average and individual MU) and strain gauge signal at the sampling frequency (2048 Hz) resolution.

same time. CV was not consistently correlated with force, rate of force development and recruitment (Table 3.3). While Hedayatpour et al. [29] demonstrated a strong dependency between the conduction velocity of individual fibers and the average conduction velocity obtained from cross correlation of EMG signals, the influence of larger (and more conductive) fibers may be underestimated with this method.

The effective (e.g. shifted) AP frequency in the fibers is estimated by assuming discrete changes in CV. With respect to the time of peak mean frequency $DR_i^{MEP} = 38\,Hz \approx DR_i^{MF}$, and considering $CV_i = 4\,m/s$ as the baseline propagation velocity, the equivalent receiving frequency at the time of maximal force is:

$$DR_f^{MF} = \left(1 + \frac{0.5\,m/s}{4\,m/s}\right) \times 32\,Hz \approx 36\,Hz \tag{3.9}$$

Table 3.2: Neural delays: EMD and FPP.

Subject	EMD (ms)	FPP (ms)
1	55.05 ± 2.59	103.76 ± 5.00
2	55.34 ± 11.78	78.21 ± 6.47
3	48.44 ± 14.59	54.59 ± 30.76
4	51.35 ± 10.51	77.96 ± 6.01
5	38.49 ± 19.31	55.91 ± 24.85
6	42.97 ± 13.60	89.01 ± 9.47
7	48.58 ± 5.83	88.79 ± 3.92
8	71.78 ± 0.00	51.27 ± 0.00
9	46.55 ± 2.94	55.01 ± 8.60
10	38.09 ± 7.92	63.31 ± 33.91
11	58.76 ± 14.32	38.25 ± 28.63
12	42.24 ± 7.96	72.75 ± 28.42
13	55.80 ± 7.99	81.89 ± 29.41
14	59.49 ± 9.97	94.73 ± 49.63
15	51.62 ± 15.30	92.35 ± 25.22
Mean	50.97 ± 8.94	73.19 ± 19.19

EMD – absolute difference between EMG onset and motor output onset; phase between DR and motor output profiles, determined from cross-correlation.

3.3.4 Motor control and EMG

The multiple linear regression yielded:

$$\ln(\mathrm{MO}) = 0.74\ln(\mathrm{DR}) + 0.32\ln(\mathrm{CV}) + 0.02\ln(\mathrm{AMU}) + 1.70$$
$$R^2 = 0.8, p = 0 \tag{3.10}$$

Where MO is the motor output (i.e. the measured force). Given that the $p - value$ is null and R^2 is close to one, there is a significant linear regression relationship between the logarithm of force and the logarithm of the peripheral and central control variables, implying a multiplicative relationship between the variables themselves.

Furthermore, there was a strong correlation between the neural control variable DR and the double differential EMG signal (Table 3.3). The amplitude of the interference EMG signal is strongly correlated with discharge rate ($R^2 = 0.84 \pm 0.06$) and moderately correlated with the proportion of active motor units ($R^2 = 0.61 \pm 0.13$).

3.4 Discussion

3.4.1 Motor Unit Recruitment

The ballistic neural discharge burst initiates before force onset (e.g. before visual and muscle spindle feedback can be processed), and the participating MUs are recruited early in the ballistic contraction, in agreement with previous observations with invasive techniques [15], Throughout the force-holding phase (i.e. after the first half second of contraction) AMU remains steady (alike CV and DR) and close to its maximal value for 70% MVC, with no signs of fatigue (Figure 3.6). In average, full recruitment of the decoded MUs occurred between 1 and 30% of peak force, in all but one outlying subject (Table 3.4). The accuracy of the force onset detection method and the larger number of

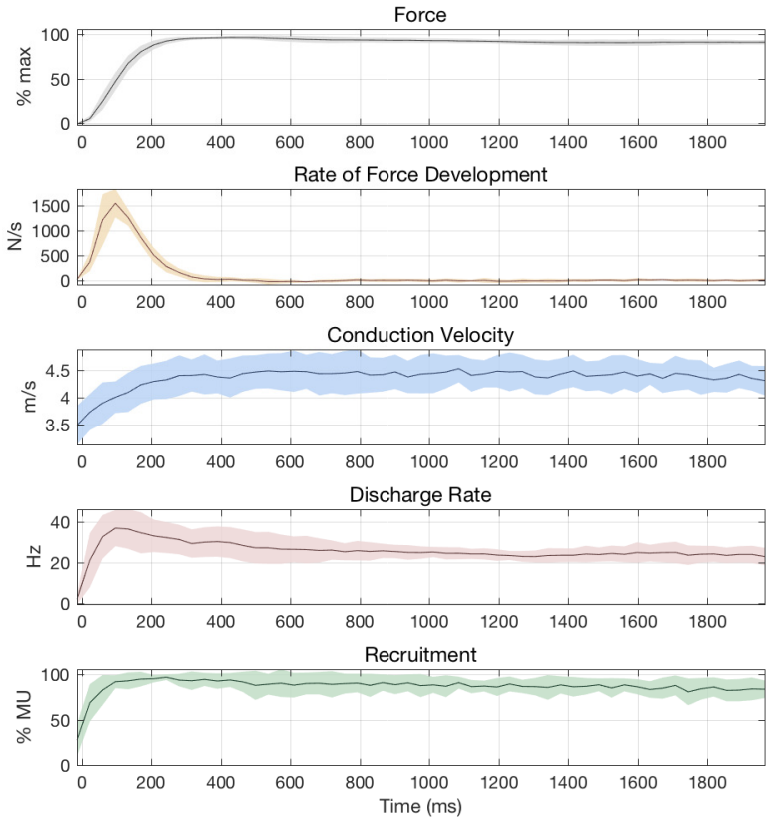

Figure 3.6: Step-and-hold contraction: mean and standard deviation of force, recruitment (proportion of active motor units), discharge rate and conduction velocity determined in 40 ms windows, averaged over subjects.

sampled units in the current study explain a marginal difference from Desmedt et al. [15], where full recruitment in ballistic contractions usually occurred before force detection.

The small differences in times of activation of different units corroborate a previous report from Dideriksen et al. [12] claiming that size-based ranking of motor unit recruitment does not yield a significant functional gain, and that its most relevant feature is the wide spectrum of innervation numbers. The present work did not provide evidence of consistency in the order of recruitment from trial to trial, which may either be a consequence of the intrinsic physiological features or the limitations of the decomposition method in cases of multiple action potential overlap. Nonetheless, it agrees with the lack of coherence in the order of activation of agonists (rectus femoris, vastus lateralis and vastus medialis) observed in ballistic isometric knee extensions [41]. Despite the indication that MU rank is not of primary relevance in neural control of ballistic contractions, this does not imply that there are no differences in control strategies. The existence of the so-called ballistic threshold could not be observed from our protocol, since that would require performing contractions with different target force levels in the same session.

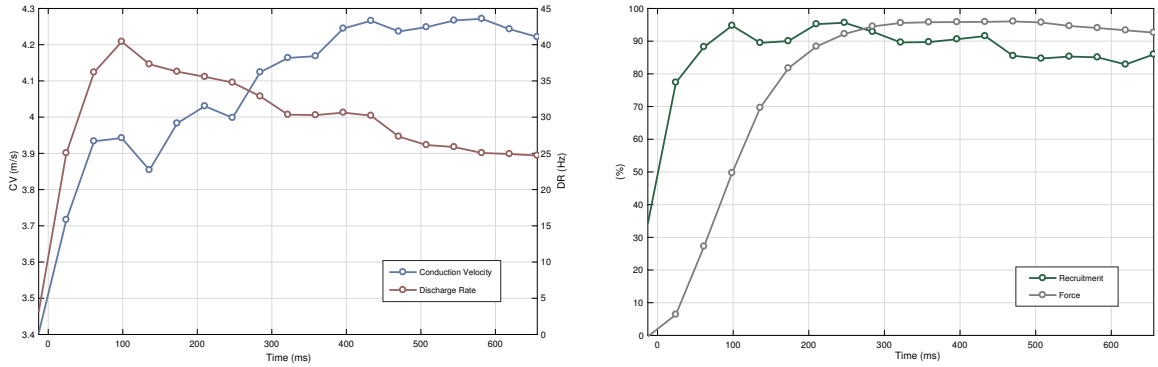

Figure 3.7: The initial 650 ms of contraction: mean force, recruitment (proportion of active motor units), discharge rate and conduction velocity determined in 40 ms windows, averaged over subjects.

Table 3.3: Correlation between sEMG features, bioelectrical factors and motor output.

	Correlation
Force vs. CV	0.62 ± 0.28
Force vs. ASD	0.33 ± 0.31
Force vs. AMU	-0.08 ± 0.29
RMS vs. ASD	0.84 ± 0.11
RMS vs. DR	0.84 ± 0.06
RMS vs. AMU	0.61 ± 0.13
RMS vs. RFD	0.53 ± 0.15
RMS vs. CV	-0.02 ± 0.29
RFD vs. ASD	0.53 ± 0.19
RFD vs. DR	0.54 ± 0.22
RFD vs. AMU	0.19 ± 0.15
CV vs. ASD	0.02 ± 0.24
CV vs. DR	0.11 ± 0.27
CV vs. AMU	0.29 ± 0.32

Correlation between variables determined in 40 ms intervals.

3.4.2 Rate Coding

The average maximal discharge rate for single motor units was consistent with the range of 60 to 120 Hz indicated by Desmedt et al. [15] (except for a single outlying subject; Table 3.4), and the firing peak was followed by a drop in instantaneous DR to much lower values (e.g. less than 50 Hz) [44]. Noticeably, the overall instantaneous DR (i.e. average over all MU DRs) reached its maximum in under 40% of peak force, in all but three subjects. The force at full recruitment and force at maximal DR were less consistent than the force at peak RFD, which was highly consistent across both trials and subjects, occurring in average at 32% of peak force. This is in agreement with the strong dependency of ballistic RFD on intrinsic contractile properties, besides neural drive, reported by Folland et al. [70]. Furthermore, we observe a relatively long period of force increase following full recruitment and peak DR, which also agrees with previous findings of a greater relative contribution of the neural drive in the earlier phase of ballistic force production, and a more pronounced impact of non-neural factors in latter phases [70].

FPP (i.e. the estimated time lag between the overall discharge profile and the motor output) was generally higher than the initial EMD (Table 3.2). FPP takes into account the delay during the force

Table 3.4: Motor output and neural activity.

Subject	FFR (% max)	FP_{DR} (% max)	FP_{RFD} (% max)	$MUDR_{max}$ (Hz)
1	16.28 ± 16.17	46.44 ± 3.07	27.02 ± 2.38	114.12 ± 14.27
2	3.25 ± 2.36	34.88 ± 25.75	27.99 ± 1.92	89.06 ± 18.40
3	10.55 ± 7.70	11.26 ± 7.67	36.42 ± 2.55	81.85 ± 18.75
4	19.80 ± 24.18	13.22 ± 13.16	30.85 ± 2.87	57.67 ± 8.42
5	5.20 ± 4.90	4.13 ± 8.45	36.23 ± 4.97	98.98 ± 25.24
6	10.44 ± 11.47	3.21 ± 8.38	32.22 ± 5.53	48.04 ± 13.20
7	30.14 ± 8.10	34.28 ± 8.10	29.49 ± 4.04	65.18 ± 7.46
8	4.97 ± 0.00	57.07 ± 0.00	30.36 ± 0.00	124.72 ± 43.97
9	20.43 ± 17.77	45.66 ± 8.36	29.20 ± 1.66	77.74 ± 12.03
10	1.21 ± 1.02	7.94 ± 15.20	33.66 ± 2.57	92.09 ± 15.10
11	12.35 ± 10.28	22.78 ± 20.65	46.10 ± 0.75	89.32 ± 20.15
12	68.22 ± 18.21	38.26 ± 5.85	22.50 ± 3.39	38.72 ± 6.23
13	6.60 ± 3.97	26.19 ± 21.45	31.33 ± 3.75	82.71 ± 11.90
14	7.65 ± 9.54	6.22 ± 7.65	36.07 ± 7.32	88.57 ± 23.81
15	24.27 ± 31.27	19.90 ± 22.12	29.83 ± 2.75	80.35 ± 31.81
Mean	$16.09 \pm 16:64$	24.76 ± 17.29	31.95 ± 5.41	75.90 ± 29.84

FFR – force at full recruitment, percentage of trial peak force; FP_{DR} – force at peak instantaneous cumulative DR (mean DR across all motor units); FP_{RFD} – force at peak rate of force development; $MUDR_{max}$ – maximal motor unit discharge rate, mean across all individual instantaneous motor unit discharge rates, over all trials.

plateau phase, and is an estimate of the phase between force and instantaneous DR profiles, whereas EMD is determined from the initial difference between EMG and force onsets. Therefore, FPP reflects the *average* period between reception and execution of a particular neural instruction over the whole contraction, while EMD reflects the single period between reception of a neural signal and the production of a mensurable output. Besides the inherently different measuring methods, the mechanisms underlying the difference between the two delays likely include the rise time of fiber twitches and the time of AP propagation to the fiber ends. Besides excitability (e.g. CV), the contractile, viscoelastic and stiffness properties of the mucoleskeletal system may vary through different stages of contraction, and thus may also influence FPP.

Nearly all motor units were kept active throughout the force holding stage, during which the fluctuations in force follow the oscillations of the motor unit instantaneous firing rates, delayed by 50 to 100 ms (Table 3.2, Figure 3.6). This similarity is a strong indicator of the decomposition accuracy. The oscillatory nature of both DR and motor output is consistent with the use of feedback control (e.g. after the ballistic phase, subjects use the visual feedback provided in the experimental setup and innate haptic mechanisms to hold force). Given the high short term synchronization (Figure 3.5), these oscillations corroborate the finding of increased force fluctuations in simulations with motor unit synchronization [56].

The findings of strong correlation between the activities of different MUs and close times of recruitment suggest that the motor units active in a step-and-hold contraction are either under similar central commands (e.g. similar synaptic input to all motor neurons [88]) or prone to synchronization. In some subjects, the loss in bimodality when the data are re-grouped according to recruitment rank could suggest the occurence of slightly different rate coding modes for the different motor units, which are preserved across trials (Figure 3.5). However, no evident discerning patterns were observed

among motor unit spike trains, and, since the means of the two apparent distributions were very close (e.g. the two means are at roughly 0.75 and 0.8 in subject 12), these observations are not powerful enough to find significance. Therefore, there was no evidence of the existence of differentiated control strategies for neural sub-populations, which is consistent with the literature presenting evidence of a continuous distribution of fiber characteristics, and suggesting that muscle units should not be classified into discrete types [2]. Although recruitment was generally progressive (Figure 3.3), since the order of recruitment was not consistent from trial to trial, the motor unit properties or associations on the base of the size principle could not be inferred. In future studies, more refined methods and larger data sets could be used to investigate the differences in rate coding strategies of different neuron populations.

When comparing single MU DR to force rather than against each other, we find strong correlations, with mean R^2 equal to 0.85. The correlation between individual MU discharge rates and motor output was similar for all motor units except in punctual trials from three (Table 3.1). This suggests that different units have somewhat similar roles in sustaining force at submaximal levels. The sum of the instantaneous DR over all units tended to have higher correlation with motor output than the average of single unit correlations (Table 3.1). However, these correlations between neural drive and motor output are completely lost when using the more popular spike average density [5] or when averaging the values over time windows (Table 3.3), as done for analysis of EMG RMS and CV. Therefore, the information lost when determining DR at a resolution much greater than the sampling period may be relevant to explain fine gradation of motor output, and, as such, the choice of method of *instantaneous* DR computation may be an important factor when studying fast and precise movements.

3.4.3 Conduction Velocity

CV rises monotonically for ca. 300 to 400 ms after force onset in sustained ballistic contractions. The increase in CV is concurrent with a strict increase in force, whereas DR and RFD have a non-monotonic behaviour in the same period, with mean DR decreasing to half of its peak value and RFD returning to zero before stabilizing (Figure 3.6). In the initial contraction phase, the rise in CV is coherent with fast recruitment, activation of parallel fibers and increasing discharge rate as expected from the literature; however, CV and force continue rising for ca. 200 ms beyond the peak of total DR.

Despite being present in published data (e.g. Broman et al. [25] and Eberstein et al. [78]), the transient rising behaviour of CV at the onset of contraction is typically disregarded, since such studies are usually concerned with the variation of CV at much longer time scales (e.g. during fatiguing contractions). Here we discuss possible mechanisms for the rise in CV and its potential contribution towards ballistic contraction performance.

Conduction Velocity and Neural Control

A close relationship between force and CV matches Masuda and De Luca's data [10] on slow ramp contractions, especially when considering the last two seconds of the upward ramp (e.g. the contraction time scale employed in the present study). An often proposed mechanism driving the rise

in CV is the activation of additional MUs as higher force levels are reached. According to the size principle, the recruited muscle units are sequentially larger and more conductive [10][29][1]. Consequently, recruitment may influence CV in a non-linear way, as different motor units do not have the same intrinsic CV. However, in ballistic contractions, the variation of CV cannot be entirely explained with the aforementioned rationale: in this case, all units are recruited within a very short time, after which CV continues rising for longer than the sum of EMD and the time of AP propagation through TA muscle fibers.

A careful analysis of Masuda and De Luca's [10] results reveals that the most pronounced increase in CV in slow ramp contractions tends to occur towards the latter phase of recruitment (e.g. after 50% MVC). On the one hand, this distinct rise in CV could be attributed to the partaking of large conductive neurons, which are recruited at later (i.e. high) thresholds in paced contractions, but closer to tension onset in ballistic contractions [15]. On the other hand, above a certain force level, the number of additionally recruited units is dramatically reduced, and thus "even though the high threshold units generate more tension, the contribution of recruitment to increases in voluntary force declines at higher force levels" (Milner-Brown et al. [7]). Since CV and force behave similarly, it is conceivable that the variation of CV at higher force levels may also be caused by factors besides additional unit recruitment. The prolonged increase in CV found in the current study, which lasts much longer than the recruitment phase in ballistic contractions, supports this hypothesis.

While CV has also been reported to vary proportionally to DR [19], in the present study CV varied differently from DR and AMU (Figures 3.6 and 3.7). After the ballistic contractions, when the target force is sustained, at lower firing rates, all variables ultimately stabilize. The final period of rise in CV cannot be imputed to an increase in DR, since during this phase the mean instantaneous discharge rate is roughly halved. Moreover, the Velocity Recovery Function (VRF) based on computational models indicates that the positive dependency of CV on DR only holds in a limited interval of instantaneous frequencies, which does not include the firing rates observed in ballistic contractions. According to Fortune and Lowery's simulation [30], the linear relationship between DR and CV occurs for instantaneous firing rates up to ca. 20 Hz, above which CV is in a supra-normal region and does not vary proportionally to DR. In general, the units sampled in the present study fired within the supra-normal range during the explosive segment of contractions – hence the absence of correlation between conduction velocity and DR is consistent with the VRF simulation results [30]. These findings stress that the positive correlation between DR and CV does not hold indefinitely and may have limited application in fast natural movements. Remarkably, K^+ channel dynamics is key in Fortune and Lowery's model [30], which supports the critical role of time-dependent biochemical changes leading to the establishment of an optimal ionic environment for fast peripheral control.

Conduction Velocity and Membrane Potential

The time constants of biochemical reactions influence the rate of contraction within single muscle fibers. The time needed for an AP to propagate through a muscle fiber (up to 20 ms, see Section 3.3.3)

[1] Conversely, progressive fatigue of active units would contribute to decrease CV (or its rate of increase) in maximal/long contractions; however, fatigue is unlikely to play a relevant role in our study.

is much lower than the rise time of evoked twitches in TA fibers (between 47 and 80 ms [8]), indicating that the biochemical events occurring locally within the fibers, from the release of Ca^+ from the sarcoplasmic reticulum to the cross-bridge cycle, are determinant for the temporal progression of force. These biochemical alterations may carry on for considerable periods. For instance, the membrane potential can decrease for several minutes after muscle fibers are stimulated [32]. Given the dependency of CV on membrane potential, CV itself may also have an inherent rise time depending, for instance, on the time required for establishing chemical gradients across the sarcolemma, that would in turn enable quicker re-polarization of the muscle fiber and thus increase CV. The existence of a CV rise time could go unnoticed in ramp contractions, particularly in Masuda and De Luca's set-up [10], where the choice of an extremely low RFD imposes slow recruitment. Specifically, the rise time of CV for the lastly recruited fibers could be greatly reduced in slow contractions, due to the prior activation of nearby fibers that is known to facilitate conduction [29] (likely by pre-establishing the optimal ionic gradient; see explanation below). The findings of the current study agree with a strong dependency of CV on transient chemical changes, resulting in a noticeable effect on its time-dependency at the scale of ballistic contractions.

Once the units are recruited, the *baseline* myocyte thermo-chemical environment (i.e. the ion concentrations and membrane channel state prior to arrival of an action potential) changes depending on factors such as the dynamics of ionic channels. The easily variable ionic gradients across the the sarcolemma determine the membrane potential and may thus influence CV. Conduction velocity may be maximized when an *optimal conducting environment* is established throughout the length of all recruited fibers, after which it is maintained as long as the neurons keep firing (even though they may fire at a lower frequency than in the initial activation burst) and fatigue does not occur (Figure 3.6). In general, temporary changes in the peri- and intra-cellular environment could be caused by altered ion channel dynamics in both sarcolemma and T-tubules, temperature or pH, metabolite build up or water content in the muscle. During ballistic contractions, changes in channel dynamics and ion concentration could explain the final rise in CV.

When the K^+ gradient across the membrane increases, the membrane becomes hyperpolarized (i.e. the membrane potential becomes more negative[2]). As a result, the repolarization time is reduced and CV increases [19]. Evidently, the gradient can be raised by increasing the intracellular ionic concentration and/or decreasing the extracellular concentration. For instance, a temperature rise may intensify the Na^+/K^+-pump activity and thus enhance the build up of K^+ inside the muscle fibers. Consequently, the extracellular K^+ concentration is reduced, and this effect can be propagated to the neighbouring fibers. Noticeably, the activity of Ca^{2+}-dependent-K^+-channels can also influence CV [30] and might be optimized with Ca^{2+} saturation, which can take up to 50 ms to be attained in ballistic contractions [70]. Conversely, a reduction of the interstitial space water content increases the extracellular K^+ concentration, with the opposite effect on CV[3]. Another proposed mechanism for

[2] Recall that the electrical equilibrium potential for a given ion is given by the Nernst Equation: $E = \frac{kT}{q} \ln\left(\frac{[\mathrm{out}]}{[\mathrm{in}]}\right)$ [26][27], where k is the Boltzmann constant, T is the temperature, q is the ion charge, $[\mathrm{out}]$ is the extra-membrane ion concentration and $[\mathrm{in}]$ is the intra-membrane ion concentration. E_{K+} has a strong direct impact on membrane potential, which can be estimated from the Millman or the Goldman-Hodgkin-Katz voltage equations, weighted by the membrane's relative conductance to K^+ [90].

[3] Interestingly, an increase of intracellular water could lead to greater conductivity through fiber swelling despite the negative

the influence of temperature on CV is the increased activation of voltage-gated Na^+ channels, which would cause the AP amplitude to decrease. A smaller AP depolarization would result in a shorter innactivation time, as in the case of hyperpolarization, and thus increase CV [16].

Early activation of low threshold fibers may contribute to enhance the overall conductivity, in agreement with several published phenomena. Indeed, a *low activation* state leads to greater CV in subsequent contractions, when compared to a complete rest state [21]. Tonic activation might *prime* the chemical gradients of some units and thus enhance the overall CV at the onset of strong contractions – this has been suggested to be the cause of supranormal CV in subjects with fibromyalgia [21]. Since the fibers of different units are amalgamated [2][77] the extracellular chemical changes (initiated by low threshold units in gradual contractions) may spread to neighboring fibers that, when activated, may be closer to their *optimal conductive state*. Changes in the membrane environment may also contribute for the increase in conduction velocity that follows fatiguing contractions: this phenomenon is mostly attributed to muscle fiber swelling and hyperpolarization due to greater sodium pump activity [84].

CV and Muscle Tension

Force increases for a period longer than FPP after DR starts decreasing. From the conservative estimations of TA conduction time, the increase in conduction velocity leads to a reduction of about 2.5 ms (see Section 3.3.3) in muscle fiber propagation time, between peak DR and peak CV. An ever faster propagation of APs from the MEP through the fiber counteracts the reduction in the frequency of APs reaching the sarcomeres. As a result, the signal intensity at the ends of the fibers is not reduced as dramatically as the DR. The reduction in fiber propagation time is about half of the increase in mean firing period ($\Delta T_{DR} = 1/32 - 1/38\,Hz \approx 5\,ms$; Figure 3.6).

The effective signal rates in the muscle, conservatively estimated both at peak DR and peak force (i.e. end of ballistic contraction), are closer to each other than the DR at the same times. This observation suggests that the rise in CV counteracts the lowering of mean DR, mitigating the decrease in signal intensity within the end-effectors (i.e. muscle fibers)[4]. Moreover, the conduction velocity measurement from EMG may underestimate the actual individual fiber CV, especially for lastly recruited fibers in gradual contractions, which are the most conductive ones [29]. Consequently, the actual maximal CV (and ΔCV) is likely to be larger than the previous estimation, and thus CV alone may peripherally compensate for the drop in mean central drive at the later stage of ballistic contractions. The maintenance of the effective cellular signal contributes to explain the concurrent rise and holding of motor output.

Besides the proposed chemical-related time dependency of CV, additional changes in the viscoelastic state or the biochemical environment in the sarcoplasm (affecting contractility) could influence the variation in motor output that is not directly related to DR. For instance, Folland et al. [70] suggests that at around 100 ms the relative contribution of the mechanical state of the muscle-tendon unit out-weights neural drive. This is in agreement with the literature suggesting that, in the first

impact on membrane K^+ concentration.

[4] Note that other baselines could be chosen, but the difference in peripheral frequencies would still be of the order of 2 ms.

100 ms of contraction, the contractile properties are predominant, whereas the impact of the individual's maximal strength capacity is revealed later in the contraction [39]. Finally, in agreement with the analysis above, force is relatively stabilized once both central (e.g. recruitment and DR) and peripheral (e.g. CV) variables reach a steady state (i.e. $\Delta CV \approx 0$). From that point on, motor output fluctuations linearly reflect overall DR at a small time-resolution (Table 3.1).

3.4.4 EMG Amplitude

The findings of the present study indicate a strong dependency of the EMG amplitude on total instantaneous DR and no correlation with CV in submaximal step-and-hold contractions (Table 3.3). The relationship between CV and EMG features has been described in the literature, especially in the context of muscle exhaustion. Eberstein and Beattie [78] correlated the rates of decline of CV and mean EMG frequency in the biceps brachii in isometric contractions held at 60 and 70% MVC. Although CV and EMG were strongly related over the course of long fatiguing contractions (e.g. 18 to 36 s), careful observation of the trial subset illustrated in their paper suggests that over the initial 4-8 seconds CV rises slightly (increasing in a range coherent with this study), and only then decreases linearly, along with EMG mean frequency, due to fatigue. This suggests that the contribution of CV towards EMG in non-exhausted states may be less relevant. A possible mechanism for the observed electrical changes in fatigued muscles is the accumulation of potassium ions in the extracellular space, leading to lower sarcolemma excitability (see Section 3.4.3) [91]. Similarly, studies in ischemic conditions propose K^+ [77] and lactate [84] accumulation as sources of reduced CV during fatigue.

More recently, CV was noted to have limited prediction value in regards to muscle fatigue progression, since CV had no correlation with the time to exertion, which is related to EMG spectral features [92]. An important implication of this finding is that the frequency spectrum is determined by control factors beyond muscle conductivity [25][92]. This study shows that similar relationships apply to EMG amplitude.

The instantaneous DR in rapid contractions is related to changes in trained or aged individuals against controls. Our results show that EMG amplitude linearly reflects instantaneous DR, which is the most variable control determinant of force production during ballistic contractions [67], and thus support the use of EMG for motor assessment, training and rehabilitation. Despite all units initially recruited remaining active throughout the contraction, there are oscillations in AMU, which is also mildly correlated with RMS.

3.4.5 Motor Output

As seen in Figure 3.6, through most of the holding phase (i.e. when peak force is sustained at a submaximal plateau) recruitment, total discharge rate and conduction velocity remain at an approximately constant level, and at this stage the instantaneous fluctuations of motor output are proportional to fluctuations in DR (Table 3.1 and Figure 3.4). Rate coding is thus a neural control mechanism used in gradation of force at high (i.e. $>$ 70% MVC) levels of force, which likely involve visual and haptic

feedback (thus the phase between electrical and mechanical profiles becoming greater than EMD; Table 3.2).

It is known that CV, DR and recruitment are moderately associated with force. However, the available literature is typically focused on measuring correlation, and fails to demonstrate strong linear relationships between control factors and motor output throughout the whole duration of ballistic contractions (e.g. across time); in some studies, the relationships between rough estimates of neural drive and contractile properties at different time-periods are interpreted in terms of changes in "relative contribution" of different factors across the contraction (e.g. Folland et al. [70]). Such analysis based on correlation inherently assumes the linearity and additivity of the contributions of central and peripheral factors towards motor output.

Since CV measures the continuous propagation of a discrete signal DR to the mechanical effectors, their cumulative effect on motor output should reflect their product rather than their sum. The present study introduces the investigation of multiplicative relationships between CV, DR and Force. Its findings suggest that peripheral and central effects have a mensurable multiplicative effect on motor output. A relationship of this type was assumed in the derivation of the effective signal intensity reaching the contractile units, inspired on the Doppler-Effect. This approximation yielded estimates of peripheral AP frequency consistent with the resulting motor output (see Sections 3.3.3 and 3.4.3). Furthermore, in order to quantify the combined effect of the different control variables over muscle tension in the time-domain, a multiple linear regression was employed on the logarithms of the different variables, up to 650 ms after force onset, resulting in a coefficient of determination $R^2 = 0.8$. The high value of R^2 indicates that ballistic force depends non-linearly on DR, AMU, and also on CV (e.g. a peripheral control factor that is not exclusively explained by neural strategies). This analysis serves as proof of principle for the recognition of their non-trivial dependencies, going beyond the linear relationships that are typically assessed in the literature [46].

3.5 Conclusions

The investigation here reported leads to new insights into the relationships between central and peripheral bioelectrical factors, e.g. neural activity and muscle fiber conduction velocity. To the author's knowledge, this has been the first attempt to investigate the evolution of conduction velocity and to analyze its impact on the motor output in combination with central control variables during submaximal fast contractions.

Conduction velocity and ballistic force were found to increase monotonically beyond the peak of DR, for longer than twice the largest estimates of neuromechanical delay (and hence longer than might be explained by the viscoelastic properties of muscle and connective tissue). The analysis here proposed shows that the dynamics of CV are in agreement with the transience of ionic gradient changes and may contribute to explain an extended rise in muscle fiber tension.

Besides regulating the excitability of the sarcolemma, and thus influencing CV, biochemical mechanisms may also contribute for prolonging tension production through direct action in the sarcomeres

(e.g. enzyme activity or calcium build up). The rise in CV in the late phase of force development may counteract the concurrent decrease in discharge rate, mitigating its impact on the effective signal reaching the contractile structures. The experimental data were successfully fit to a tentative model of the motor response as a non-linear function of central and peripheral bioelectric factors (R^2=0.8), but further research has to be conducted in order to validate this relationship.

Future studies may investigate the biochemical agents (e.g. membrane channels, enzymes) that lead to a persistent increase in CV during ballistic contractions. Furthermore, although the filtering effect of passive tissue on the contractile tension is minimized in isometric contractions, in further investigations the magnitude of the the extra-fascicular (e.g. connective) delaying factors should be evaluated (e.g. using an AR model of the biomechanical system similar to the one employed in Chapter 2 and electrical stimulation).

The motor neuron activity decoded from non-invasive EMG matched the only existing report on spinal control of ballistic contractions[15], where motor neurons were invasively probed. However, the present protocol did not allow the study of ballistic thresholds. This may be assessed in future studies of ballistic contractions to varied target levels. Additional improvements to the protocol should include the identification of structural features of motor units, estimation of individual muscle fiber conduction velocity and further evaluation of the existence of differentiated firing patterns during fast contractions. EMG amplitude was highly correlated with DR and moderately related to AMU. Global EMG features may be useful to assess both central and peripheral control in biofeedback applications. Blind source separation of high density EMG should be adopted in future studies to continue unraveling the firing strategies that influence fast and accurate motor performance.

4

Final Conclusions and Further Development

The methodological and physiological findings of this dissertation contribute for the scientific research on spinal and peripheral control of fast contractions. Motor output (e.g. force and RFD) in early stages of ballistic contractions is associated with neuro-muscular parameters in athletes and subjects with impaired motor skills. However, measures of motor output are particularly susceptible to onset overestimation in the context of explosive contractions. Despite its accuracy, manual onset detection is time-consuming and restrains analysis of large data-sets, whereas the single-threshold methods proposed in the literature may introduce systematic biases and confound results. The first investigation here presented (Chapter 2) addresses this experimental problem, so that manual processing can be circumvented in the second research (Chapter 3), which addresses neuro-muscular control of ballistic contractions. The precision of several automatic methods is validated in a range of different experimental conditions and simulations. The automatic methods here proposed perform as well as, and even outperform, the gold standard of manual detection.

The best performing method is the AGLR algorithm, proposed by Staude for kinematic signals [69], which has here been shown to be equally powerful to estimate onsets in other bio-mechanical signals. Similar results are observed in both real and simulated data. Ballistic simulations are obtained with a new force model that allows testing at different noise levels and robust comparison of performances against the real onset. This result opens the door to analysis of high volume data in a variety of scientific and industrial applications, and is employed in the second part of the project.

The second research project investigates neuro-mechanical control, using high-density surface EMG and state-of-the-art processing methods. It addresses the gap in the literature on control of ballistic contractions, and introduces an original analysis of both central and peripheral determinants of performance during sustained explosive contractions. The results validate the use of non-invasive EMG acquisition and state-of-the-art signal decomposition to study the neural control of ballistic contractions, as it ensures random sampling of motor-units, a large number of observed units and extraction of individual spike trains. The activity of large populations of spinal motor neurons was extracted using blind source separation of multi-channel EMG. This algorithm identifies the neural drive underlying voluntary actions with very high sensitivity with respect to the reference invasive method detection. The central motor control is thus characterized from the individual MU spike trains, while muscle fiber conduction velocity is estimated from the cross-correlation of the high-density EMG.

Although it has been warned that "caution is necessary when attempting to deduce the neural drive to muscle from interference EMG recordings" [4], in the current study, the surface signal amplitude was highly correlated with the underlying neural activity, especially rate coding. These findings suggest that the use of sEMG may be appropriate to estimate the strength of neural drive during explosive contractions.

In step-and-hold contractions, the force plateau is reached upon stabilization of both central and peripheral electromechanical signal transmission mechanisms (e.g. Recruitment, DR and CV). All MUs are activated similarly, having close recruitment times and highly correlated instantaneous DRs. Furthermore, when considering either the total instantaneous DR (i.e. averaged across MU's) and all the individual MU DR's, there is a very strong correlation between DR and the force throughout the

holding phase, if the signals are aligned to compensate for FPP. Moreover, FPP is larger than the EMD, since it reflects not only the production of a mechanical process from an electrical signal, but rather the precise motor execution of a well defined rate-coded electric command.

On the other hand, during the initial ballistic phase, full recruitment and maximal discharge rate occur early in the contraction, whereas CV (alike force) increases through the whole contraction. The prolonged rise and maintenance of force, despite the reduction in DR, is likely influenced by the following factors: 1) passive mechanical filtering of the cumulative muscle fiber tension by the connective tissues and muscle itself; 2) improved propagation (e.g. conduction) of the control signals through the sarcolemma; 3) improved contractility of the myofibriles. While the viscoelastic properties (1) may not explain the whole duration of the monotonic rise in force concurrent with a drop in DR, the increase in CV is coherent with the temporal progression of transient biochemical events inside the myocytes. Such cellular changes can both decrease repolarization time (2) and influence contractility (3).

The DR profile used in the analysis combining CV, DR and motor output was based on determination of neural activity in a relatively large time-scale. This approach was justified by the literature reporting that the low frequencies are mostly determinant for force development. On the other hand, the total instantaneous DR profile evidenced in Figure 3.4 suggests that high frequency bursts, which can be mitigated at a larger time-scale, are closely followed by the force profile. Therefore, the averaged DR may be misleading, and further studies should address this limitation by improving the estimation of CV so that it can be measured at a smaller time-resolution.

The observed lasting rise in CV, which was not predicted from the existing literature, might be explained with changes in ionic gradient causing faster hyperpolarization and simultaneous recruitment of adjacent fibers. The rising conduction velocity, especially of larger (and stronger) fibers, may contribute for the maintenance of the stimuli intensity to the sarcomeres during the final increase in force, despite the decrease in DR. Within the supranormal region of CV as a function of DR, CV is governed by non-neural factors and may have a significant contribution towards force development. The analysis of the interactions between peripheral and central control factors suggests that the product of discharge rate and muscle fiber conduction velocity is reflected by the motor output. The data were successfully fit to a tentative model of the motor response as a non-linear function of central and peripheral bioelectric factors (R^2=0.8), but further research has to be conducted in order to validate this relationship.

The analysis here presented brings a new insight into how recruitment and excitation influence contractility, and may contribute for the comprehension of the neurophysiology of motor performance. We have discussed how biochemichal changes may transiently enhance control by increasing conduction velocity and miofibrilar contractility. Future investigations may also explore how these cellular mechanisms can induce long term adaptations (e.g. hypertrophy, neuroplasticity). Ultimately, research on neuromechanics shall clarify how the determinants of skillful movement can be conditioned or decoded. This understanding will give rise to new therapies and training methods for targeting neuromuscular pathologies or improving performance and fitness.

Bibliography

[1] A. Del Vecchio, F. Negro, F. Felici, and D. Farina, "Distribution of muscle fibre conduction velocity for representative samples of motor units in the full recruitment range of the tibialis anterior muscle," *Acta Physiologica*, vol. 222, no. 2, 2018.

[2] R. Merletti and D. Farina, *Surface Electromyography: Physiology, Engineering and Applications*, 1st ed., ser. IEEE Press Series on Biomedical Engineering. IEEE Press, Mar. 2016.

[3] S. J. Hall, *Basic Biomechanics*, 6th ed. New York: McGraw-Hill, 2012.

[4] R. M. Enoka and J. Duchateau, "Inappropriate interpretation of surface EMG signals and muscle fiber characteristics impedes understanding of the control of neuromuscular function," *Journal of Applied Physiology*, vol. 119, no. 12, pp. 1516–1518, 2015.

[5] A. Del Vecchio, F. Negro, F. Felici, and D. Farina, "Associations between Motor Unit Action Potential Parameters and Surface EMG Features," *Journal of Applied Physiology*, vol. 123, no. 4, pp. 835–843, 2017.

[6] E. Henneman, "Relation between Size of Neurons and Their Susceptibility to Discharge," *Science*, vol. 126, no. 3287, pp. 1345–1347, 1957.

[7] H. Milner-Brown, R. Stein, and R. Yemm, "The orderly recruitment of human motor units during voluntary isometric contractions," *The Journal of Physiology*, vol. 230, no. 2, pp. 359–370, 1973.

[8] B. Y. S. Andreassen and L. Arendt-Nielsen, "Muscle fibre conduction velocity in motor units of the human anterior tibial muscle: a new size principle parameter," *The Journal of Physiology*, vol. 391, no. 1, pp. 561–571, 1987.

[9] A. Hodgkin and S. Nakajima, "The effect of diameter on the electrical constants of frog skeletal muscel fibers," *The Journal of Physiology*, vol. 221, no. 1, pp. 105–120, 1972.

[10] T. Masuda and C. J. De Luca, "Recruitment threshold and muscle fiber conduction velocity of single motor units," *Journal of Electromyography and Kinesiology*, vol. 1, no. 2, pp. 116–123, 1991.

[11] T. Sadoyama, T. Masuda, H. Miyata, and S. Katsuta, "Fiber conduction velocity and fibre composition in human vastus medialis," *European Journal of Applied Physiology*, vol. 57, no. 6, pp. 767–771, 1988.

[12] J. L. Dideriksen and D. Farina, "Motor unit recruitment by size does not provide functional advantages for motor performance," *The Journal of Physiology*, vol. 591, no. 24, pp. 6139–6156, 2013.

[13] K. Murakami, H. Fujisawa, J. Onobe, and Y. Sato, "Relationship between Muscle Fiber Conduction Velocity and the Force-time Curve during Muscle Twitches," *Journal of Physical Therapy Science*, vol. 26, no. 4, pp. 621–624, 2014.

[14] D. Farina and A. Holobar, "Characterization of Human Motor Units From Surface EMG Decomposition," *Proceedings of the IEEE*, vol. 104, no. 2, pp. 353–373, 2016.

[15] J. E. Desmedt and E. Godaux, "Ballistic contractions in man: characteristic recruitment pattern of single motor units of the tibialis anterior muscle," *The Journal of Physiology*, vol. 264, no. 3, pp. 673–693, 1977.

[16] S. Methenitis, N. Karandreas, K. Spengos, N. Zaras, A. N. Stasinaki, and G. Terzis, "Muscle Fiber Conduction Velocity, Muscle Fiber Composition, and Power Performance," *Medicine and Science in Sports and Exercise*, vol. 48, no. 9, pp. 1761–1771, 2016.

[17] L. R. Brody, M. T. Pollock, S. H. Roy, C. J. De Luca, and B. Celli, “pH-induced effects on median frequency and conduction velocity of the myoelectric signal,” *Journal of Applied Physiology*, vol. 71, no. 5, pp. 1878–1885, 1991.

[18] T. Clausen, “Na-K Pump Regulation and Skeletal Muscle Contractility,” *Physiological Review*, vol. 83, no. 4, pp. 1269–1324, 2003.

[19] S. R. Gray, G. De Vito, M. A. Nimmo, D. Farina, and R. A. Ferguson, “Skeletal muscle ATP turnover and muscle fiber conduction velocity are elevated at higher muscle temperatures during maximal power output development in humans,” *American Journal of Physiology-Regulatory Integrative and Comparative Physiology*, vol. 290, no. 2, pp. 376–382, 2005.

[20] L. Padua, E. Stalberg, P. Caliandro, G. Muscogiuri, C. Pazzaglia, G. P. Sorice, G. Granata, S. Enrica, A. Pontecorvi, and A. Giaccari, “Single-fiber conduction velocity test allows earlier detection of abnormalities in diabetes,” *Muscle and Nerve*, vol. 43, no. 5, pp. 652–656, 2011.

[21] E. G. Klaver-Krol, J. J. Rasker, N. R. Henriquez, W. G. Verheijen, and M. J. Zwarts, “Muscle fiber velocity and electromyographic signs of fatigue in fibromyalgia,” *Muscle and Nerve*, vol. 46, no. 5, pp. 738–745, 2012.

[22] P. J. Blijham, B. G. M. V. Engelen, G. Drost, D. F. Stegeman, H. J. Schelhaas, and M. J. Zwarts, “Diagnostic yield of muscle fibre conduction velocity in myopathies,” *Journal of the Neurological Sciences*, vol. 309, no. 1, pp. 40–44, 2011.

[23] M. J. Zwarts, T. W. Van Veerden, T. P. Links, H. T. M. Haenen, and H. J. G. Osterhuis, “The muscle fiber conduction velocity and power spectra in familial hypokalemic periodic paralysis,” *Muscle and Nerve*, vol. 11, no. 2, pp. 166–173, 1988.

[24] T. H. V. A. Fritz, “Computer-aided analysis of muscle fibre conduction velocity in neuromuscular diseases,” *Neurological Sciences*, vol. 27, no. 1, pp. 51–57, 2006.

[25] H. Broman, G. Bilotto, and C. J. De Luca, “Myoelectric signal conduction velocity and spectral parameters: influence of force and time,” *Journal of Applied Physiology*, vol. 58, no. 5, pp. 1428–1437, 1985.

[26] P. Dayan and L. F. Abbott, *Theoretical Neuroscience : Computational and Mathematical Modeling of Neural Systems*. Cambridge, Mass.: MIT Press, 2014.

[27] G. Wulfram, W. M. Kistler, R. Naud, and L. Paninski, *Neuronal Dynamics: from Single Neurons to Networks and Models of Cognition*. Cambridge: Cambridge University Press, 2014.

[28] L. Zhang, K. J. Morris, and Y. C. Ng, “Fiber type-specific immunostaining of the Na+,K+-ATPase subunit isoforms in skeletal muscle: Age-associated differential changes,” *Biochimica et Biophysica Acta - Molecular Basis of Disease*, vol. 1762, no. 9, pp. 783–793, 2006.

[29] N. Hedayatpour, L. Arendt-Nielsen, and D. Farina, “Motor unit conduction velocity during sustained contraction of the vastus medialis muscle,” *Experimental Brain Research*, vol. 180, no. 3, pp. 509–516, 2007.

[30] M. Fortune E. & Lowery, “Simulation of the Interaction Between Muscle Fiber Conduction Velocity and Instantaneous Firing Rate,” *Annals of Biomedical Engineering*, vol. 39, no. 1, pp. 96–109, 2011.

[31] J. T. Mortimer, R. Magnusson, and I. Peterson, “Conduction Velocity in Ischemic Muscle: Effect on EMG Frequency Spectrum,” *The American Journal of Physiology*, vol. 219, no. 5, pp. 1324–1329, 1970.

[32] C. Juel, “Potassium and sodium shifts during in vitro isometric muscle contraction, and the time course of the ion-gradient recovery,” *Pflügers Archiv*, vol. 406, no. 5, pp. 458–463, 1986.

[33] K. R. Mills, L. Arendt-Nielson, and A. Forster, “Changes in muscle fibre conduction velocity during prolonged submaximal contractions of human vastus lateralis,” *Electroencephalography and Clinical Neurophysiology*, vol. 61, no. 3, p. 125, 1985.

[34] M. Zwarts, H. Haenen, and T. v. Weerden, “Muscle fiber conduction velocities and power spectra during sustained isometric muscle contractions,” *Electroencephalography and Clinical Neurophysiology*, vol. 61, no. 3, p. 59, 1985.

[35] L. Arendt-Nielson and K. Mills, “The relationship between mean power frequency of the EMG spectrum and muscle fibre conduction velocity,” *Electroencephalography and Clinical Neurophyslology*, vol. 60, pp. 130–134, 1985.

[36] P. Ravier, D. Farina, and O. Buttelli, “Time-varying delay estimators for measuring muscle fiber conduction velocity from the surface electromyogram,” *Biomedical Signal Processing and Control*, vol. 22, pp. 126–134, 2015.

[37] E. Koutsos, S. Member, C. Vlad, P. Georgiou, and S. Member, “A Muscle Fibre Conduction Velocity Tracking ASIC for Local Fatigue Monitoring,” *IEEE Transactions on Biomedical Circuits and Systems*, vol. 10, no. 6, pp. 1119–1128, 2016.

[38] A. Holobar, “A new optical flow model for motor unit conduction velocity estimation in multichannel surface EMG,” *Computers in Biology and Medicine*, vol. 83, no. 1, pp. 59–68, 2017.

[39] L. L. Andersen and P. Aagaard, “Influence of maximal muscle strength and intrinsic muscle contractile properties on contractile rate of force development,” *European Journal of Applied Physiology*, vol. 96, no. 1, pp. 46–52, 2006.

[40] R. Ema, M. Saito, S. Ohki, H. Takayama, Y. Yamada, and R. Akagi, “Association between rapid force production by the plantar flexors and balance performance in elderly men and women,” *AGE*, vol. 38, no. 5, pp. 475–483, 2016.

[41] N. A. Tillin, P. Jimenez-Reyes, M. T. G. Pain, and J. P. Folland, “Neuromuscular performance of explosive power athletes versus untrained individuals,” *Medicine and Science in Sports and Exercise*, vol. 42, no. 4, pp. 781–790, 2010.

[42] C. J. De Ruiter, D. Van Leeuwen, A. Heijblom, M. F. Bobbert, and A. De Haan, “Fast unilateral isometric knee extension torque development and bilateral jump height,” *Medicine and Science in Sports and Exercise*, vol. 38, no. 10, pp. 1843–1852, 2006.

[43] L. Grimby and J. Hannerz, “Recruitment order of motor units on voluntary contraction: changes induced by proprioceptive afferent activity.,” *Journal of Neurology, Neurosurgery and Psychiatry*, vol. 31, pp. 565–573, 1968.

[44] J. Duchateau and S. Baudry, “Maximal discharge rate of motor units determines the maximal rate of force development during ballistic contractions in human,” *Frontiers in Human Neuroscience*, vol. 8, no. 4, pp. 9–11, 2014.

[45] P. Aagaard, E. B. Simonsen, J. L. Andersen, P. Magnusson, and P. Dyhre-Poulsen, “Increased rate of force development and neural drive of human skeletal muscle following resistance training,” *Journal of Applied Physiology*, vol. 93, no. 4, pp. 1318–1326, 2002.

[46] N. A. Maffiuletti, P. Aagaard, A. J. Blazevich, J. Folland, N. Tillin, and J. Duchateau, “Rate of force development: physiological and methodological considerations,” *European Journal of Applied Physiology*, vol. 116, no. 6, pp. 1091–1116, 2016.

[47] D. Ruegg, “Ia afferents of the antagonist are inhibited presynaptically before the onset of a ballistic muscle contraction in man,” *Experimental Brain Research*, vol. 74, no. 3, pp. 663–666, 1989.

[48] J. Fuglevand, D. Winter, and E. Patla, “Models of recruitment and rate coding organization in motor-unit pools,” *Journal of Neurophysiology*, vol. 70, no. 6, pp. 2470–2488, 1993.

[49] D. Farina, A. Holobar, R. Merletti, and R. M. Enoka, “Decoding the neural drive to muscles from the surface electromyogram,” *Clinical Neurophysiology*, vol. 121, no. 10, pp. 1616–1623, 2010.

[50] L. L. Andersen, S. P. Magnusson, M. Nielsen, J. Haleem, K. Poulsen, and P. Aagaard, “Neuromuscular Activation in Conventional Therapeutic Exercises and Heavy Resistance Exercises: Implications for Rehabilitation,” *Physical Therapy*, vol. 86, no. 5, pp. 683–697, 2006.

[51] R. Dotan, G. Jenkins, T. D. O’Brien, S. Hansen, and B. Falk, “Torque-onset determination: Unintended consequences of the threshold method,” *Journal of Electromyography and Kinesiology*, vol. 31, pp. 7–13, 2016.

[52] A. Sakamoto and P. James, “Muscle activations under varying lifting speeds and intensities during bench press,” *European Journal of Applied Physiology*, vol. 112, pp. 1015–1025, 2012.

[53] M. D. Jakobsen, E. Sundstrup, C. H. Andersen, P. Aagaard, and L. L. Andersen, “Muscle activity during leg strengthening exercise using free weights and elastic resistance: Effects of ballistic vs controlled contractions,” *Human Movement Science*, vol. 32, no. 1, pp. 65–78, 2013.

[54] C. J. de Ruiter, “Initial phase of maximal voluntary and electrically stimulated knee extension torque development at different knee angles,” *Journal of Applied Physiology*, vol. 97, no. 5, pp. 1693–1701, 2004.

[55] V. Linnamo, P. V. Komi, and A. Davie, “Neuromuscular responses to explosive and heavy resistance loading,” *Journal of Electromyography and Kinesiology*, vol. 10, pp. 417–424, 2000.

[56] W. Yao, A. J. Fuglevand, R. M. Enoka, A. J. Fuglevand, and R. M. Enoka, “Motor-unit Synchronization Increases EMG Amplitude and Decreases Force Steadiness of Simulated Contractions,” *Journal of Neurophysiology*, vol. 83, no. 1, pp. 441–452, 2000.

[57] J. L. Dideriksen, D. Farina, M. Baekgaard, and R. M. Enoka, “An integrative model of motor unit activity during sustained submaximal contractions,” *Journal of Applied Physiology*, vol. 108, no. 6, pp. 1550–1562, 2010.

[58] S. J. Day and M. Hulliger, “Experimental simulation of cat electromyogram: evidence for algebraic summation of motor-unit action-potential trains.,” *Journal of Neurophysiology*, vol. 86, pp. 2144–2158, 2001.

[59] D. Farina, R. Merletti, and R. M. Enoka, “The extraction of neural strategies from the surface EMG,” *Journal of Applied Physiology*, vol. 96, no. 4, pp. 1486–1495, 2004.

[60] K. G. Keenan, D. Farina, K. S. Maluf, R. Merletti, and R. M. Enoka, “Influence of amplitude cancellation on the simulated surface electromyogram,” *Journal of Applied Physiology*, vol. 98, no. 1, pp. 120–131, 2005.

[61] A. Vigotsky, I. Halperin, G. Lehman, G. Trajano, and T. M. Vieira, “Interpreting Surface Electromyography Studies in Sports and Rehabilitation Sciences,” *Frontiers in Physiology*, vol. 8, no. 1, p. 15, 2018.

[62] Z. K. Pope, G. M. Hester, F. M. Benik, and J. M. DeFreitas, “Action potential amplitude as a noninvasive indicator of motor unit-specific hypertrophy,” *Journal of Neurophysiology*, vol. 115, no. 5, pp. 2608–2614, 2016.

[63] Y. Jonmohamadi, G. Poudel, C. Innes, and R. Jones, “Source-space ICA for EEG source separation, localization, and time-course reconstruction,” *NeuroImage*, vol. 101, pp. 720–737, Nov. 2014.

[64] F. Negro, S. Muceli, A. M. Castronovo, A. Holobar, and D. Farina, “Multi-channel intramuscular and surface EMG decomposition by convolutive blind source separation,” *Journal of Neural Engineering*, vol. 13, no. 2, p. 17, 2016.

[65] M. R. Sheridan and K. A. Flowers, “Movement variability and bradykinesia in Parkinsons-disease,” *Brain*, vol. 113, no. March, pp. 1149–1161, 1990.

[66] N. Teasdale, J. Phillips, and G. E. Stelmach, “Temporal movement control in patients with Parkinson’s disease,” *Journal of Neurology, Neurosurgery, and Psychiatry*, vol. 53, no. 10, pp. 862–868, 1990.

[67] N. A. Tillin, M. T. G. Pain, and J. P. Folland, “Identification of contraction onset during explosive contractions. Response to Thompson et al. "Consistency of rapid muscle force characteristics: Influence of muscle contraction onset detection methodology"," *Journal of Electromyography and Kinesiology*, vol. 23, no. 4, pp. 991–994, 2013.

[68] B. J. Thompson, E. D. Ryan, T. J. Herda, P. B. Costa, A. A. Walter, E. J. Sobolewski, and J. T. Cramer, “Consistency of rapid muscle force characteristics: Influence of muscle contraction onset detection methodology,” *Journal of Electromyography and Kinesiology*, vol. 22, no. 6, pp. 893–900, 2012.

[69] G. H. Staude, “Precise onset detection of human motor responses using a whitening filter and the log-likelihood-ratio test,” *IEEE Transactions on Biomedical Engineering*, vol. 48, no. 11, pp. 1292–1305, 2001.

[70] J. P. Folland, M. W. Buckthorpe, and R. Hannah, “Human capacity for explosive force production: Neural and contractile determinants,” *Scandinavian Journal of Medicine and Science in Sports*, vol. 24, pp. 894–906, 2014.

[71] H. J. Wyatt, “Detecting saccades with jerk,” *Vision Research*, vol. 38, no. 14, pp. 2147–2153, 1998.

[72] G. H. Staude, W. M. Wolf, U. Appel, and R. Dengler, “Methods for onset detection of voluntary motor responses in tremor patients,” *IEEE Transactions on Biomedical Engineering*, vol. 43, no. 2, pp. 177–188, 1996.

[73] P. Soda, S. Mazzoleni, G. Cavallo, E. Guglielmelli, and G. Iannello, “Human movement onset detection from isometric force and torque measurements: A supervised pattern recognition approach,” *Artificial Intelligence in Medicine*, vol. 50, no. 1, pp. 55–61, 2010.

[74] C. Richartz, M. Levenez, J. Boucart, and J. Duchateau, “Initial conditions influence the characteristics of ballistic contractions in the ankle dorsiflexors,” *European Journal of Applied Physiology*, vol. 110, no. 4, pp. 805–814, 2010.

[75] E. Burdet, D. Franklin, and T. Milner, *Human Robotics: Neuromechanics and Motor Control*, 1st ed. London, England ; Cambridge, Massachusetts: The MIT Press, 2013.

[76] D. Farina, L. Arendt-Nielsen, R. Merletti, and T. Graven-Nielsen, “Assessment of single motor unit conduction velocity during sustained contractions of the tibialis anterior muscle with advanced spike triggered averaging,” *Journal of Neuroscience Methods*, vol. 115, no. 1, pp. 1–12, 2002.

[77] M. Gazzoni, F. Camelia, and D. Farina, “Conduction velocity of quiscent muscle fibers decreases during sustained contraction,” *Journal of Neurophysiology*, vol. 94, no. 1, pp. 387–394, 2005.

[78] A. Eberstein and B. Beattie, “Simultaneous measurement of muscle conduction velocity and EMG power spectrum changes during fatigue,” *Muscle and Nerve*, vol. 8, no. 9, pp. 768–773, 1985.

[79] D. Farina, M. Gazzoni, and F. Camelia, “Low-threshold motor unit membrane properties vary with contraction intensity during sustained activation with surface EMG visual feedback,” *Journal of Applied Physiology*, vol. 96, pp. 1505–1515, 2004.

[80] R. Merletti, M. Knaflitz, and C. J. De Luca, “Myoelectric manifestations of fatigue in voluntary and electrically elicited contractions,” *Journal of Applied Physiology*, vol. 69, no. 5, pp. 1810–1820, 1990.

[81] J. Y. Hogrel, “Use of surface EMG for studying motor unit recruitment during isometric linear force ramp,” *Journal of Electromyography and Kinesiology*, vol. 13, no. 5, pp. 417–423, 2003.

[82] D. Farina and D. Falla, “Effect of muscle-fiber velocity recovery function on motor unit action potential properties in voluntary contractions,” *Muscle and Nerve*, vol. 37, no. 5, pp. 650–658, 2008.

[83] H. Nishizono, H. Kurata, and M. Miyashita, “Muscle fiber conduction velocity related to stimulation rate,” *Electroencephalography and Clinical Neurophysiology*, vol. 72, no. 6, pp. 529–534, 1989.

[84] M. J. Zwarts, T. v. Weerden, and J. H. v. d. Hoeven, “Long-lasting supernormal conduction velocity after sustained maximal isometric contraction in human muscle.,” *Muscle and Nerve*, vol. 16, no. 3, pp. 312–320, 1993.

[85] M. Mihelin, J. V. Trontelj, and E. Stålberg, “Muscle fiber recovery functions studied with double pulse stimulation,” *Muscle and Nerve*, vol. 14, no. 8, pp. 739–747, 1991.

[86] M. Jesunathadas, M. Klass, J. Duchateau, and R. M. Enoka, “Discharge properties of motor units during steady isometric contractions performed with the dorsiflexor muscles,” *Journal of Applied Physiology*, vol. 112, no. 11, pp. 1897–1905, 2012.

[87] D. Farina, W. Muhammad, E. Fortunato, O. Meste, R. Merletti, and E. Rix, “Estimation of single motor unit conduction velocity from surface electromyogram signals detected with linear electrode arrays,” *Medical and Biological Engineering and Computing*, vol. 39, no. 2, pp. 225–236, 2001.

[88] D. Farina, F. Negro, S. Muceli, and R. M. Enoka, “Principles of Motor Unit Physiology Evolve With Advances in Technology,” *Physiology*, vol. 31, no. 2, pp. 83–94, 2016.

[89] J. A. J. Friederich, “Muscle fiber architecture in the human lower limb,” *Journal of Biomechanics*, vol. 23, no. 1, pp. 91–95, 1990.

[90] D. Junge, *Nerve and muscle excitation*, 3rd ed. Sunderland, Mass.: Sinauer Associates, 1992.

[91] K. Mills and R. Edwards, “Muscle Fatigue in Myophosphorylase Deficiency: Power Spectral Analysis of the Electromyogram,” *Electroencephalography and Clinical Neurophysiology*, vol. 57, no. 4, pp. 330–335, 1984.

[92] T. W. Beck, X. Ye, and N. P. Wages, “Local muscle endurance is associated with fatigue-based changes in electromyographic spectral properties, but not with conduction velocity,” *Journal of Electromyography and Kinesiology*, vol. 25, no. 3, pp. 451–456, 2015.